EFFECT OF PARTICLE PROPERTIES ON FROTH STABILITY

By

Innocent Achaye
(Msc, Bsc)

Thesis presented for the **Degree of Doctor of Philosophy** in the Department of Chemical Engineering

UNIVERSITY OF CAPE TOWN

MARCH 2017

DECLARATION

I, Innocent Achaye, hereby declare that the work on which this thesis is based is my original work (except where acknowledgements indicate otherwise) and that neither the whole work nor any part of it has been, is being, or is to be submitted for another degree in this or any other university. I authorise the University to reproduce for the purpose of research either the whole or any portion of the contents in any manner whatsoever.

Signature: Signed by candidate

Signature Removed

Date:

12th/March/2017

ACKNOWLEDGEMENTS

I would like to thank everyone who helped me either directly or indirectly during the course of my studies. In this regard, I acknowledge the following people who contributed enormously to see to it that this thesis is a success.

Firstly, I take this opportunity to thank the Chemical Engineering department at UCT for granting me the scholarship. I also would like to acknowledge individuals within the unit that helped me during the study, notably:

- My supervisors Dr. Belinda McFadzean and Mrs. Jenny Wiese for their undivided efforts, direction, guidance, and continuously believing in me.
- Mr. Martin Harris for envisioning the project.
- Prof. David Deglon for helping with the flotation column design.
- Mrs. Shireen Govender, the laboratory manager, under whom I spent enormous amounts of time doing experiments. Her professionalism helped get the experiments done.
- Staff of the CMR laboratories, most especially Kenneth Maseko, Rubin Van Schalkwyk and Monde Bekaphi, who were always on standby to assist with handiworks.

Secondly, special thanks go to my wife, Toffister, and my daughter, Shiphrah, for standing strong while I was away.

Finally, I am indebted to the administration of Gulu University for granting me study leave to pursue this course to the very end.

PUBLICATIONS AND CONFERENCE PRESENTATIONS

McFadzean, B., Achaye, I., Wiese, J., Chidzanira, T., and Harris, M. (2016). *The effect of particle properties on froth stability.* Paper presented at the XXVIII International Mineral Processing Congress - IMPC 2016, Quebec City, Santiago, Canada.

Achaye, I., McFadzean, B., and Wiese, J. (2015, 16-19 November 2015). *The effect of Particle size on froth stability.* Paper presented at the International Flotation Conference (Flotation '15), Cape Town.

Achaye, I., Wiese, J., and McFadzean, B. (2015). *The effect of particle size on froth stability.* Paper presented at the MINPROC '15, Cape Town.

Achaye, I., Wiese, J., and McFadzean, B. (2014). *Particle size effects on froth stability in a laboratory bench-scale flotation column.* Paper presented at the MINPROC '14, Cape Town.

SYNOPSIS

The froth flotation process has found substantial usage in the mineral processing industry for over a century and as long as minerals continue to exist in the earth's crust, the demand for upgrading and recovery of these natural yet valuable resources will continue to exist. It relies on the principle that a bubble-particle collision process should be accompanied by the formation of an attachment between the pair. Of particular importance to the flotation process is the stability of froths. This will affect the mass pull, which, in turn, will affect recovery and the grade that is attainable. Froth stability is affected by many factors, viz. machine properties, hydrodynamics within the flotation cell, reagent suites, as well as mineral particle properties. Of particular interest to reagent suites is the frother dosage and its influence on the prevention of coalescence which has been fairly well studied. Regarding froth stability, the frother influences the amount of water that reports to the concentrate as well as the bubble surface viscosity, limiting drainage and subsequent bubble coalescence. Most of the other factors influence the amount of particles that report to the froth, but it is the particle properties that have the overriding influence on the froth stability. It is in the interest of flotation modelling and optimisation to be able to find relationships for the impact of particle properties on froth stability.

This project has focussed on the influence of two main particle properties, i.e. size and hydrophobicity, and their interactive effects on froth stability. In order to establish relationships between particle properties and froth stability, two devices were built in the laboratory, i.e. a non-overflowing stability column to measure froth stability and a bench-scale continuous flotation cell to provide metallurgical information, besides being able to measure froth stability using water recovery and froth surface bubble burst rate.

In the first part of the investigation, particles of discrete sizes as well as mixtures of particles sizes were utilised at a constant hydrophobicity. Results obtained show a power law relationship between froth stability and particle size, with all particle combinations falling on the same relationship. Froth stability decreased with increasing particle size. A large increase in froth stability occurred for feed particles of average size below 50 µm. This was attributed to particles in the finer range reporting to the

froth by both true flotation and entrainment. These fine particles would result in a higher interfilm viscosity resulting in reduced drainage.

A useful linear relationship between froth stability and the reciprocal of feed particle size was obtained. The reciprocal of feed particle size was used to represent the specific surface area of the particles. It was found that as the specific surface area of the particles increased, their froth stabilising effect also increased in a linear fashion.

In the second part of the investigation, the influence of particle hydrophobicity and the interactive effects of particle size and hydrophobicity on froth stability were explored. In common with other studies, it was found that froth stability increased with increasing particle hydrophobicity up to an optimum value between 66° and 69° and thereafter it decreased. The smallest size particles (28 µm) produced the highest variation in froth stability with increasing hydrophobicity. The response of the coarse particles to froth stability with increasing hydrophobicity was less pronounced. Particle size was found to have a greater influence on froth stability than particle hydrophobicity. Variations in froth stability were about 1.5 times greater for changes in particle size than changes in hydrophobicity over the relatively large ranges of size and hydrophobicity tested.

The relationship between froth stability and feed particle specific surface area was investigated at different hydrophobicities and found to be linear for most practical particle sizes. However, a deviation from linearity occurred at very small particles sizes (28 µm) for particles of optimum hydrophobicities. The slopes of the froth stability versus feed specific surface area relationships in the linear region were found to increase with increasing hydrophobicity, up until an optimum contact angle of between 64° and 68°, whereafter they decreased. Thus, this family of curves would allow the prediction of froth stability of varying hydrophobicities on a size-by-size basis. This relationship was shown to hold for two real ores: a platinum-bearing UG2 ore and an Itabirite iron ore. Thus, a simple linear calibration of grind versus froth stability would allow a prediction of froth stability for a particular ore.

A Langmuir-type model was developed to relate the froth stability to the concentrate particle surface area. It was found to be a good fit to the experimental data. This shows that it is possible to model froth stability in terms of the particle packing at the air-water interface in much the same way that surfactant molecular packing at the interface is modelled. The increasing particle surface area affects the surface tension of the films

and reduces film drainage. In studying the interactive effects of particle size and hydrophobicity, it was found that all data points of all hydrophobicities fell on the same relationship when froth stability was plotted as a function of concentrate surface area. It was therefore, concluded that particle size and hydrophobicity define the amount of particles that will report to the froth phase, but once in the froth, it is the surface area of the particles that will define the froth stability.

STATEMENT OF NOVELTY

Particle size and hydrophobicity effects on froth stability have been investigated in two specially designed laboratory devices, viz; a bench-scale continuously operated flotation column and a non-overflowing stability column. The novelty resulting from this study are outlined below:

- Developed a novel bench-scale flotation device for the characterisation of small samples such as drill core, or synthetic ore samples.
- Shown linear relationships between feed particle specific surface area and froth stability for most practical particle sizes. This was shown to apply to particles of different hydrophobicities in a synthetic pyrite/quartz ore, as well as two real ores.
- Developed a model of the relationship between froth stability and particle surface area that shows that froth stability is dependent only on particle surface area and not on the hydrophobicity of the particles in the froth.

TABLE OF CONTENTS

TABLE OF FIGURES

NOMENCLATURE

A	Area
Å	Angstrom
AAS	Atomic absorption spectroscopy
B.E.T	Brunauer, Emmett, and Teller
cm	Centimetre
cm/s	Centimetre per second
cm^3/min	Cubic centimetres per minute
ΔG	Gibb's free energy
$\sum$	Sigma
g	Grams
g/min	Grams per minute
Hmax	Maximum height attained by the froth
Jg	Superficial air velocity
Kg	Kilogram
L	Litre
L/min	Litres per minute
m	Metre
m^2/g	Square metres per gram
mL	Millilitre
ppm	Parts per million
°	Degree
°C	Degree centigrade
%	Percentage
PAX	Potassium amyl xanthate
PGM	Platinum group minerals
Q	Air flow rate
Rf	Froth recovery
rpm	Revolutions per minute
t	Time
µm	Micrometre
UG2	Upper group 2

CHAPTER ONE

1. INTRODUCTION

1.1. Froth flotation process

Froth flotation is a separation technique that exploits the surface properties of solids (particles) by adjusting and controlling the respective interfacial tensions. This possibility of varying the relative properties of different interfaces makes froth flotation one of the most versatile and universal industrial separation techniques used today (Bulatovic, 2007).

The surface properties of the different solids are controlled by different classes of reagents, each with a specific function. In addition to chemical reagent control, the overall process of selective separation by froth flotation depends on many other factors such as: the physical and mechanical features of thinning of liquid films, hydrodynamics of solid-in-water slurries, gas dispersion in such slurries, kinetics of chemical reactions, and of physical processes such as wetting, and the attachment of particles at air-water interfaces. At constant temperature, any differences in interfacial tensions and surface charges exhibited by various minerals can be exploited if the particles are contacted with two phases i.e. a liquid and a gas. The difference in interfacial tensions leads to a preferential non-wetting of some solids by water. This differentiation enables the non-wetted (hydrophobic) solids to be separated into a froth by contact with air bubbles.

1.2. Froth phase and froth stability

The froth phase in flotation cells is of paramount interest because it is the grade-determining phase and, in many instances, is also the recovery-determining phase. The presence of particles has a great influence on the stability of froths. The main particle properties which affect froth stability are particle size and hydrophobicity (Ata *et al.*, 2003; Aveyard *et al.*, 1994; Chipfunhu *et al.*, 2011; Dippenaar, 1982a,b; Farrokhpay, 2011; and Rahman *et al.*, 2012). The instability of froths is reflected by the rupture of thin films, bubble coalescence and loss of froth volume (Schwarz and Grano, 2005). The hydrophobicity, size and shape of particles are the properties that govern the degree of penetration of the particles in the film (Bulatovic, 2007). This

degree of penetration is related to the ability of the particle to rupture an individual film in the froth. Therefore, for constant particle hydrophobicity and shape, the rate of film rupture and, consequently, the froth stability can be related to the size and number of particles present in the froth. Particle size, hydrophobicity and concentration all affect froth stability interactively. As such, it is difficult to model the effect of one parameter while ignoring the others.

1.3. Problem statement and justification

Froth flotation plays an important role in the processing of mineral ores. However, the understanding of the processes occurring in the froth phase has had its pitfalls and challenges. Work done in the Amira P9 project proposed a phenomenological model of the froth based on froth mobility and froth stability (Harris, 2011). This work will focus on providing a quantitative framework for froth stability prediction. A number of studies have shown that the sizes of particles, and their hydrophobicity, have a significant effect on the structure and stability of the froth. However, there is a general gap in the knowledge in terms of the interactive effects of these two particle properties on froth stability, and how these two particle properties can be used to quantitatively predict the stability of froths.

In this project, the effects of particle size and hydrophobicity and their interactive effects were investigated in great depth. A bench-scale continuously operated flotation column and a non-overflowing stability column were used to measure froth stability in a three phase system in which a synthetic ore made up of three components i.e. pyrite, talc and quartz was used. The froth stability measurement proxies explored are water recovery and top-of-froth bubble burst rate in the bench-scale flotation column, and dynamic froth stability factor in the stability column.

1.4. Objectives

The objectives of this investigation were as follows:

a) To determine the froth stability at varying particle size distributions.
b) To determine the froth stability for particles of varying hydrophobicities;
c) To determine the interactive effects of particle size and hydrophobicity on froth stability; and

d) To develop a method to calibrate the froth stability of a given ore at different grind sizes.

1.5. Research questions

(i) What forms the basis of a good experimental measure for froth stability?

(ii) What is the relationship between froth stability and particles of varying size distributions?

(iii) What is the relationship between froth stability and particles of varying hydrophobicities?

(iv) What are the interactive effects of particle size and hydrophobicity on froth stability?

1.6. Hypotheses

Hypothesis 1: Froth stability increases with decreasing particle size and this is due to increased viscosity of the thin liquid films between bubbles which leads to a slower liquid drainage rate.

Hypothesis 2: Froth stability will increase as a function of the increasing particle surface area in the froth because thin film liquid drainage will be directly affected by the surface area of particles retarding drainage.

Hypothesis 3: Froth stability is greatest at a critical contact angle, below or above which froth stability decreases. This is due to bridging effects causing film rupture in highly hydrophobic particles.

Hypothesis 4: Optimum froth stability is obtained with small particles of intermediate hydrophobicity. This is because large particles and particles of very high hydrophobicity rupture liquid films and so suppress the froth stability.

1.7. Scope

In this project, a synthetic ore made up of three components, i.e. pyrite, quartz and talc was used. A bench-scale continuous column flotation cell was used for flotation tests and measuring froth stability using two proxies, i.e. water recovery and top-of-froth bubble burst rate. A non-overflowing stability column was used to measure froth stability by following the froth growth rate. By carefully controlling the feed, the effects

of different parameters on froth stability were investigated. This study investigated the effects on froth stability of:

a) varying particle size distributions;
b) varying particle hydrophobicities;
c) interactive effects of groups of particles of varying size distributions and varying hydrophobicities.

The project took hydrodynamic effects, such as bubble size, superficial gas velocity, and gas holdup into account, but did not investigate them. This study did not investigate the effect of surfactants; a constant frother dosage was used in all experiments. A polypropylene glycol ether, Dowfroth 250, was used as frother at 100 ppm dosage. It has been postulated that two particle parameters can comprehensively describe froth stability and froth mobility, i.e. size and hydrophobicity. This study investigated these two particle properties in relation to froth stability.

1.8. Thesis layout

This thesis is structured as outlined below:

1) Chapter 1: This chapter provides a background to the flotation process with emphasis on the froth phase and its stability. In this chapter, the boundaries of the project are established, stating clearly the problem to be tackled.
2) Chapter 2: In this chapter, a critical synthesis of the literature relevant to this study was carried out. It is reported that several froth stability measurement techniques have been generated and this has been well discussed. Particle size and hydrophobicity effects on froth stability has been discussed, with emphasis put on the stabilisation mechanisms.
3) Chapter 3: This chapter details the design and operation of a novel bench-scale flotation column that was built in the laboratory to carry out test work. The material of construction was Perspex for the pulp section and glass for the froth section. The flotation column was designed to operate continuously at steady state.
4) Chapter 4: This chapter details the set-up of the experiments including all reagents and materials used. A detailed description of the non-over-flowing stability column used for froth stability prediction is included. This section also

details how samples were prepared and analysed, and how data obtained was analysed

5) Chapter 5: In this chapter, it was seen clearly that particle size has a substantial effect on froth stability. The relationships between particle size, particle surface area and froth stability were established and the underlying mechanisms responsible for the relationships discussed with reference to established scientific principles.
6) Chapter 6: In this chapter, experimental results originating from studying the effect of particle hydrophobicity and the interactions of size and hydrophobicity in influencing froth stability are reported. Discussions explaining the observed phenomena are made and conclusions are drawn.
7) Chapter 7: In this chapter, the defining outcomes of this project are clearly spelt out. The research questions earlier stated in chapter 1 are answered and hypothesis either accepted or rejected.

CHAPTER TWO

2. LITERATURE REVIEW

2.1. Overview

There are many important drivers of froth stability in flotation: machine properties, ore characteristics, hydrodynamics within the flotation cell, effect of reagent suites, as well as mineral particle characteristics. Decoupling the effects of these important drivers assists in better understanding the flotation process. In addition, flotation modelling and prediction is facilitated once these effects are known.

This chapter provides a review of the current understanding of froth stability and its measurement. The influence of particles on the stability of three phase froths, their stabilisation mechanisms and eventual flotation performance in terms of grade and recovery will also be reviewed. The particle properties under investigation in the current study are size, hydrophobicity and concentration.

2.2. Kinetics of the flotation process

Froth flotation is a mineral processing technique used for separating valuable minerals from gangue, a waste material present in the ore, by use of surfactants and wetting agents. The separation process takes place in a flotation cell which, on laboratory scale, can be made to operate in either batch mode or on a continuous basis.

On laboratory scale, batch flotation cells have found application for investigating the effects of various operating parameters on flotation performance due to a number of reasons, i.e. batch flotation tests can be rapidly carried out and are an inexpensive way of assessing mineral flotation response at various operating conditions. Coupled with the above, it is easy to evaluate the effects of altering flotation variables which is accomplished by fitting batch data to first order kinetic rate equations – kinetic modelling of flotation processes being important from both a design and operating perspective, providing a basis for the simulation of industrial flotation circuits (King, 1978; Mathe *et al.,* 1999; Woodburn *et al.,* 1976).

Flotation is a process occurring in time; the results being determined by many random factors. Formation of a permanent attachment between a particle and a bubble requires collision. The kinetic energy must be high enough to overcome the barrier of

the potential of the particle-bubble interaction but low enough to make this interaction stable. It is further noted that the particle-bubble collision and the value of particle kinetic energy are of random character (Brożek and Mlynarczykowska 2006).

In batch flotation systems, it is assumed that the overall flotation response of different minerals follows first order kinetics with respect to the concentration of floatable minerals (Mathe *et al.,* 1999; Zuniga, 1935), i.e. kinetic models based on chemical analogy describes the flotation process mathematically as:

$$\frac{dC_t}{dt} = -kC_t^n \qquad \text{Equation 2.1}$$

Where k is the flotation rate constant, C_t is the concentration of floating materials remaining in the flotation chamber at any time, t and n is the order of the flotation process.

According to Brożek and Mlynarczykowska (2006), Equation 2.1 describes the flotation kinetics of particles which are homogeneous in their surface properties i.e. equal floating particles which possess the same value of the flotation rate constant.

Solving Equation 2.1 for $n = 1$, we obtain the recovery of the floatable particles to the froth phase from the expression:

$$R(t) = 1 - e^{-kt} \qquad \text{Equation 2.2}$$

Boundary condition for solving Equation 2.2 is:

$$\lim_{t\to\infty} R(t) = R_\infty \qquad \text{Equation 2.3}$$

Where R_∞ = equilibrium recovery and $R(t)$ = overall recovery at any time, t.

Integrating Equation 2.1 using the boundary condition in Equation 2.3 gives Equation *2.4* which is a general first order kinetic expression for the flotation process.

$$R(t) = R_\infty\left(1 - e^{-kt}\right) \qquad \text{Equation 2.4}$$

$R(t)$ is the overall flotation recovery which is a measure of the performance of the separation process; it is defined as the ratio of the mass of particles collected in the

concentrate launder by true flotation to the mass of particles in the feed. The flotation rate constant may be evaluated using first order, second order or non-integral order equations (Hernáinz and Calero, 2001). Under conditions of true flotation, only particles that attach themselves to gas bubbles are considered to be overflowing in the concentrate launder. Particles recovered by entrainment are not considered.

Equation 2.4 represents a single-stage model for batch flotation cells which assumes 100% recovery of minerals within the froth phase. This is one of the major limitations of the batch flotation cell as a design and optimisation tool. A two-stage model (as shown in Figure 2.1), which is seen as a more realistic representation of the flotation process, has also been advanced in flotation column modelling (Finch and Dobby, 1990; Yianatos, *et al.,* 1998).

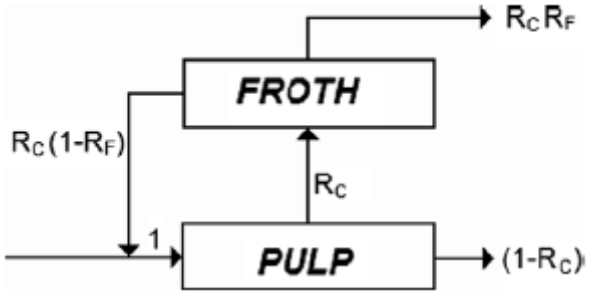

Figure 2.1: Representing the two-stage flotation model which considers both the pulp and froth as distinct phases (Adapted from Yianatos et al., 2008).

The overall flotation recovery (due to true flotation) is thus related to the recoveries of the collection and froth zones and this is described by the relationship:

$$R = \frac{R_C R_f}{1 - R_C(1 - R_f)} \qquad \text{Equation 2.5}$$

Where R = overall flotation recovery, R_C = collection zone recovery, R_f = froth zone recovery.

2.3. Froth recovery, R_f

Considering the flotation process as perfect mixer, the first order flotation rate constant, k, for a continuous process can be defined as:

$$k = \frac{R}{\tau(1 - R)} \qquad \text{Equation 2.6}$$

Where τ = mean residence time.

In order to develop a comprehensive flotation model the flotation recovery in the froth phase, R_f, must be taken into account. R_f has been defined by Savassi *et al.* (1998) as:

$$R_f = \frac{\text{Mass rate of particles reporting to the concentrate via true flotation}}{\text{Mass rate of attached particles at the pulp} - \text{froth interface}} \qquad \text{Equation 2.7}$$

Froth recovery can be calculated by dividing the overall flotation rate constant, k by the pulp zone rate constant, k_c.

$$R_f = \frac{k}{k_c} \qquad \text{Equation 2.8}$$

Vera *et al.,* (2002) has noted that R_f has a significant effect on overall recovery. A particle may be recovered in the collection zone and be transported to the froth phase. However, if the froth zone recovery is low, the particle will drop back to the pulp zone instead of being recovered to the concentrate. From experience, it has been seen that collection zone recovery varies from 60% to 99% while froth zone recovery varies from 10% to 90%. Up to 50% of the overall flotation recovery might be lost owing to inefficiencies in the performance of the froth zone (Vera *et al.,* 2002).

Because of its significance in determining the overall flotation recovery, it is important to experimentally measure and quantify R_f. A technique developed by Vera *et al.,* (1999) building on previous works of Feteris *et al.,* (1987) and Laplante *et al.,* (1983) has been proposed. This technique involves simultaneous determination of the collection zone rate constant, k_c, and subsequently the froth zone recovery, R_f. Two assumptions are made in carrying out the methodology:

(1) That the transfer of particles from the body of the pulp to the pulp-froth interface depends only on events occurring in the pulp zone;
(2) That the transfer of particles from the froth to the concentrate depends only on events occurring in the froth phase.

At zero froth depth, R_f is equal to 100%. The flotation rate constant at zero froth depth is defined as the collection zone rate constant, k_c. At all froth depths greater than zero, the froth recovery will be less than or equal to 100%. Vera *et al.* (1999), utilised

Equation 2.8 to further develop a relationship between flotation rate constant, k and froth depth, FD. It has earlier been reported that k varies linearly with FD with a negative slope (Engelbrecht and Woodburn, 1975; Feteris *et al.,* 1987; Hanumanth and Williams, 1990; Laplante, 1980). The linear relationship can be represented as:

$$k = a - b(FD) \qquad \text{Equation 2.9}$$

Where a and b are constants. The linear relationship can also be represented graphically as shown in Figure 2.2.

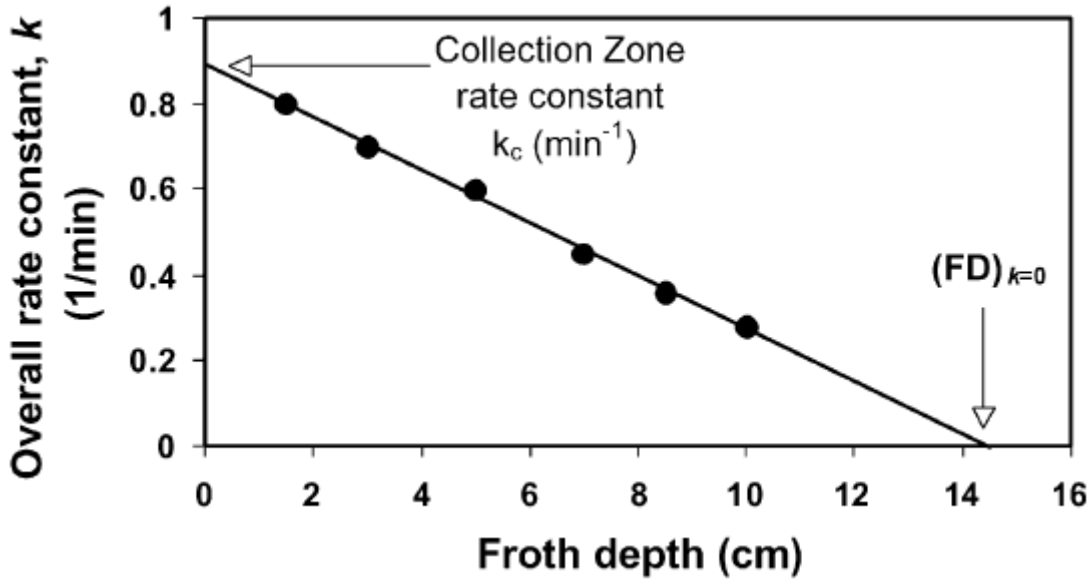

Figure 2.2: Flotation rate constant, k, as a function of froth depth, FD. (Vera et al., 1999).

The intercept, a = k_c at zero froth depth. For a very deep froth for which no material is transferred from the froth to the concentrate (k = 0), the intercept of the straight line is $(FD)_{k=0}$, and b = k_c / $(FD)_{k=0}$. Substituting for a and b into Equation 2.9:

$$k = k_c\left\{1 - \frac{(FD)}{(FD)_{k=0}}\right\} \qquad \text{Equation 2.10}$$

Substituting Equation 2.10 into Equation 2.8 yields:

$$R_f = \left\{1 - \frac{(FD)}{(FD)_{k=0}}\right\} \qquad \text{Equation 2.11}$$

Equation 2.11 shows that the froth recovery per unit froth depth is constant (Vera *et al.,* 1999). However, the varying froth depth technique for measuring froth recovery only estimates recovery losses in the froth alone and not any other loses that may

occur at the pulp-froth interface as the particle laden bubbles decelerate and form the froth (Seaman *et al.,* 2006). It requires that the cell reaches steady state at each froth depth before measurements are taken. According to Runge *et al.* (2010), it is difficult to perform this technique at industrial scale as hours of steady state operation is difficult to achieve. For a scavenger cell, measurement of recovery is very difficult because the differences in grade between the feed and the tailings are very small. This is the simplest method to determine froth recovery in a laboratory setting and is the technique used in this study.

Another technique that has been developed to measure froth recovery is the direct measurement of bubble load. Devices have been developed to measure the flow of particles over the concentrate launder so that froth recovery can be estimated (Falutsu and Dobby, 1992; Seaman *et al.,* 2006; Yianatos *et al.,* 2008). Particle laden bubbles are allowed to rise within a tube over a timed period. The particles are then removed, dried, weighed and assayed. Figure 2.3 shows diagrammatic representations by Runge *et al.* (2010) of the devices developed by Seaman *et al.* (2006), Yianatos *et al.* (2008) and Falutsu and Dobby (1992) to measure bubble load.

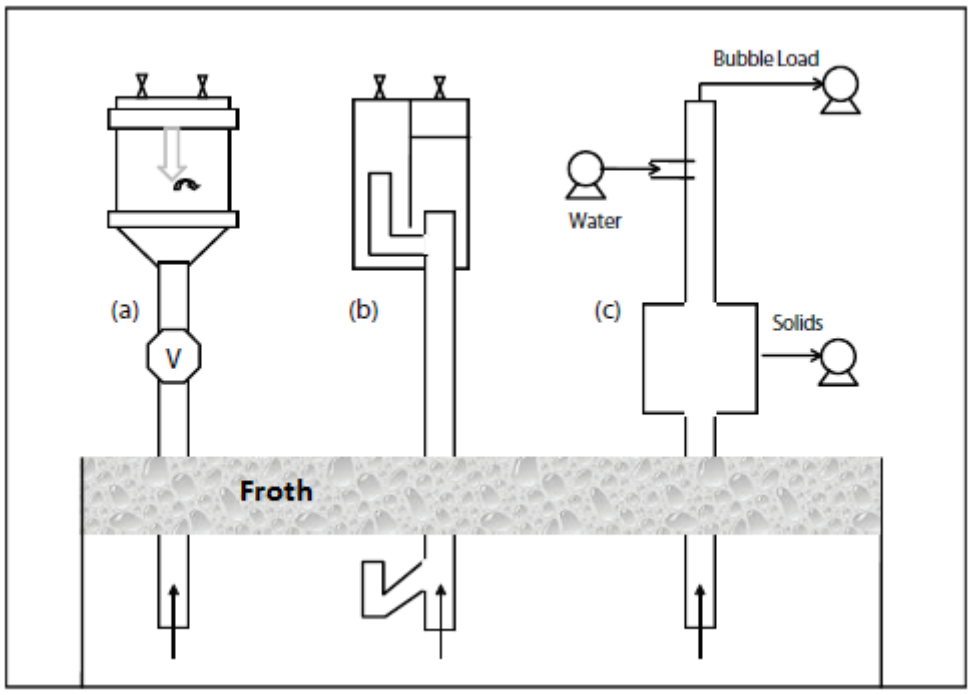

Figure 2.3: Figure 2.3: Bubble load devices. (a) Seaman et al. (2006), (b) Yianatos et al. (2008) and (c) Falutsu and Dobby (1992). (Adopted from Runge et al. 2010).

Besides the above techniques, estimation of bubble load has been done from mass balances. Savassi *et al.* (1997) first proposed this technique which involves pumping samples through a funnel directly from the pulp by means of a vacuum pump. The funnel was oriented in two directions, viz. vertically to aid preferential rise and collection of particle laden bubbles and horizontally to enable bubbles to rise past the funnel preventing their collection. A device for collecting a sample of the pulp which contains no particle laden bubbles was also developed by Savassi *et al.* (1997). A mass balance is performed using the mass of solids, water content and mineral assay of the three samples in order to determine the mass of solids attached per litre of air (or bubble load). This technique is however, unable to estimate froth recovery in flotation cells in which there is only a small difference in assay between the particles attached to the bubbles and the particles suspended in the pulp phase.

An adaptation of the Savassi technique which simplifies the sampling methodology and mass balancing problem was proposed by Alexander *et al.* (2003). In this technique, a sample is collected to determine the air holdup. Two more samples are collected to infer the assay of the particles in the suspended pulp and the particles attached to air bubbles. The following assumptions are made:

- The assay of the suspended particles in the pulp is equal to that of the tailings assay, and this holds if the cell is perfectly mixed.
- There is no selective shedding of attached particles within the froth phase. As such, the assay of the particles attached to the bubbles at the surface of the froth is the same as that entering from the pulp.

The mass balancing techniques have the advantage of being relatively simple and straightforward to perform. Since a sample of the attached particles can be obtained, it is possible to investigate its characteristics in terms of size, liberation, surface speciation, etc. There is, however, concern whether these devices can produce a representative sample of the attached particles reporting to the froth.

2.4. Entrainment

Three main processes are responsible for the transport of particles from the pulp through the froth to the concentrate launder (Wills and Napier-Munn, 2006), viz.

- True flotation (selective attachment to air bubbles). This is the most important mechanism and the majority of particles report to the concentrate through this process.
- Entrainment (non-selective recovery in the water which reports to the concentrate). The degree of entrainment determines the separation efficiency between the valuable mineral and the fully liberated gangue minerals.
- Physical entrapment between particles in the froth attached to air bubbles (also referred to as aggregation).

These mechanisms occur parallel to each other and are responsible for the overall recovery of particles in flotation. Kinetics of particle recovery by true flotation as applicable in a batch cell has been discussed earlier. It is important that the entrainment mechanism be discussed here as well because it has a significant effect not only on the quality of froths obtained, but on the eventual grade and recovery attainable. Both hydrophobic and hydrophilic particles are recovered by entrainment. Entrainment is defined as the non-selective mechanical carry over of both hydrophobic and hydrophilic particles from the pulp phase through the froth and out of the concentrate launder. Entrainment is the primary mechanism by which gangue minerals are recovered (Smith and Warren, 1989), and is controlled by factors such as particle size distribution and amount of slimes in the feed, pulp density, aeration rate, froth thickness, etc (Kirjavainen, 1989, 1992, 1996; Laplante *et al.,* 1989; Smith and Warren, 1989; Warren, 1985).

A representation of the two mechanisms responsible for particle recovery in flotation is shown in Figure 2.4.

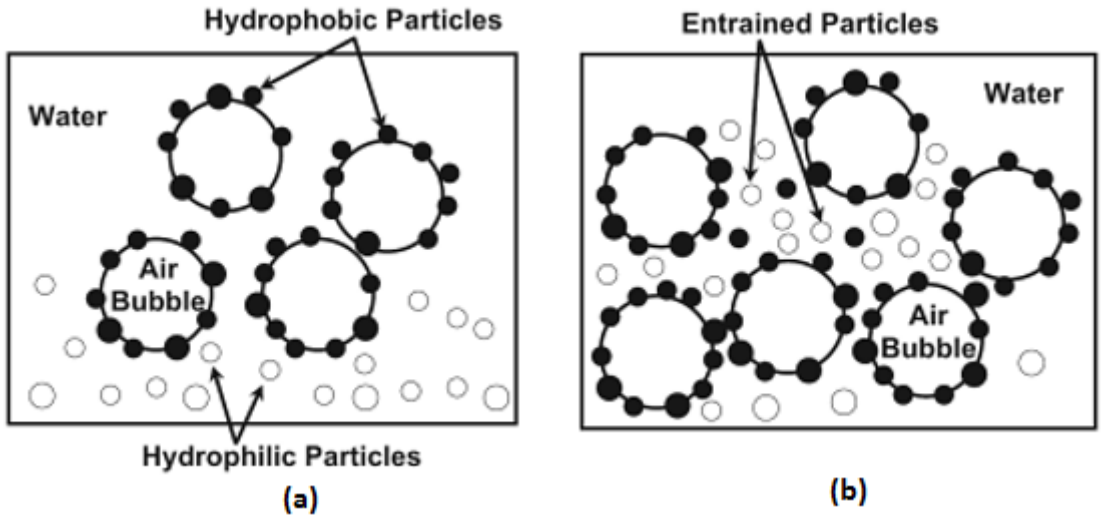

Figure 2.4: Mechanisms of particle recovery by (a) true flotation, (b) entrainment (Kawatra and Carlson, 2013).

Using fine-sized free gangue particles, pioneering studies have been able to correlate entrainment with the recovery of water into the froth (Johnson *et al.,* 1974; Trahar and Warren (1976); Thorne *et al.,* 1976; Warren, 1985). The relationship between gangue recovery and water recovery has been described using Equation 2.12 (Smith and Warren, 1989; Warren, 1985).

$$R_g = e_g . R_w \qquad \text{Equation 2.12}$$

Where R_g = fine-sized gangue recovery, e_g = degree of entrainment or entrainment factor, and R_w = water recovery in a given time.

Earlier studies have shown that the recovery of gangue minerals is directly related to the amount of water recovered. The classic work of Engelbrecht and Woodburn (1975) is one such example (Figure 2.5) which shows the recovery of silica particles of various sizes as a function of particle size. The key findings from the plot of gangue recovery as a function of water recovery are (Neethling and Cilliers, 2002):

- For most of the regions of interest, a linear relationship exists between gangue recovery and water recovery. This relationship has recently been shown to hold by Kracht *et al.* (2016);
- Extrapolating this linear relationship produces a zero intercept on the water recovery axis for very fine particles, but an increasingly positive intercept with increasing particle size;

- A non-linear relationship is observed between gangue recovery and water recovery at low water recoveries;
- The slope of the linear portion of the recovery of gangue recovery as a function of water recovery plots decreases with increasing particle size.

Particle size plays an important function in determining the degree of entrainment. According to Smith and Warren (1989), particles larger than 50 μm experience little to no entrainment. As such, as size increases, particles will most likely drain hydraulically on reaching the froth phase.

The structure of the froth has a significant effect on entrainment (Engelbrecht and Woodburn, 1975; Kirjavainen, 1996; Subrahmanyam and Forssberg, 1988). For a stable froth which is composed of small bubbles, there will be a high recovery of both entrained and attached particles because of low drainage and less coalescence of bubbles. An unstable froth will have a low degree of entrainment.

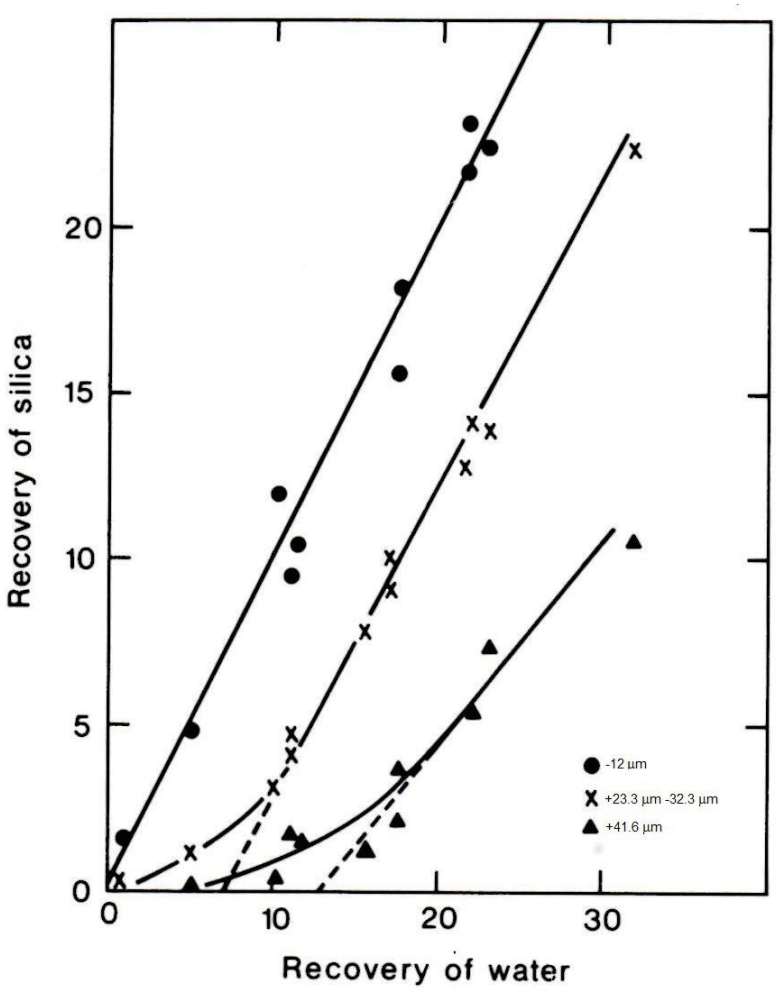

Figure 2.5: Recovery of silica gangue of different sizes as a function of water recovery (Engelbrecht and Woodburn, 1975).

2.5. The structure of the froth

In describing the structure of three-phase froths, knowledge of two-phase foams has been substantially used (Bikerman, 1973; Ventura-Medina, 2002). Pugh (1996) states that pure liquids are incapable of foaming unless a surface-active material is present in them. A gas bubble introduced below the surface of a pure liquid will almost immediately burst as soon as the liquid has drained away. In the study of foams and froths therefore, dilute surfactant solutions are used so as to create a relatively strong air-liquid interface brought about by elasticity in the film.

In a two-phase system, gas cells are enclosed by liquid; the gas cells are the dispersed phase while the liquid is the continuous phase. The bubbles of a foam have a polyhedral shape with the thin films or surfaces forming the faces or lamellae. Where the thin films meet is called the Plateau borders (usually seen as lines) and four

Plateau borders meet at vertices (usually seen as nodes). The thin liquid film which separates two adjacent bubbles is therefore termed as the lamella, while the channel formed by the intersection of three lamellae is the Plateau border. Figure 2.6 shows the diagrammatic representation of different constituents of the foam system.

In relation to a two-phase system, the froth can be defined as a three phase structure consisting of solids, liquid and air bubbles. The solids contained in the froth are either valuable material attached to lamellae or a mixture of valuable material and gangue material contained freely within the Plateau borders (Triffett and Cilliers, 2006). The entire froth is made up of a continuous network of narrow water channels in which water and solid particles can flow.

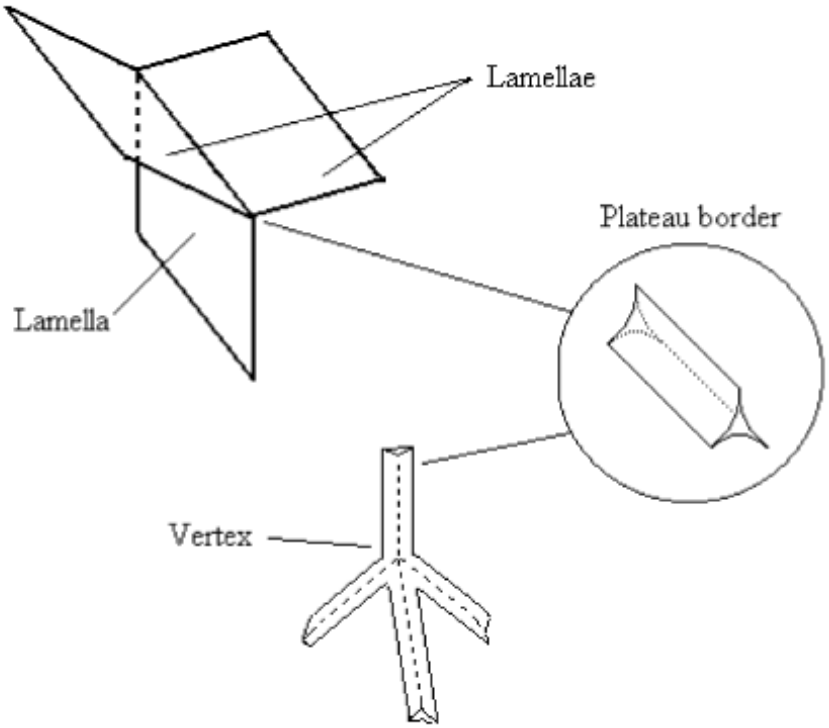

Figure 2.6: Structure of the lamella, Plateau border, and vertex in a foam system (Ventura-Medina, 2002).

A foam or froth system usually undergoes three main sub-processes which are responsible for defining its structure, i.e. drainage, film rupture (bursting), and coarsening (coalescence and diffusion). Due to gravity and capillary forces, liquid drains from the liquid films and Plateau borders. Liquid flow from thin films to Plateau borders is aided by differences in curvature. The liquid will flow till it reaches the vertices. This will lead to thinning of the liquid films, which will eventually induce film

rupture and coalescence of two adjacent bubbles. Diffusion is brought about by differences in capillary pressures. Small bubbles have higher capillary pressure than large bubbles; as such gas will diffuse from the small bubbles to the large bubbles (Bikerman, 1973; Weaire and Hutzler, 1999). This process is known as disproportionation. The driving force for the disproportionation to occur is the Laplace pressure over a curved surface. It has been reported by de Vries (1957) that the diffusion process can reduce the total number of bubbles to about 10% of the initial count without rupture of the foam lamellae. Pugh (1996) notes that this process is, however, most important in cases where the gas is soluble in the liquid e.g. in soft drinks where the solubility of carbon dioxide is 50 times greater than nitrogen. Disproportionation occurs over a substantially longer time frame than coalescence and therefore coalescence will dominate in a flotation froth (Ventura-Medina & Cilliers, 2002).

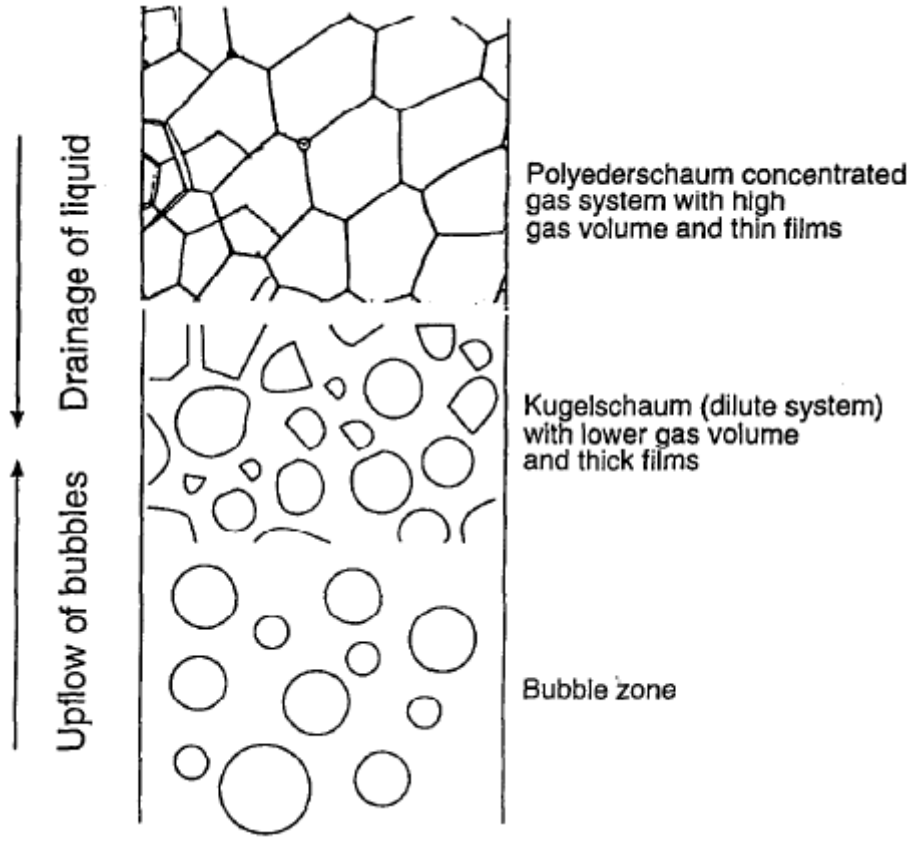

Figure 2.7: Froth structure occurring during formation and drainage of the foam in a column (Pugh, 1996).

According to Pugh (1996) and as depicted in Figure 2.7, two types of foam structures exist:

1. Kugelschaum or sphere foam is initially produced in freshly prepared systems and consists of small, roughly spherical bubbles separated by thick films of viscous liquid. This type of foam structure may be considered as a temporary dilute dispersion of bubbles in the liquid, but on aging, the structure undergoes gradual changes with the bubbles transformed into polyhedral gas cells with thin flat walls.

2. Polyderschaum is formed after drainage has taken place through the plateau borders. The liquid film thins to about 1000 nm with the resulting thin film structure referred to as a Polyderschaum. A high gas content structure is usually formed near the surface of the froth and the foam density decreases with the froth height. A foam will collapse from the top to the bottom of the column, as thin films in the polyderschaum foams are more susceptible to rupture by shock, temperature gradients, or vibration.

2.6. Froth structure and stability

It has been stated earlier that the presence of a surface-active material is important in foaming/frothing. Pugh (1996) notes that a simple test for the purity of water can be carried out by shaking a sample of it in a closed vessel and the water purity estimated from the bubble persistence time. A bubble persistence time of even one second on water would imply the presence of a surface active impurity, such as dust. In order to prepare foams/froth systems, two techniques may be used. The dispersion technique involves mechanical shaking or whipping of a surfactant solution or slurry. This method is, however, not particularly good since accurate control of the amount of air introduced to the liquid/slurry is difficult to achieve. A more robust technique, known as sparging, used in industry or for quantitative laboratory analysis involves passing a stream of gas through an orifice and growing bubbles in the solution/slurry.

Stability of the froth is defined by Aktas *et al.,* (2008), as the time of its persistence and is related to froth structure and bubble size distribution. According to Tsatouhas *et al.,* (2006), it also refers to the foam decay process, during which time there is no further generation of gas bubbles. It is used to describe the general phenomena of thin film rupture, bubble coalescence and loss of froth volume. Triffett and Cilliers (2006) define froth stability as the ability of bubbles in a froth to resist coalescence and bursting. A more stable froth is expected to have fewer coalescence and bursting

events, a smaller mean bubble size, and may carry more water. With regard to stability, two types of foams can be defined, i.e. an unstable (or transient) foam with a lifetime of seconds, and a metastable (or permanent) foam with a lifetime of hours or days (Pugh, 1996).

Formation of a liquid film occurs when a gas bubble rising in liquid approaches either another bubble or the surface of the liquid. According to Dippenaar (1982a), the stability of a froth is related to the stabilities of these liquid films. The rupture of thin liquid films that separate two adjacent bubbles is one of the main reasons proposed for bubble coalescence in the froth. Coalescence of bubbles occurs when the liquid content in the froth falls below a critical value. The presence of particles and surfactants help to prevent film rupture (Ata, 2012).

The objective of froth flotation is to obtain a stable froth which will recover a large amount of valuable particles attached to air bubbles. However, a more stable froth would mean recovery of more gangue minerals by entrainment as well. Accordingly, from a view point of maximising recovery and concentrate grade, there is an optimum froth stability for any given flotation cell and any given operating conditions for that cell (Triffet and Cilliers, 2006).

2.7. Frothers and froth stability

The use of frothers is an important aspect in flotation chemistry. Frothers are surface-active compounds that have the ability to adsorb at the air-water interface. A frother molecule consists of hydrophobic (non-polar) and hydrophilic (polar) parts as shown in Figure 2.8(a). At the air-water interface, the frother is oriented such that the hydrophobic part is in the air phase and the hydrophilic part is in the water phase. The frother therefore, has a mixed polarity as the two ends are oriented in different phases. Figure 2.8(b) shows the structure of two frothers (methyl isobutyl carbinol, MIBC and a polypropylene glycol ether, Dowfroth 250).

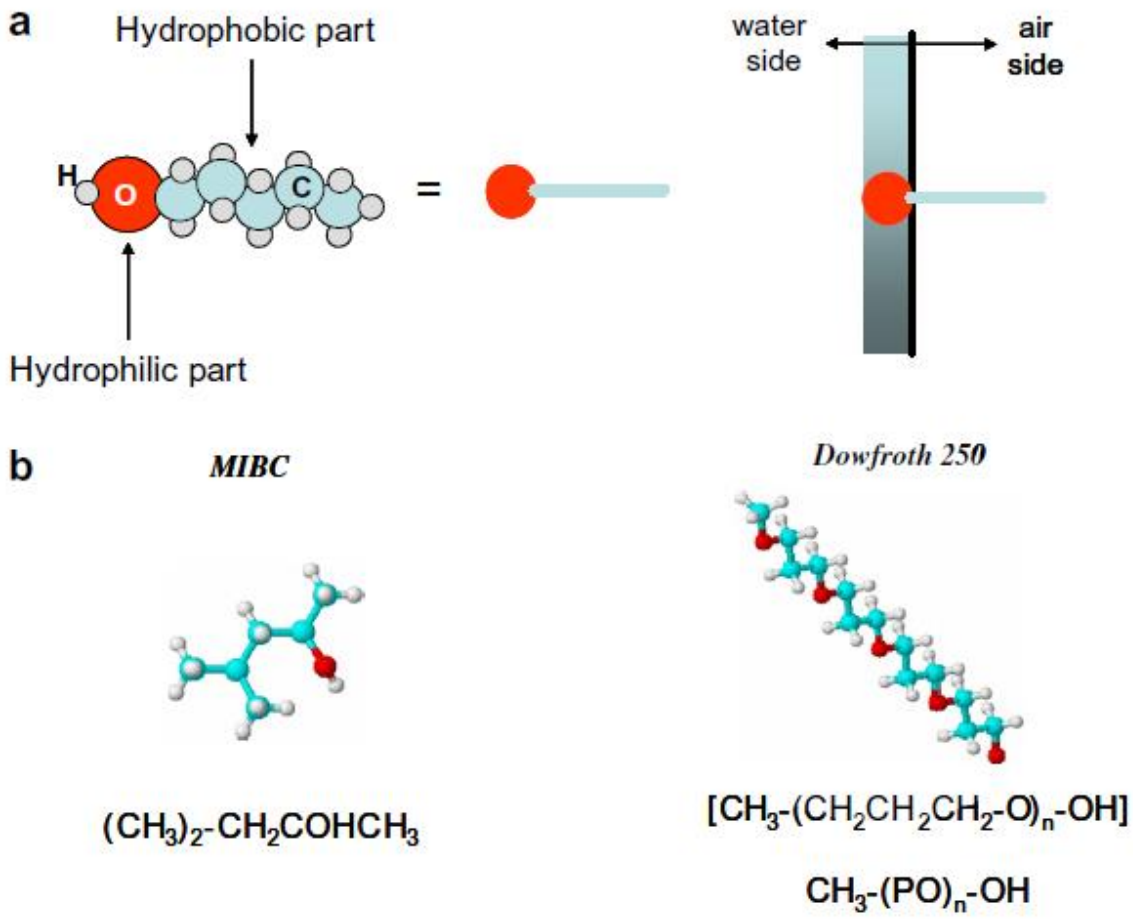

Figure 2.8: (a) General structure of frother (based on alcohol) showing mixed polarity (left) and orientation at the air–water interface (right). (b) Examples of two common frothers, an alcohol and a polyglycol (Finch et al., 2008).

The role of the frother in flotation is two-fold: to control bubble size, and to aid in froth generation (Finch *et al.*, 2008). Nesset *et al.* (2006) studied the impact of frothers on bubble size and found that both the Sauter mean (D_{32}) and the number mean (D_{10}) decreased to a constant value as shown in Figure 2.9. The collector dosage which gives the lowest bubble size is referred to as the critical coalescence concentration (CCC). Beyond the CCC, no further reduction in bubble size can be obtained. The decrease in bubble size can also be seen with the size distribution, initially bi-modal, but becoming progressively unimodal, finer and narrower. The frother plays an important role in reducing bubble size, thereby stabilising the froth. This tendency of frothers reducing bubble size has been a subject of numerous other studies (Castro *et al.*, 2013; Chow and Laskowski, 2002; Laskowski, 2003; Przemyslaw, 2013). The mechanism put forward is that the surfactant acts to reduce the tendency of the bubbles to coalesce (Laskowski, 2003). Another mechanism proposed by Finch *et al.* (2006) that seeks to compliment the coalescence mechanism argues that frothers also

control the breakup of the air stream at the point of injection. In the breakup mechanism, the frother molecules at the air-water interface will bulge because they are closer together, forcing a break-away of a bubble which will correspondingly be smaller. Fine bubbles are a requirement for a froth to be stable and as the frother concentration is increased, the froth stability will improve.

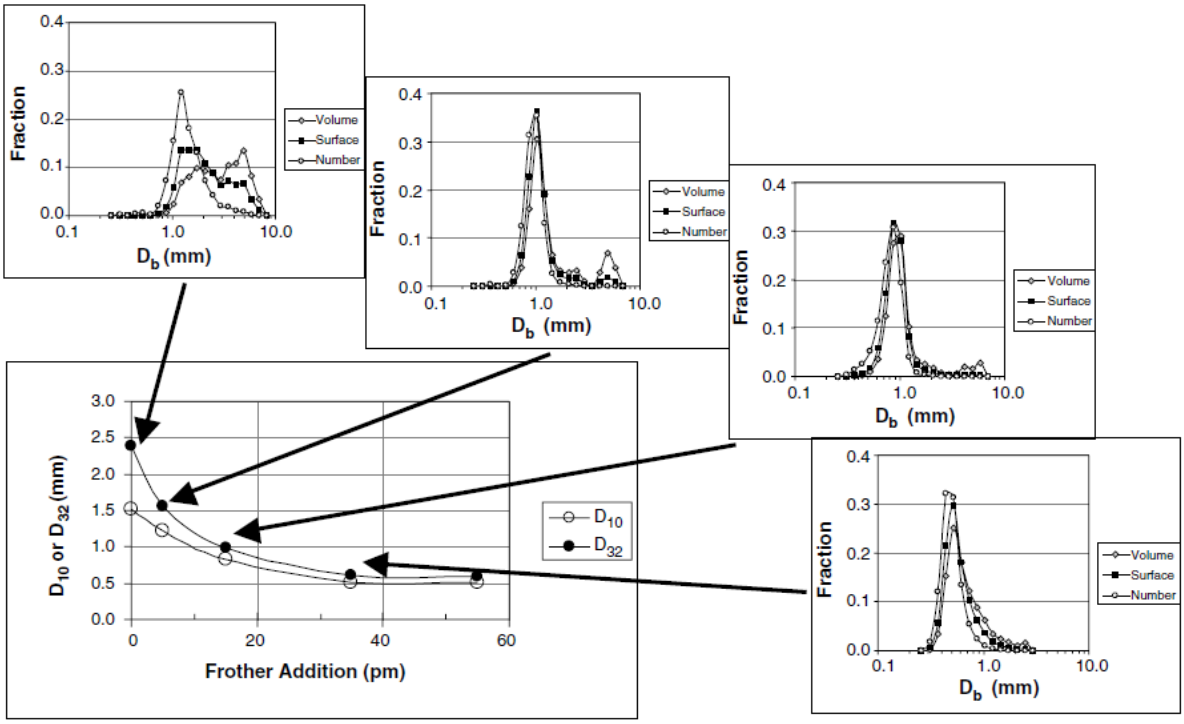

Figure 2.9: Impact of frother dosage on mean bubble size (D_{32} and D_{10}) and on frequency distributions (number, surface area, volume) at selected frother (Nesset et al., 2006).

2.8. The importance of particle size

Particle size effects on froth stability have been studied by a number of authors. These studies have investigated the effects of discrete particle size fractions as well as mixtures of size classes on froth stability and overall flotation recovery. Ip *et al.* (1999) and Johansson and Pugh (1992) conducted studies on quartz systems in sparsely mineralised froths consisting of about 2% by volume of solid particles. Ip *et al.* (1999), in studying aluminium metal foams, found an inverse linear relationship between particle size and froth stability (measured by the average foam life) for particles of mean size ranging from 40 to 140 µm. Johansson and Pugh (1992) demonstrated that the 26 – 44 µm size class had a higher stability (maximum froth height) than the 74 – 106 µm size class for the same frother concentration.

Studies have also been extended to real ore systems in which froth stability has been quantified by water recovery and a dynamic froth stability factor (Aktas *et al.,* 2008; Feng and Aldrich, 1999). Water recovery as well as dynamic froth stability were found to decrease with increasing particle size. Feng and Aldrich (1999) studied the comparative effects of particle size on the flotation of two complex sulphide ores viz. Merensky and UG2. They found that when batch flotation was carried out with fine size fractions (-38 µm), froth stability was higher, and froth volume was greater than for coarse size fractions (+75-106 µm), where the froth was unstable, and the froth volume was lower. In both types of ore, medium particle size fractions (+38-53, and +53-75 µm) resulted in better flotation performance in terms of concentrate grade and recovery. The optimal size range for the UG2 ore (represented by U) was however, finer than for the Merensky ore (represented by M). The UG2 ore with comparatively smaller bubbles than the Merensky ore exhibited higher flotation rates under corresponding experimental conditions. This is best illustrated by the results they obtained shown in Figure 2.10. These results may, of course, have been influenced by valuable mineral liberation, which would have influenced recovery and froth stability. In addition, these experiments were carried out in a batch flotation cell, which assumes that the particles that become attached to bubbles in the pulp all report to the concentrate, without any significant drop back from the froth (Connolly and Dobby, 2009) so that the froth zone recovery, R_f, is usually close to 100%. Also to be taken into consideration is the optimal pulp flotation size for collision and attachment, which is in the medium size ranges.

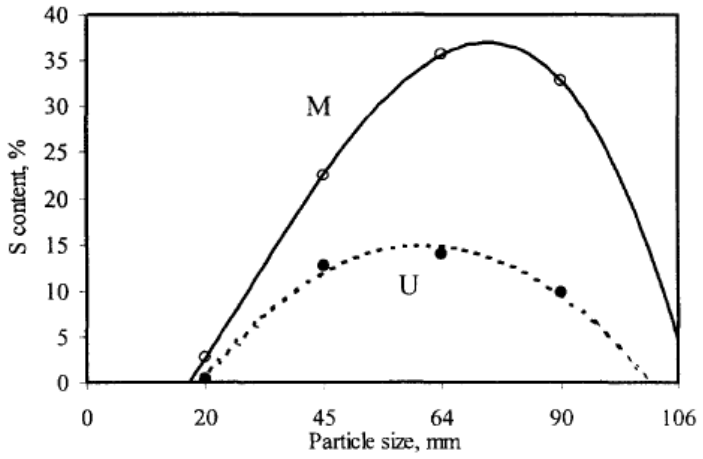

Figure 2.10: Variation in sulphur grade as a function of particle size fraction for Merensky (M) and UG2 (U) ores, Feng and Aldrich (1999).

According to Bulatovic (2007), the presence of particles in three phase froths greatly affects the stability of these froths. It is expected that there is an optimum particle size which acts as a froth stabiliser. Very large particles and very fine slimes show smaller effects than particles of intermediate size. A possible explanation for a decrease in froth stability at smaller particle sizes comes from the amount of particles that may report to the froth phase when the feed size is smaller. There is a decrease in probability of collision between particle and bubble with decreasing size, which is largely responsible for the difficulty in floating fine particles. This can, however, be improved by a reduction in bubble size. Another reason proposed for poor recovery of fine particles is that smaller particles, having lower momentum may not be able to break the liquid barrier surrounding a bubble. However, this limitation can be overcome by utilising flotation exploiting electrostatic interactions. It has been put forward by Trahar and Warren (1976) that the floatable size range of particles varies with minerals and reagent conditions, for instance, 6 – 70 µm for galena, 8 – 90 µm for sphalerite, 15 – 60 µm for chalcopyrite, and 20 – 150 µm for pyrite. In addition, it was found that fine particles of diameter < 10 µm generally exhibit low flotation rates and recovery. According to Sutherland and Wark (1955) the best flotation rate and recovery occurs in the 10 – 100 µm particle size range.

Szatkowski and Freyberger (1985) have shown that fine particles retard bubble coalescence and promote the production of a stable froth. Soto (1992) demonstrated that the froth phase is the barrier to coarse particle flotation. Operating without a froth phase and using a column with a short collection zone was shown to significantly improve coarse phosphate recovery.

Rahman *et al.* (2012) acknowledge that the stability of the froth depends significantly on the solids it contains. Particles greatly affect froth stability by reducing bubble coalescence, thus maintaining more bubble surface area throughout the froth zone. The reason for this is that coarse particles rupture the thin liquid films easily due to their higher mass, resulting in froth collapse and destabilisation. They carried out experiments on the flotation behaviour of different particle size fractions in a column flotation cell and monitored their response to changes in flotation variables. Mixtures of fine ($d_{80} = 72\ \mu m$) and coarse ($d_{80} = 299\ \mu m$) silica were used as feed. The results of their studies reveal that the overall fine particle recovery was much higher than for

coarser particles. Experiments were also carried out with 40%, 70%, 80% and 95% fine silica mixed with coarse silica at a constant superficial air velocity of 1 cm/s and a froth depth of 250 mm. Their results show that with an increasing percentage of finer silica in the feed, the recovery in both the collection and froth zones increased. It was found that froth recovery seems to be sensitive to the ratio of fine to coarse particles in the feed, i.e. with an increasing percentage of finer silica in the feed, an increasing trend in coarse particle recovery was noticed. For the case of the froth zone recovery, the reason given for this is that the fine particles, positioned at the air-liquid interface might have made a rigid and strong structure, therefore, providing a barrier to the coarse particles dropping out of the froth.

Similar experiments were performed by Vieira and Peres (2007) to investigate the influence of fine quartz (-74 to +38 μm) in the feed on the flotation recovery of medium (-150 to +74 μm) and coarse (-297 to +150 μm) quartz. They observed that in the absence of fine quartz, low recoveries of coarse and medium quartz were achieved. However, the effect of the presence of fine quartz was found to be more significant in the case of coarse quartz than for medium sized quartz. Hence, the presence of fine particles seems to enhance the collection of coarse particles in both collection and froth zones. This is because fine particles render the bubbles smaller and more stable.

Recently, experimental studies were carried out by Chipfunhu *et al.* (2012) on the flotation behaviour of methylated quartz particles of different sizes, but within the size range from 0.20 – 50 μm and varying contact angles in a mechanical flotation cell. The size range is noticeably finer than in other studies mentioned and, therefore, “fine” and “coarse” within this context are relative. Their results showed that the flotation rate and maximum recovery increased with an increase in both particle size and contact angle across all size fractions. Fine particles floated at lower rates than coarser particles having similar contact angles. They plotted maximum recovery as a function of particle size and contact angle. They determined that there exists a critical contact angle, θ_{crit}, which is particle size dependent, below which particles do not float. The critical contact angle is higher for the fine particles and lower for the coarser ones.

In a similar study, Muganda *et al.* (2011) characterised the flotation response of chalcopyrite as a function of particle size and advancing contact angle. They carried out flotation experiments under constant hydrodynamics and feed particle size

distribution. Their results are in agreement with the experimental findings of Chipfunhu *et al.* (2011). Likewise, maximum recovery increased with advancing contact angle for each size fraction as depicted in Figure 2.11. Particles within the same size fraction and within the same contact angle range were found to display similar flotation behaviour. Maximum recovery was obtained at intermediate particle sizes – there was lower recovery at very fine and coarser particle sizes. This study, however, was conducted using a batch flotation cell with low froth heights and, as such, was indicative of the pulp zone recovery. This would quantify the amount of particles that would report to the froth, but not what would occur once they made it to the froth zone.

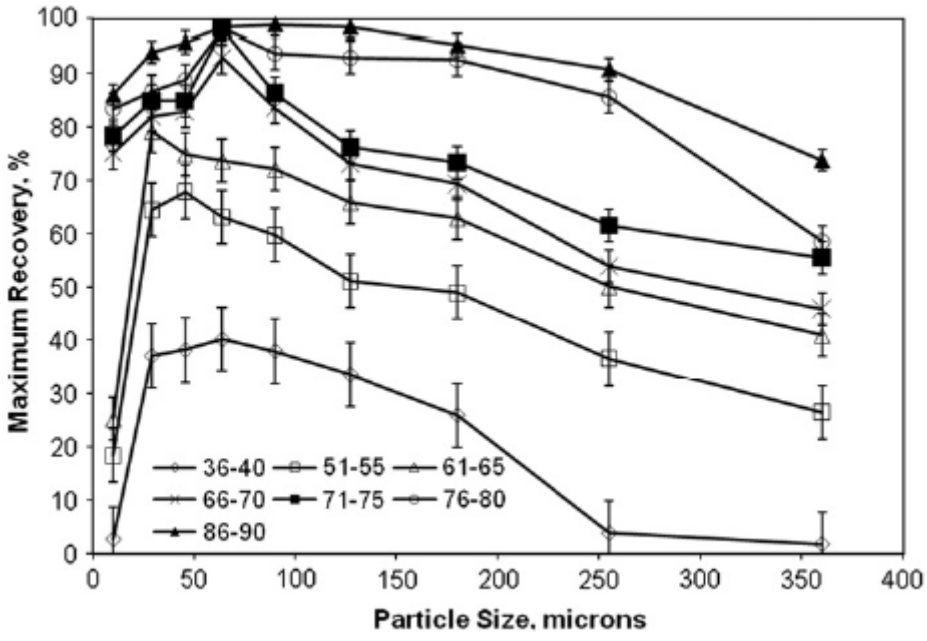

Figure 2.11: Maximum recovery as a function of particle size for different contact angle ranges, Muganda et al. (2011).

In conclusion, the studies appear to be in consensus that smaller particles stabilise froths. However, certain studies suggested that there was an optimum size range, where smaller and larger particles produced less stable froths. Not all studies agree with this, with some studies showing that froth simply became more stable, the smaller the particle size. Most of the froth studies did not define relationships of froth stability with particle size, but produced qualitative data. There is a need for a quantitative investigation of the effect of particle size on froth stability.

2.9. Particle hydrophobicity

One of the main particle parameters affecting flotation performance is the hydrophobicity of mineral particles (Johansson and Pugh, 1992; Prestidge and Ralston, 1996). Collectors selectively convert the surfaces of particular minerals from a hydrophilic condition to a hydrophobic condition, which creates a condition for attachment to air bubbles. Particle hydrophobicity can be estimated by means of contact angle measurements. The presence of hydrophobic particles can cause bubble coalescence in the froth.

The link between hydrophobicity and froth stability can be explained by considering the attachment of a particle to a bubble immersed in a liquid phase. When a bubble contacts a mineral particle surface in contact with a liquid, the total surface is minimised as it curves round the inhibited phase (Binks, 2002; Hunter *et al.*, 2008) in pursuit of a stable configuration. Figure 2.12 shows the idealised attachment of a particle to an air bubble in water (liquid phase). In reality, the solid particle would be approximately an order of magnitude smaller than the bubble. An angle of contact, denoted by θ is made between planes tangential to the surfaces of the solid and the liquid at the wetting boundary. This wetting boundary is a small zone where the three phases (i.e. solid, liquid, and gas) meet and is referred to as the three phase line of contact (TPLC). TPLC is the boundary between the solid particle phase, the receding liquid phase, and the advancing gas phase.

The free energy change is given by (Rosenholm, 2007):

$$dG_{SL} = \sum_i \gamma_i dA_i = \sigma_{SV} dA - \gamma_{LV}(dA\cos\theta_{SL}) - \sigma_{SL} dA \qquad \text{Equation 2.13}$$

Where: the subscript i represents a component, V = Vapour, L = Liquid, and S = Solid; γ = surface or interfacial tension of the liquid, σ = surface energy of the solid particle, and A = area. And if the $\Delta G_a < 0$ (i.e. negative), then the process of air-mineral particle contact is spontaneous.

Equation 2.13 relates the change in free energy at the interface of the three phases to the surface energy of the solid, the interfacial tension of the liquid, and the angle of contact that the solid makes with the liquid and vapour phases. This angle of contact is dependent on the particle hydrophobicity.

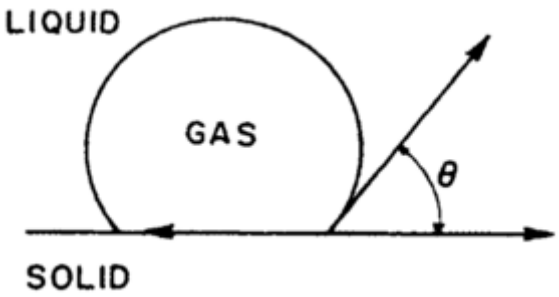

Figure 2.12: Schematic presentation of equilibrium contact between an air bubble and a solid immersed in water (Adapted from Rao, 2013).

At equilibrium:

$$dG_{SL}/dA \approx \Delta G_{SL}/A = 0 = \sigma_{SV} - \gamma_{LV}(\cos\theta_{SL}) - \sigma_{SL} \qquad \text{Equation 2.14}$$

Which can be written as:

$$\sigma_{SV} = \gamma_{LV}(\cos\theta_{SL}) + \sigma_{SL} \qquad \text{Equation 2.15}$$

Equation 2.15 is the Young's equation which is used to express the thermodynamic equilibrium of the three phase contact in terms of the interfacial tensions. This indicates that from the knowledge of the three surface energies involved, it is possible to predict the contact angle that a solid surface makes with the liquid.

The Dupré equation for the work of adhesion is also used to define the change in free surface energy:

$$dG_{SL}/dA \approx \Delta G_{SL}/A = \Delta G_A^S = -W_A = \sigma_{SV} - \gamma_{LV} - \sigma_{SL} \qquad \text{Equation 2.16}$$

Where ΔG_A^S = change in free energy for the work of adhesion at the surface.

Combining the Young and Dupré equations we obtain Equation 2.17:

$$\Delta G = \gamma_{LV}(\cos\theta_{SL} - 1) \qquad \text{Equation 2.17}$$

Equation 2.17 shows that the change in free energy during the bubble-particle contact is a function of the contact angle. The free energy change, ΔG is the energy required to remove a particle from an air/water interface, and it is at a maximum when $\theta = 90^o$. Thermodynamically, it means that an increase of the air/solid interface area and a decrease of the solid/water interface area occurs when an air bubble attaches to a solid particle (Leja, 1982). Cosθ must be less than 1 for a finite contact angle for

attachment of the bubble to the particle. For this to happen, γ_{SV} has to be low. The mineral particle is thus treated with collector in order to create a surface with low γ_{SV} by adsorption. Low energy surfaces are hydrophobic while surfaces with high energies are hydrophilic.

Particle hydrophobicity effects on froth stability can be explained by the bridging-dewetting mechanism of foam film rupture by solid particles (Aveyard *et al.,* 1994; Denkov and Marinova, 2006; Frye and Berg, 1989; Garrett, 1980). According to Aveyard *et al.* (1994), particles can cause film rupture by bridging the film. Film rupture is highly dependent on contact angle. If the contact angle, θ, is less than a critical degree of wetting (θ<90˚, in this case), a stable orientation is attained and the life of the film is prolonged (as illustrated in Figure 2.13a). However, in the case where the bridging particle has a contact angle greater than the critical degree of wetting (θ>90˚, in this case), the particle will easily dewet through both sides of the lamella, resulting in film rupture (Figure 2.13b).

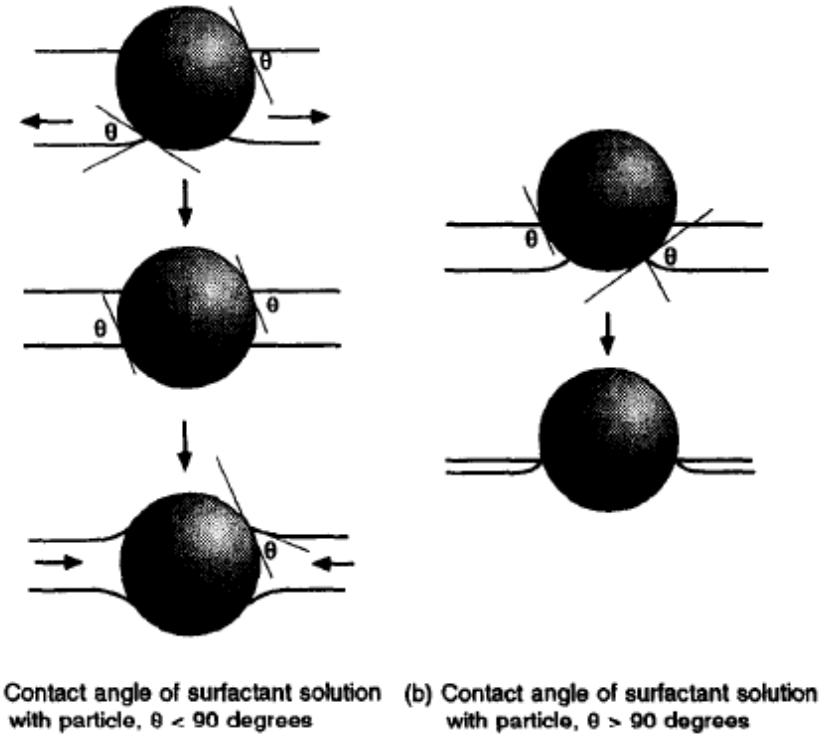

Figure 2.13: Bridging particle behaviour in a foam. (a) moderately hydrophobic (b) highly hydrophobic particle (Aveyard et al., 1994).

Ata *et al.* (2003) carried out experiments in a continuous flotation cell to study the collection of hydrophobic particles in the froth phase. Glass particles with well-defined

hydrophobicities prepared using controlled silanation were used. Three levels of hydrophobicity were investigated i.e. weakly, intermediate, and strongly hydrophobic corresponding to contact angles of 50˚, 66˚ and 82˚ respectively. The results obtained indicated that the strongly hydrophobic particles (θ = 82°) were more capable of destabilising the froth (by rupturing bubble films) than the moderately hydrophobic particles, but still gave the highest flotation recovery. The question which arises then is why the highest recovery is obtained with the strongly hydrophobic particles. This was explained based on the high reattachment rate of particles to bubbles in the froth zone due to their high level of hydrophobicity.

Schwarz and Grano (2005) carried out similar studies using methylated quartz particles which were 90% passing 38 µm in size and with different average advancing water contact angles (35˚, 53˚, 63˚ and 69±2˚) measured by the Washburn technique. Polyproplene glycol was used as the frother. They found that froth recovery increased with increasing contact angle up to a maximum near 63˚ above which it started decreasing. This decrease in froth recovery at high contact angles was linked to increased burst rate of froth bubbles which was manifested in an increase in froth bubble size.

Experiments were carried out by Pugh (2005) to study the structure and stability of froths. Surface modified quartz particles of different sizes were used. The relationship between flotation yield and the hydrophobicity of the quartz particles for two particle size fractions (26 – 44 µm and 74 – 106 µm) were investigated. The flotation yield was found to increase with contact angle for both particle sizes, but the smaller size particles showed a greater flotation yield throughout the hydrophobic range of contact angles between 20˚ – 80˚.

Studies carried out by Ulusoy *et al.* (2004) pointed to an interesting connection between particle shape and hydrophobicity. The shapes of calcite and barite particles ground by ball, rod and autogenous mills were examined using scanning electron microscopy (SEM). The results were correlated with the critical surface tension of wetting as determined by contact angle and micro-flotation methods. The results obtained revealed that particles with higher flatness and elongation ratio had higher apparent hydrophobicities without being affected by the mill type. This resulted in greater flotation performance. However, particles with higher roundness and relative

width had lower apparent hydrophobicities. These minor differences in hydrophobicity in terms of shape properties would, in all likelihood be overridden by the addition of collector as shown by Vizcarra *et al.* (2011).

In a similar study, Pugh (2005) used dynamic frothing tests to characterise froths containing 2% quartz particles whose surfaces were modified by reaction with trimethylchlorosilane in cyclohexane under a dry environment following standard procedures. A modified Bikerman test consisting of a glass column where the maximum equilibrium volume of the froth was determined at a flow rate of 60 l/h was used. Four commercial frothers i.e. polypropylene glycol monomethyl ether with n = 3 and n = 4, α-terpeneol and methyl isobutyl carbinol were used. The results obtained expressed the dynamic froth characteristics in terms of maximum froth height as a function of the hydrophobicity of the particles (expressed in terms of the flotation yield). It was found that with small particle sizes of 26 – 44 µm, there appeared to be a distinct maximum corresponding to a flotation yield of about 70%, which corresponds to a critical degree of hydrophobicity of 60˚. These results were reproducible for both high and low concentrations of the different frothers used. With larger particles (size fractions of 74 – 106 µm), these effects were not observed. The large particles seemed not to influence the stability of the system. Again similar trends were observed for both high and low frother concentrations for the large size fractions. Pugh (2005) extended their studies using static stability tests. The sets of data again showed a high static froth stability (slow rate of collapse) corresponding to a critical degree of hydrophobicity at both frother concentrations with pronounced effects occurring with the polypropylene glycol monomethyl ether at the lower concentration of 20 mg/l. Pugh (2005) was therefore able to show that dynamic and static stabilities could be increased in two ways i.e. reduction in mineral particle size and an increase in particle concentration and this is at a particular contact angle.

In an earlier study carried out by Johansson and Pugh (1992), the influence of quartz particles (of well-defined size fractions with different degrees of hydrophobicity) on the stability of froths was studied by measuring dynamic and static froth stabilities using a froth column. They reported that larger particles (74 – 106 µm) had a less pronounced effect on froth stability, smaller quartz particles (26 – 44 µm) showed maximum froth stability at an intermediate degree of hydrophobicity ($\theta \approx 50–65^{\circ}$), while weakly

hydrophobic particles did not have an influence on froth stability and strongly hydrophobic particles (θ > 90°) destabilised froths. It was also found that the higher the concentration and smaller the particle size, the greater the stability of the foam. According to Morris *et al.* (2008), contact angles of particles found in flotation froths usually lie within the range of 0 – 90° with low hydrophobicity being in the range 0 – 30°, intermediate 30 – 70° and high over 70°.

Contact angle determination

To determine the contact angles of sulphide minerals which are representative of particles in a pulp, Prestidge and Ralston (1995) note that powder technologies are available which reduce problems associated with single-surface studies. For a bed of powders, the contact angle measurement techniques are based on the flow of liquid through a packed bed of particles and they can either be dynamic or static in nature. Dynamic methods (Washburn, 1921) employ the measurement of the liquid penetration rate into a bed of particles while static methods (Dunstan and White, 1986; Diggins *et al.*, 1990) determine powder contact angles from equilibrium measurements of the capillary pressure increment required to prevent the movement of liquid through a packed bed of mineral particles.

A description of the Washburn technique for contact angle measurement has been reported by Siebold *et al.* (2000). Considering the Poiseuille's law, liquid capillary rise rate in a porous media is given by:

$$\frac{dh}{dt} = \frac{R_D^2}{8\eta}\frac{\Delta P}{h} \qquad \textit{Equation 2.18}$$

Where *h* = height reached by the liquid at time t (since the height reached by the liquid is linearly related to the mass increase, mass is commonly substituted for height in this equation), R_D= mean hydrodynamic radius of pores, η = viscosity of the liquid, and ΔP = pressure difference which is given by:

$$\Delta P = \frac{2\gamma cos\theta}{R_S} - \rho g h \qquad \textit{Equation 2.19}$$

Where γ = liquid surface tension, ρ = liquid density, θ = advancing contact angle of the liquid on the solid, R_S = mean static radius of pores, and g = acceleration due to gravity.

If it is assumed that the hydrostatic pressure is negligible in the early stages of the process, Equation 2.18 can be integrated to give the well-known Washburn's expression:

$$h^2 = \frac{r\gamma cos\theta}{2\eta} t \qquad \textit{Equation 2.20}$$

Where $r = R_D^2/R_S$

From Equation 2.20, h^2 varies linearly with t. In order to determine r, a perfectly wetting liquid (θ = 0, and cos θ = 1) is used. Once r is known and using glass tubes of constant packing characteristics, the contact angle, θ, of a non-wetting liquid ($0<\theta<90^{\circ}$) can be determined.

2.10. Stabilisation mechanisms of froths by mineral particles

Various mechanisms have been proposed to explain froth stabilisation by hydrophobic particles.

Kaptay (2012) offered an explanation for the role of particle hydrophobicity in influencing froth stability. He states that the subject of froth stability is a complex one which needs to be analysed taking into account two phenomena i.e. the stability of particles in the liquid/air interface and the stability of the liquid film.

Considering the stability of the particle at the interface, a useful parameter that seeks to explain how well particles of different hydrophobicities stabilise froths is the particle detachment energy (ΔG_{remove}). This is the energy required to remove a particle from the liquid/air interface to the bulk liquid phase and it is related to the free energies involved in the process. This particle detachment energy can be represented by Equation 2.20 (Kaptay, 2006).

$$\Delta G_{remove} = \pi R^2 \sigma (1 \pm \cos\theta)^2 \qquad \text{Equation 2.21}$$

Where R = the radius of the spherical solid particle; σ = the interfacial energy between the liquid and gas; θ = the contact angle of the liquid phase on a solid particle; sign '+' refers to particle removal into the gas phase, while sign '-' refers to the removal of the particle into the liquid phase. According to Equation 2.21, ΔG_{remove} should be highest at a contact angle of 90° and large particle sizes.

The detachment energy theory can only partially explain foam stability by particles. It considers the stability offered by particles at the interface. However, it is also important that the stability provided by particles residing in the interfilm between two interfaces be considered. Practically, maximum foam stabilities have been observed at contact angles below 90°. A mechanism proposed to explain this phenomenon is the effect of particles on the capillary pressure between two bubbles. The thin liquid films between bubbles are stabilised by the maximum capillary pressure, P_c^{max}. This is the pressing force required to bring two bubbles to coalescence. This observation was made by Denkov *et al.* (1992) who considered theoretical liquid films formed by a particle monolayer pressed between two emulsion interfaces. Utilising the works of Denkov *et al.* (1992), Kaptay (2006) derived an expression for P_c^{max} as:

$$P_c^{max} = p\frac{2\sigma}{R}\cos\theta \qquad \text{Equation 2.22}$$

Where R = particle radius, σ = interfacial tension, θ = contact angle, and p = theoretical packing parameter, which is a function of particle concentration and packing on the capillary pressure.

Equation 2.22 dictates that a froth system will only be stable if the maximum capillary pressure is positive and is much larger than the combined sum of all forces (centrifugal, electric or magnetic fields, etc.) that seek to collapse the thin liquid films between the bubbles. This equation also predicts that froth stability is possible if θ < 90° and the maximum stability will be obtained for a contact angle of 0° and at small particle sizes. This maximum capillary pressure theory is in contrast to the predictions made by the particle detachment theory. However, a critical look at this shows that this is expected since the liquid film will drain less when a particle resides more in the interfilm, reaching a minimum at a contact angle of 0°; the point at which the particle resides within the film. This does not take gravitational forces into consideration. The interactive effect of the detachment energy and capillary pressure was modelled by Kaptay (2006) for a single layer of particles between two bubbles. For a foam system containing particles, the highest stability was obtained at a contact angle of about 70°.

Johannson and Pugh (1992) studied the influence of particle hydrophobicity on froth stability and proposed a schematic to represent this phenomena (Figure 2.14). When small mineral particles have a low hydrophobicity (θ < 40°) they will remain dispersed

within the lamella phase, and so their influence on froth stability will be low (a). However, particles with intermediate hydrophobicity will penetrate the interface and remain in the film during thinning (b). For a very large contact angle, a drop in the capillary pressure will cause the particle to dewet the liquid causing rupture (c). The experiments conducted by Johannson and Pugh (1992) utilised sparsely mineralised froths (2% wt quartz).

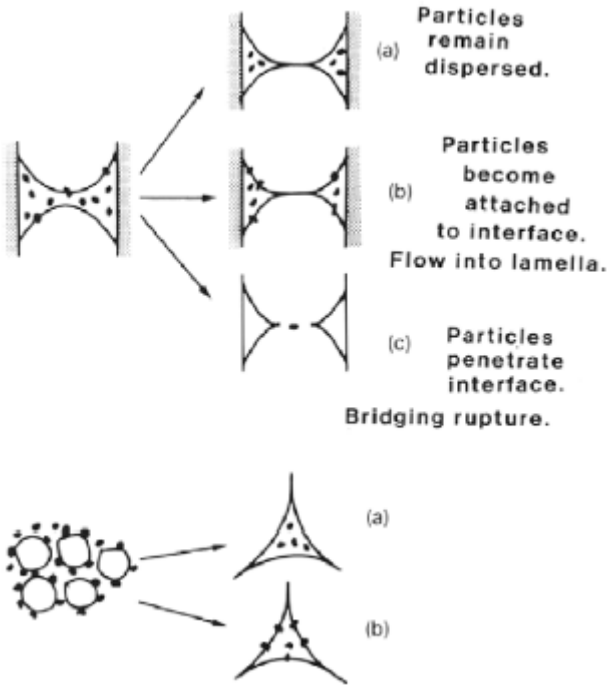

Figure 2.14: Suggested stabilization and destabilization mechanisms of the mineralised froths (a) Particles with fairly low degree of hydrophobicity corresponding to a contact angle of $< 40°$ on quartz plate, (b) intermediate degree of hydrophobicity $\theta \approx 65°$, and (c) fairly high degree of hydrophobicity $\theta > 80°$ (Johannson and Pugh, 1992).

Thus far this review has focussed on the stability of froths and foams aided by particle-interface interactions. Another central consideration in explaining stabilities of froths is particle-particle interaction (Hunter *et al.,* 2008). These interactions between particles at short separation distances are of utmost importance and may determine to a large extent the overall stability or instability of the froth system. It relies on the principle of particle network structures generating a steric barrier to coalescence brought about by film drainage and thinning between bubbles. As film thinning occurs and reaches its final stages, dark spots (or holes) are formed. These will expand until the film becomes unstable and ruptures. However, for a stabilised particle-bubble system, the bubble surface is well covered and the possibility of thinning and rupture is minimised. As such, an energy barrier must be overcome to form a critically sized dark spot (or hole)

in the film wall. The degree of coalescence can then be related to the amount of energy required for the formation of holes. For a strongly adsorbed particle system, it is difficult to remove the particle into the open medium during thinning as it preferentially moves laterally along the contact line. This brings into play the forces related to particle-particle interactions such as electric double layer repulsion and dipole-dipole repulsion as well as van der Waals attractions and capillary forces.

Theories on the contributions made by the particle packing mechanism in Plateau borders to froth stabilization have also been proposed. Horozov (2008) proposed that liquid films can be stabilised by either a bridging monolayer of particles, a bilayer of hexagonally packed particles, or a network of particle aggregates inside the film as shown in Figure 2.15. This packing mechanism possibly acts to prevent liquid outflow from the thin films, thus stabilising the froth.

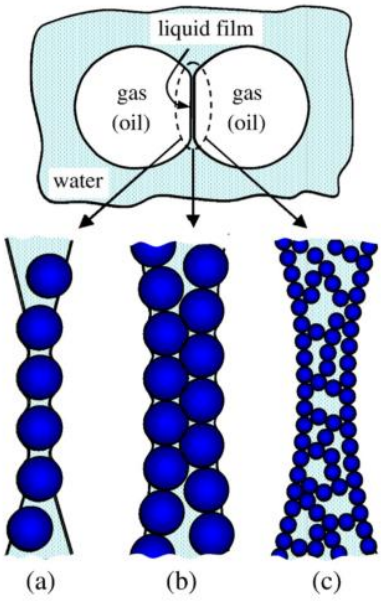

Figure 2.15: Mechanisms of liquid film stabilisation: (a) a monolayer of bridging particles; (b) a bilayer of close-packed particles; (c) a network of particle aggregates (gel) inside the film (Horozov, 2008).

It has also been reported that a strong correlation between the viscosity of the liquid and the stability of the foam/froth exists (Leja, 1982). If the liquid from which the bubbles form is viscous, the drainage of liquid from between the bubbles is slow. This will inevitably increase the froth stability. Thus, fine particles that increase viscosity will slow liquid drainage and increase froth stability.

2.11. Measuring froth stability

Froth structure and froth stability play significant roles in determining the mineral grade and recovery achievable from a flotation operation. However, quantifying froth stability consistently, both at laboratory and industrial scales remains a significant challenge (Farrokhpay, 2011; Barbian *et al.,* 2005).

A number of techniques have been developed and reported on the measurement of froth stability in continuous flotation column operations. These include: water recovery, air recovery (Barbian et. al., 2003; Hadler and Cilliers, 2009; Ventura-Medina and Cilliers, 2002), and image analysis (de Jager *et al.,* 2004; Morar *et al.,* 2006). Non-continuous froth stability measurements using the dynamic froth stability column have also been significantly used in flotation column research (Barbian *et al.,* 2005; Bikerman, 1953; Iglesias *et al.,* 1995).

2.11.1. Froth stability column

Aktas *et al.* (2008), Pugh (2005) and Barbian *et al.* (2003) have suggested two methods that can be used to measure the stability of the froth, viz. dynamic methods and static methods. In dynamic methods, observations are made during the formation and build-up of the foam. Static methods involve observation of the decay of the foam. In laboratory-scale tests, both of these methods assess froth stability individually and do not address froth stability of a continuous process with simultaneous measurements of recovery and grade.

The froth stability column, originally proposed by Bikerman (1973) is based on the dynamic stability test for non-overflowing froth columns. Dynamic froth stability involves the measurement of the dynamic stability factor, denoted as $\sum$, defined as the ratio of the volume of froth to air flow rate in the system.

Triffet and Cilliers (2006) used the dynamic test method to measure two froth stability parameters namely; the maximum height attained by the froth in the column and the rate or velocity of movement of froth up the column. They used a Perspex column with the following dimensions; 30 x 30 x 165 cm. They plotted froth height as a function of time for their test work and generated a curve as shown in Figure 2.16. The graph displays raw data as well as a fitted model for the data.

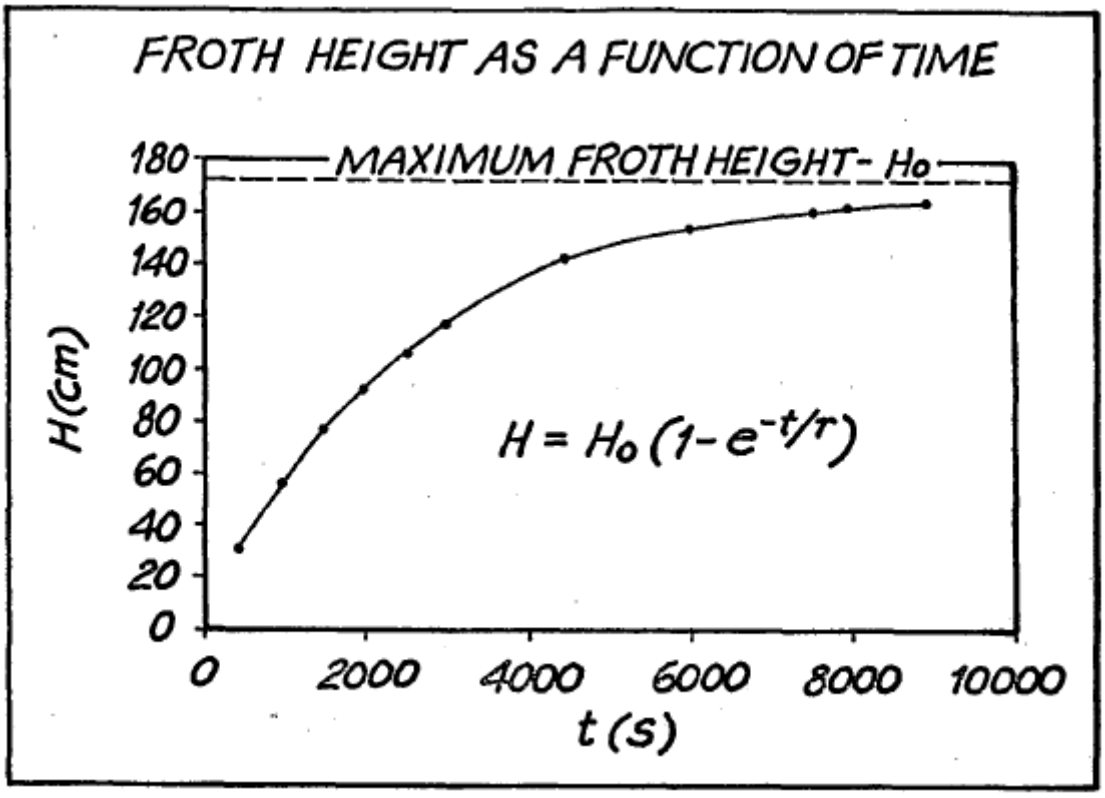

Figure 2.16: A plot of froth height, H, as a function of time, t (adapted from Triffet and Cilliers, 2006).

The fitted model for the data obtained was of the form (Barbian *et al.,* 2003):

$$\mathrm{H} = \mathrm{H}_{\circ}\left(1 - \mathrm{e}^{-\mathrm{t}/\tau}\right) \qquad \text{Equation 2.23}$$

Where τ = fitted stability parameter and t = time, H_o = maximum height attained by the froth

A measure of the dynamic froth stability factor was performed by Barbian *et al.* (2003) in which air flow rate and frother concentrations were the key operating variables. They measured the rate of froth growth and the maximum equilibrium height reached for different air flow rates and frother concentrations. The maximum equilibrium froth height was found to increase with increasing air flow rate and frother concentration, however, at higher aeration rates and frother concentrations, the maximum equilibrium height decreased. Under these conditions, the froth collapsed as it was no longer stable. The dynamic stability factor was thus found to be affected by both air flow rate and frother concentration. However, their test work could not ascertain the relationship between air flow rate and flotation performance. If this relationship were known, then it would be possible to manipulate the froth height to produce an optimal froth stability and flotation performance. Barbian *et al.,* (2005) extended this study and determined

that as the air flow rate increased into the cell, the fraction of air overflowing the weir, α, the dynamic froth stability, ∑, and the froth stability factor, β, all decreased indicating a loss of stability in the froth.

Iglesias *et al.* (1995) investigated the behaviour of short-life foams in which the decay occurs by drainage and/or film breakage, and whose lifetime is too short for inter-bubble diffusion to become significant. Their foam decay experiments were carried out in a graduated borosilicate glass column measuring 5 cm in diameter and 150 cm in height. A sample of solution containing surfactant, 50 ml in volume was introduced into the column and pre-humidified nitrogen gas was bubbled through the solution from the bottom through a hypodermic needle at a constant aeration rate of 140 ml/min. After dynamic equilibrium was achieved (when there is no tendency for the foam height to change), the gas flow was cut off, and the variation in foam height over time (decay process) monitored. Figure 2.17 shows the foam decay rate variation for the different surfactants used. A linear variation of foam height, H with time, t, can be mathematically expressed as:

$$H = a\ log(t) + b \qquad \text{Equation 2.24}$$

Where a and b are constants.

A differential form of Equation 2.24 which gives the rate of foam height change is given by:

$$\frac{dH}{dt} = -\frac{k}{t} \qquad \text{Equation 2.25}$$

Equation 2.25 shows that the rate of change of the foam height is inversely proportional to its age.

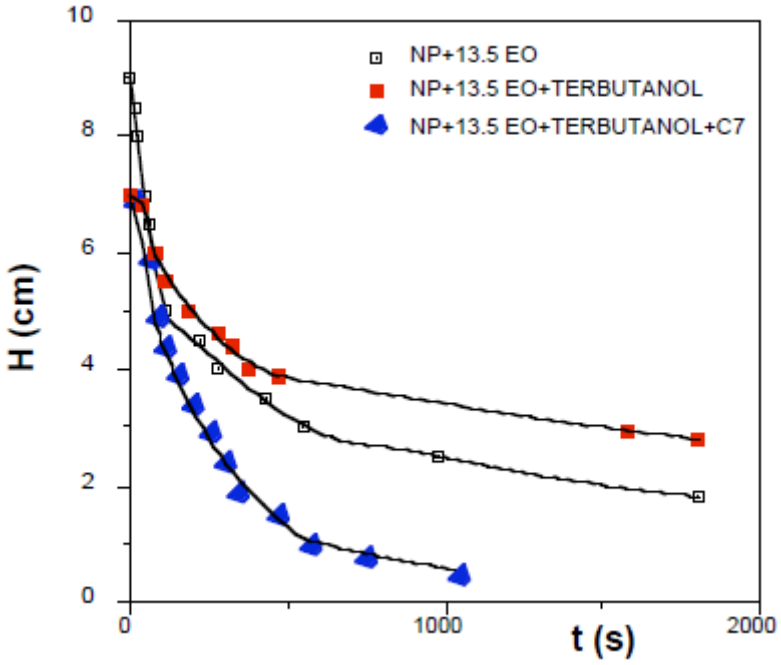

Figure 2.17: Typical decay pattern of foam height as a function of height for surfactant solutions investigated (Iglesias et al., 1995).

Iglesias *et al.* (1995) suggested a characteristic time, $t_{1/2}$, can be used to interpret the foam decay process data. $t_{1/2}$, known as foam half-life, is the time at which the column height is half the original height, H_o. An expression relating $t_{1/2}$ and H_o is given by:

$$H/H_o = 1/2 - b\ log\left(t/t_{1/2}\right) \qquad \text{Equation 2.26}$$

Where b is a dimensionless constant with typical values in the range 0.3 – 0.4. A plot of H/H_o versus $log\left(t/t_{1/2}\right)$ is a straight line graph as depicted in Figure 2.18. Their proposed experimental method and data processing technique has generated two main characteristic parameters of the froth, viz. the foam half-life $t_{1/2}$, and the original height, H_o. Whereas $t_{1/2}$ gives estimates of the foam stability, H_o accounts for both the stability and foamability.

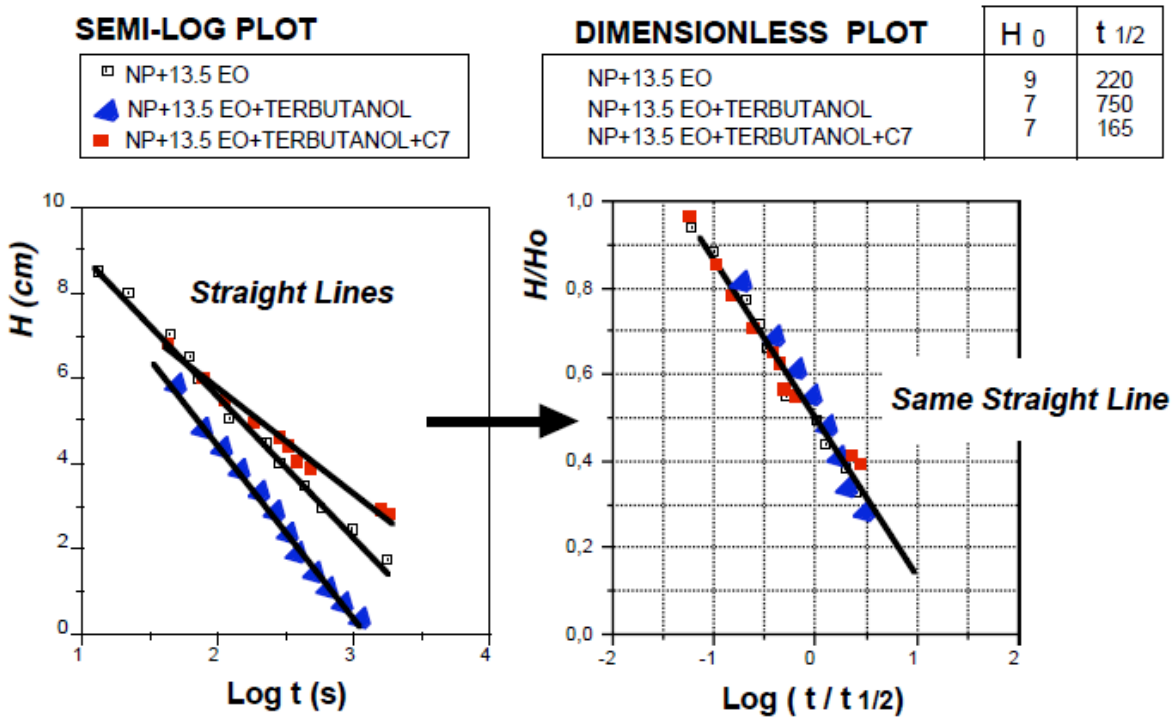

Figure 2.18: Processing the results of the foam decay rate (Iglesias et al., 1995).

2.11.2. Water recovery as a froth stability measure

Water recovery is defined as the fraction of the water entering the flotation cell that is recovered in the concentrate. In a flotation cell, water recovery is the result of a two-step transfer process, i.e. transfer of the water in the pulp phase to the froth phase and transfer of the water in the froth phase to the concentrate launder. These two steps are not independent of each other. Zheng *et al.* (2006) elaborates that only a certain fraction of the water entering the froth phase may be recovered into the concentrate; the rest returns to the pulp phase via the mechanism of drainage. The amount of water entering the froth phase may to a large degree determine the characteristics of the froth in terms of froth stability and mobility, and hence influences the recovery of the water and solid particles in the froth phase to the concentrate launder.

It has been widely reported by many authors that recovery of water has a significant effect on gangue recovery and concentrate grade and recovery. Hydrophilic particle recovery in flotation occurs mainly by entrainment which is related to froth stability. Tao *et al.* (2000) suggest that establishing a relationship between particle entrainment and froth stability is important for a better understanding of the mechanisms of

collection of different particles. They established a linear relationship between water recovery and recovery of hydrophilic solids:

$$R_a = F_a + e_a R_w \qquad \text{Equation 2.27}$$

Where: R_a = hydrophilic particle recovery, R_w = water recovery, F_a = recovery of gangue accompanying the solids, e_a = entrainment factor

They further obtained a linear relationship between water recovery and hydrophobic particle recovery:

$$log(1 - R_c) = log a + b\ log(1 - R_w) \qquad \text{Equation 2.28}$$

Where: R_c = hydrophobic particle recovery, a and b are constants. When R_w = 0, $R_c = 1 - a$, and this can be considered as the contribution from true flotation. Their computations reveal that for values of R_w between 0 and 0.18, the best fitting values for a and b are 0.218 and 4.683. However, Tao *et al.* (2000) note that the relative contribution of true flotation and entrainment to the overall recovery of hydrophobic particles is strongly dependent on the size of particles.

Water recovery is an essential component for modelling of a flotation column. It has a significant effect on both entrainment and recovery of valuable particles. It determines the circulating flow and residence time in the individual process units in the plant (Zheng *et al*., 2006; Neethling and Cilliers, 2002). It is important that water recovery from the pulp-froth interface to the product launder is minimised (by the froth), allowing water to drain out of the froth as this drainage will minimise unselective recovery of unattached particles present by the entrainment mechanism (Schwarz and Grano, 2005).

Zheng *et al.* (2006) argue that as much as both empirical and fundamental models of water recovery in flotation processes tend to fit the data reasonably well, empirical models which relate the water recovery to the solids recovery or describe the water recovery as a function of the mean froth residence time are generally unable to distinguish the effect of different cell operating conditions such as froth height and air rate – they can thus be used only within a relatively narrow range of cell operating conditions.

2.11.3. Air recovery as a froth stability measure

Air recovery is defined as the fraction of air that overflows to the concentrate as unburst bubbles. The link between air recovery and froth stability was made by Barbian *et al*. (2003). They showed that froth stability can be quantified by measuring air recovery in flotation cells.

The concept of air recovery was first introduced by Woodburn *et al.* (1994) who proposed that the froth structure, specifically the flow of bubble surface, was related to the flow of solids and water to the concentrate in a free flowing froth. They defined the air recovery, $\propto$, as:

$$\propto = \frac{Q_{out}}{Q_{in}} = \frac{\zeta \times v_f \times h_w \times w}{Q_{in}} \qquad \text{Equation 2.29}$$

Where Q_{out} = volume of air overflowing the weir, Q_{in} = volume of air added to the cell, ζ = fraction of air in the overflowing froth and is generally considered as unity, v_f = velocity of the overflowing froth, h_w = is the height of froth overflowing at the weir, w = weir lip length. v_f can be determined using image analysis of the froth.

Ventura-Medina and Cilliers (2002) used image analysis to estimate the amount of air that overflows the weir as unburst bubbles at industrial scale. They determined that for a single cell, the air recovery increased with increasing aeration rate and frother concentration. However, at the highest aeration rate and frother concentration, air recovery decreased, indicating a decrease in froth stability. There exists, therefore, a peak air recovery (PAR) with cell aeration. Smith *et al.* (2010) and Hadler and Cilliers (2009) proposed that the compliment to air recovery is the fraction of bubbles bursting at the froth surface (1–$\propto$). A high air recovery, therefore, indicates a low loss of air through bursting bubbles, and consequently a more stable froth. Hadler *et al.* (2010) agree with the above findings and stated that air recovery is a robust, non-intrusive measure of froth stability that passes through a peak as cell air rate is increased. They showed that when operating a cell at the air rate that yields the “Peak Air Recovery” an improvement in flotation performance, particularly mineral recovery, can be obtained. Their work on two concentrators, one at Modikwa and the second at Western Limb Tailings Retreatment Plant (WLTRP) involved carrying out preliminary air recovery tests during which the air rates to the first two cells in the bank were varied

and the air recovery measured. Surveys were also carried out at the "As Found air rates" and at the optimised Peak Air Recovery (PAR) air rates. Their findings are shown in Figure 2.7 below:

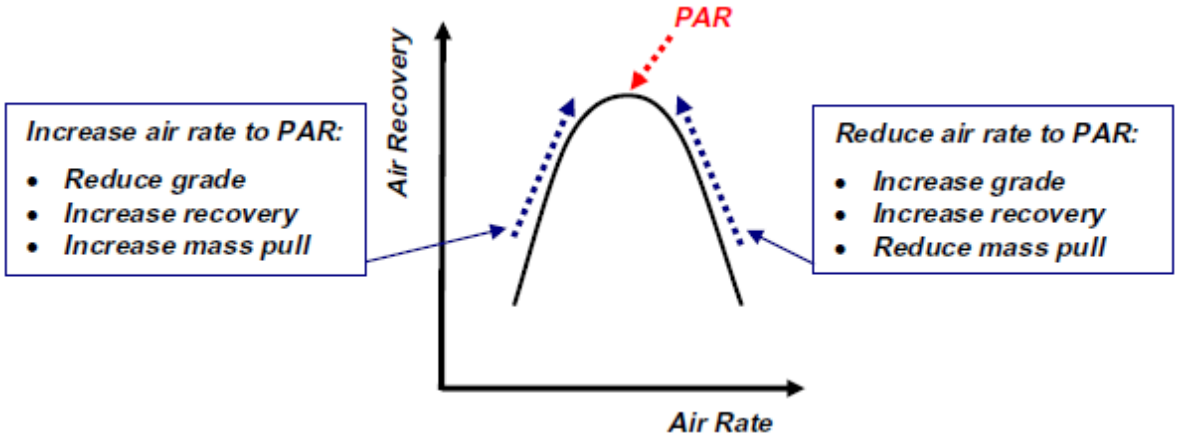

Figure 2.19: Schematic showing the general effect of air recovery optimisation on flotation performance (Hadler et al., 2010).

Their findings indicate that by increasing the air rate from "As Found" to PAR, (for operation at Modikwa), an increased mass pull and recovery were obtained for a small drop in concentrate grade. Conversely, dropping the air rate to obtain PAR conditions (for operation at WLTRP), yielded both a higher grade and recovery with a decrease in mass pull.

Zheng *et al.* (2006) noted that an accurate measurement of air recovery is difficult. They proposed that the fraction of unburst bubbles on the surface of the flotation cell can be considered to be linearly proportional to the froth height:

$$\propto = 1 - \frac{H_f}{H_f(max)} \qquad \text{Equation 2.30}$$

Where H_f(max) is the maximum froth height that can be obtained under the given operating conditions and at this maximum froth height all the bubbles burst, H_f is the froth height.

Estrada-Ruiz and Perez-Galibay (2009) proposed a semi-phenomenological model to estimate air recovery:

$$\propto = \frac{Q_{sl\_overflow} \times d_b^3}{Q_g \left\{ \left[d_b + a \left(Q_{sl\_overflow} - Q_{w\_overflow} \right) / A_c \right]^3 \right\} - d_b^3} \qquad \text{Equation 2.31}$$

Where: d_b = bubble diameter, $Q_{w\_overflow}$ = water flow rate in the overflow, $Q_{sl\_overflow}$ = slurry flow rate in the overflow, A_c = cross sectional area of the column, and Q_g = Air flow rate. It should be noted, however, that the independent variables in Equation 2.31 are difficult to measure on an industrial scale.

2.11.4. Characterisation of froth stability behaviour by image analysis

The use of machine vision for froth characterization is finding increasing application in mineral processing industries. Measurements describing properties of the froth such as: bubble size distribution, bubble shape distribution, colour, number, density, speed and stability are provided by these instruments. However, much of the challenge encountered in the use of these machine vision based instruments has been in relating the information extracted from the images to flotation performance. Moolman *et al.* (1995) explained that the characterization of flotation froth stability is a good example of the utilization of visual data as a supplement to conventional plant data. In their experiments, images from pyrite batch flotation tests conducted after a factorial design as well as images from a copper flotation plant were used to understand the relationship between froth characteristics and flotation performance. Their findings show that most of the froth characteristics (e.g. stability, mobility, viscosity, colour, and average bubble size) can be explained in terms of the concentration of solids in the froth and factors that affect the solids concentration. Froth stability measurement using image analysis is characterized based on the following arguments: if the froth is excessively stable, i.e. the rate of bubble collapse is slow, fewer local changes in light intensity between successive frames (light to dark or dark to light) should occur than in an unstable froth. In an unstable froth, the high rate of bubble collapse and the formation of new bubbles imply a quick change in the highlights on the tops of bubbles (caused by the spotlight) and the bubble boundaries (light areas).

Ventura-Medina *et al.* (2004) carried out experiments on solids loading on froth surface bubbles as a function of the superficial gas velocity for different froth depths at standard and high frother concentration, respectively in the rougher cell at Pyhasalmi copper concentrator in Northern Finland. Solids-loading in bubble lamellae was directly measured by sampling using microscope glass slides and image processing. They found that the average solids loading decreased as air flow rate (superficial gas

velocity) increased. Also, the average solids loading in bubbles increased with increasing froth depth at constant air flow rate.

Barbian *et al.* (2007) proposed that the bubble solids loading, Γ, can be calculated using the expression:

$$\Gamma = \frac{m}{A} \qquad \text{Equation 2.32}$$

Where m is the amount of solids collected on a slide and A is the surface area of the bubble-print. They state that under steady state conditions, it is also possible to collect enough material attached in the bubble lamellae by multiple sampling to determine the average grade.

Morar *et al.* (2012a, b) reported that froth stability is reflected by three main attributes which are visible on the froth surface, these are: froth surface bubble burst rate, froth surface bubble size and solids loading. These authors developed a machine vision technique to measure the burst rate of bubbles on the froth surface as a practical measure of froth stability for an industrial environment. The developed algorithm outputs for the number, size, and volume information of bubbles bursting per pair of frames analysed. Copper and platinum flotation systems were used for their experiments to represent slow and fast floating materials respectively. Their results show that burst rate tends to increase with an increase in bubble size. In the platinum system, it was found that the size that bubbles are able to attain is limited by the burst rate and the solids loading. At lower solids loading, smaller bubbles were present. Conditions of higher solids loading were attained with larger bubbles. However, the same scenario was not reproducible in the copper system. Thus, burst rate and solids loading measurements are able to augment the bubble size information obtained on the froth surface to characterize froth stability.

2.11.5. Electrical impedance spectrum as a froth stability measure

Hu *et al.* (2009) proposed a technique for quantifying froth stability using the electrical and dielectric properties of the froth. In their model, they propose that a body of froth between two electrodes can be regarded as a complex network of electrical conductance, inductance and capacitance as shown in Figure 2.20**.**

It is suggested that the solids and water contained in the inter-bubble lamellae may have an electrical resistance (R) and a conductance (C), while the bubbles may have an electrical inductance (L). In their experiments, the measurement system consisted of an electrical impedance spectrometer-Solartron 1260 Frequency Response Analyser (used to measure electrical impedance spectrum) and a pair of electrodes which were attached to the non-conductive column wall in the froth phase. A stability index (SI) defined below in Equation 2.33 has been used to quantify froth stability.

$$SI = \sqrt{\sum_{f=1}^{n} \left(S_f - S_m\right)^2 / (n-1)} \qquad \text{Equation 2.33}$$

Where: $S_f = \sqrt{\sum_1^5 \left(Z_{fi} - Z_{fm}\right)^2}$; $S_m = \sum_{f=1}^{n} S_f / n$; n is the total number of frequency points, Z_{fi} is the real impedance component of ith measurement at frequency point f; Z_{fm} is the mean of five measurements at frequency point f**.** S_f is the measure of variability in repeated measurements at frequency point, f. SI is a statistical measure of variations among repeated measurements of the electrical impedance spectrum in the froth phase. Hu *et al.* (2009) carried out experiments to establish the link between SI values and flotation response. Process variables consisting of feed flow rate, air flow rate, feed solids concentration, froth depth and collector and frother dosages were varied. At steady state, five sets of electrical impedance spectra were measured and a stability index evaluated. The results obtained showed that a flotation process with a relatively low stability index value would generally give a high flotation yield. Froth stability is therefore associated with low stability indices. This is illustrated in Figure 2.21.

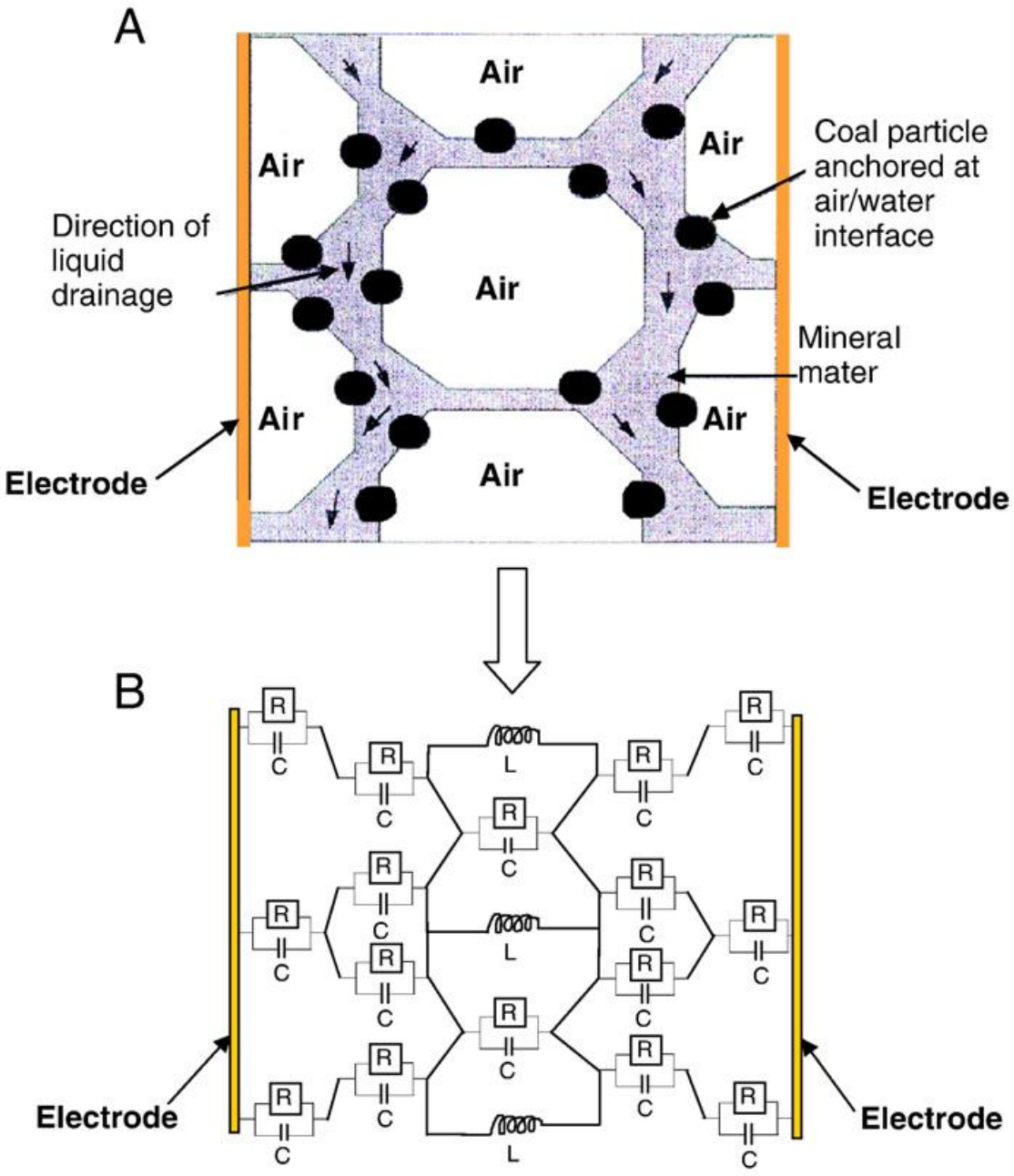

Figure 2.20: Schematic diagram of (A) froth structure and (B) possible electrical equivalent circuit representing its electrical and dielectric properties (R - resistance; C - capacitance; L - inductance (Hu et al., 2009).

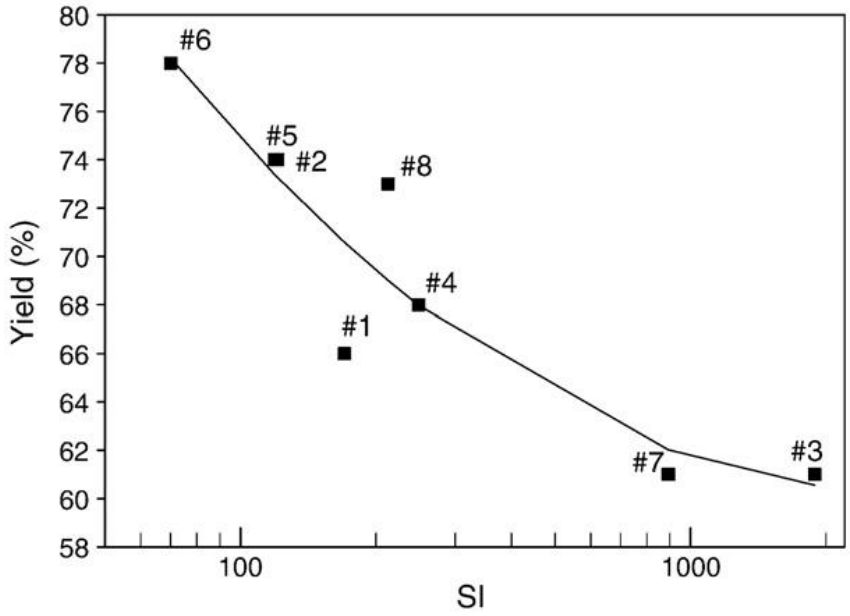

Figure 2.21: Effect of the froth stability index on flotation yield of plant operation for nine differents runs labelled #1 to #9. (Hu et al., 2009).

However, exclusive prediction of froth stability from the froth stability index cannot be absolutely relied on as a low value of SI would not guarantee a high flotation yield. This is depicted in Figure 2.21 above where runs 1 and 8 show contrasting results. Process run 1 had a lower SI than run 8 and was expected to have a higher yield, but this was not the case.

In conclusion, it should be emphasized that froth stability is an important aspect of the flotation process and its measurement and ultimately prediction is at the heart of the operations within the mineral processing industry. As such, the selection of the technique for froth stability measurement was a crucial component of this thesis. The development of a measurement technique was not a focus for this project, but rather to utilise a proven technique to achieve the desired goal of quantifying froth stability. Based on its simplicity, the froth stability column was chosen for measuring froth stability. However, because metallurgical information could not be obtained by utilising the froth stability column, a bench-scale continuously operated flotation column was built in the laboratory to achieve this purpose. This utilised two of the froth stability measurements discussed, viz. water recovery and top-of-the-froth bubble burst rate.

2.12. Summary

This review has discussed the importance of the froth phase in flotation, how to measure froth stability, the effect that mineral particles have on froth stability and the mechanisms that cause these effects. Because it is a valuable mineral grade/recovery determinant, an understanding of how the froth phase is affected by process variables (in this context, particle size and hydrophobicity) is crucial. Such is the value of froth stability as a process optimisation tool, that it is currently being trialled in a flotation control system for performance optimisation (Shean *et al.,* 2017).

The stability of the froth has been found to depend on the thickness of the liquid film between Plateau borders. Mineral particles, depending on their size and hydrophobicity, will either promote the liquid film thickening (stabilising the froth), or enhance drainage (in this case destabilising the froth). Dippenaar (1982b) reported that the thinning of the liquid film is the rate-determining step in the destabilisation of froths. The liquid film thickness is affected by the size of particles as well as their hydrophobicity which in flotation studies is manipulated by use of collectors.

The study of the literature has shown that there is agreement that coarse particles tend to produce less stable froths, but there is no consensus on the effect of particles at the fine end of the flotation range. Some studies say that froths continue to become more stable as particles become finer, while others propose that froth stability goes through a maximum and then becomes less stable at the finest flotation sizes. The only known relationship between particle size and froth stability was investigated in metal foams at very low solids concentrations. There is clearly a need for a comprehensive investigation into the effect of particle size on froth stability within the flotation context.

Most flotation studies agree that a maximum froth stability exists for particles of contact angles between 60° and 70°. However, most studies have investigated the effects of particle size and hydrophobicity on froth stability individually. It is of importance that studies on the interactive effects of these two particle properties on froth stability are investigated.

Theories that seek to explain how particles stabilise froths have also been advanced. The maximum capillary pressure of coalescence theory explains froth stability based

on the pressure gradient between a bubble and the interfilm fluid. Since this measures the resistance of the bubble phase to a pressing force, the higher this pressure the more stable the froth is. It predicts that the froth is most stable when the particle contact angle is 0˚ and the particle size is small. However, an opposing theory for describing froth stabilisation by hydrophobic particles known as the particle detachment theory has also found substantial application. It predicts that the froth stability will be highest for large particles of contact angle of 90°. However, Kaptay (2006) used these two theories in his model and predicted an optimum contact angle of 70° for maximum froth stability. The packing of particles within the Plateau borders has also been advanced as an important mechanism which influences froth stabilisation. Particles may pack to form a bridging monolayer, a bilayer of hexagonally packed particles, or a network of particle aggregates inside the film. Also, the stability of the froth is related to the liquid viscosity. A liquid with a high viscosity will slow the rate of drainage of the liquid in the thin liquid films thus stabilising the froth.

The froth stability measurement techniques relate a given property of the froth to its stability. Proxies employed by past research include water recovery, dynamic froth stability factor, air recovery, electrical impedance spectrum and bubble burst rate, among others. It was in the interests of this thesis to utilise proven techniques for quantifying froth stability. The dynamic non-overflowing froth stability column was chosen because it is simple to use and its results are scalable. However, because of its inability to provide metallurgical information, a bench-scale continuously operated flotation column was built in the laboratory for this purpose, which was also able to measure froth stability using water recovery and top-of-froth bubble burst rate.

CHAPTER THREE

3. DEVELOPMENT OF THE BENCH-SCALE FLOTATION COLUMN

3.1. Introduction

A vital step in meeting the objectives of this research project was to construct a device capable of measuring differences in froth stability, while at the same time predicting the flotation performance. The equipment was required to operate on a continuous basis at steady state. It needed to be able to operate using small enough amounts of material so as to meet logistical challenges associated with using large amounts of materials in a big column. Discrete particle size fractions of controlled hydrophobicity were carefully prepared and used in this test work.

The column flotation cell found practical use in the upgrade of mineral ores as early as the 19th Century. Industrial flotation columns are either round or rectangular vertical chambers in which the particles in a slurry move downwards counter-current to a swarm of air bubbles generated by spargers installed at the bottom of the cell. Because they are designed without impellers, particles experience hindered settling with a distribution of residence times. Columns provide an improvement in metallurgical performance as they are operated with deep froths, often with wash water. They have also been seen to reduce operating costs owing to fewer moving parts as compared to mechanical cells. Since its inception, the design of flotation columns has followed an experience-based approach and “know how”, rather than a detailed engineering solution (Ityokumbul, 1992; Finch, 1995).

The column flotation cell constructed for this project is based on the design originally described by Xu *et al.* (1996). The bench-scale flotation column represents an attempt to design a system that provides more information than the traditional batch flotation cell. In contrast to the mechanical batch flotation cell, the flotation column has a well-established froth and operates continuously at steady state. It uses small amounts of well characterised particles and has been purposely designed to meet logistical challenges foreseen in as far as meeting the objectives of this project were concerned.

Since the focus of this project was on measuring the stability of the froth, a deep froth was desired.

3.2. Design considerations

The bench-scale flotation column (shown in Figure 3.3) was designed using a Perspex pulp and glass froth sections. Glass was chosen as the material of construction for the froth zone so as to minimise wall effects associated with Perspex. Perspex is hydrophobic, which causes froth bubbles to stick to the walls. The collection and froth zones are completely separable from each other. The collection zone has an internal diameter of 3.6 cm and length of 30 cm. Its height is 73% of the overall column height considering the longest froth zone height of 11 cm. Dimensions were chosen to give a volume that was practical from a sample preparation point of view.

3.2.1. Sparger design

Spargers are typically employed in the minerals industry to generate uniform small bubbles, enabling hydrophobic mineral particles to collide with and attach onto them. The sparger used in this design consisted of a porous ceramic tube enclosed in a casing made of Perspex as shown in Figure 3.1. Bubbles were formed by sheer as a result of passing the recycled slurry across the porous tube. Bubble size was controlled by the shear rate. Pulp bubble size has been shown to have an effect on the measured froth stability (Geldenhuys, 2017). Smaller bubbles produce a more stable froth. However, bubble size was kept constant at a constant slurry flow rate of 580 g/min. In addition, slurry flow through the sparger resulted in a higher energy bubble-particle collision zone than in traditional column flotation cells where bubbles and particles are contacted through a counter-current flow system of relatively low energy.

A rotameter with an air flow rate range from 0 to 1 L/min was used. Numerous tests were carried out to determine an appropriate aeration rate that could be used for all experiments. A constant airflow rate of 0.7 L/min corresponding to a superficial gas rate of 0.98 cm/s was maintained using a rotameter.

Figure 3.1: Sparger

3.2.2. General column design

Glass columns of variable lengths each of internal diameter 4 cm were constructed and used as the froth zone. It was necessary to keep the collection zone of a constant height in order to have a consistent collection zone rate constant. Therefore, froth zones of variable lengths i.e. 4, 7 and 11 cm (as shown in Figure 3.2b) were constructed so as to calculate the froth recovery using the variable froth depth technique, a method used by several authors (Feteris *et al.,* 1987; Laplante *et al.,* 1989; and Vera *et al.,* 1999). Since the froth height was varied, a detachable launder was constructed and positioned on top of the froth zone. A series of tests was carried out to obtain the highest possible froth height and it was determined that the 11 cm column height was adequate for all test conditions explored.

The froth flowing out of the flotation system is directed through the concentrate launder before being collected. The launder sits at an angle of 20 degrees to the froth zone section.

(a) Froth section of flotation column

(b) The three glass columns; from left to right: 11, 7, and 4 cm height

Figure 3.2: (a) Set-up of froth section of continuous column flotation cell (b) Glass froth zone columns of varying height.

Translucent silicone tubing was used for flow distribution within the system. This enabled blockages to be identified especially when floating large particles in the coarsest size fraction (+150-300 µm) which settled easily in the tubes owing to their high mass.

Three peristaltic pumps were used to drive flow through the system, viz. for the feed, tails and recycle streams. The level in the cell was controlled by the tailings flow rate.

Figure 3.3: Bench-scale flotation column

3.3. Setup and operation

Experiments using the bench-scale flotation column were set-up as shown in **Error! Reference source not found.**. A slurry feed of 7 kg (which contains 5% pyrite, 1.2% talc and the rest quartz), prepared using the synthetic ore, was required to carry out each flotation test at three different froth heights consecutively. A feed pulp density of 25% was maintained for all tests. This was the highest density attainable for stable operation of the column. The slurry feed flow rate was 580 g/min at a residence time of 1 min, the superficial gas rate was 0.98 cm/s and frother dosage was 100 ppm. Operating conditions were chosen by systematically varying flow rates and frother dosages in order to find a set of conditions at which operability was achieved for all particle size conditions. This was a difficult task as the very fine particles had significantly different frothing effects to the very large particles. A balance needed to be struck between conditions which allowed both fine and coarse particles to float. In addition, the glass froth section was hydrophilic and froth drainage was high at the surface and required high frother dosages. It is acknowledged that the frother dosage is higher than normal and well above the critical coalescence concentration. However, it was simply a requirement due to the varying particle conditions and did not in any way mask the effects of particle size as these were still clearly observed. The particle

effects that were observed in this investigation are expected to be extrapolated to any frother dosage.

The solid particles in the feed tank were kept in suspension by means of an impellor. The feed and air were fed through a sparger where particle-bubble contacting took place before entering the column. A recycle stream that assisted in keeping the particles in suspension was maintained between the base of the pulp section and the feed stream.

The air supply was first turned on, followed by the recycle and tailings pumps. The feed pump was then turned on and the system was allowed to reach steady state in closed circuit for 10 minutes, after which the cell was open-circuited and given three residence times to reach steady state. Thereafter, three concentrate and three tailings samples were collected in open circuit at 30 seconds intervals.

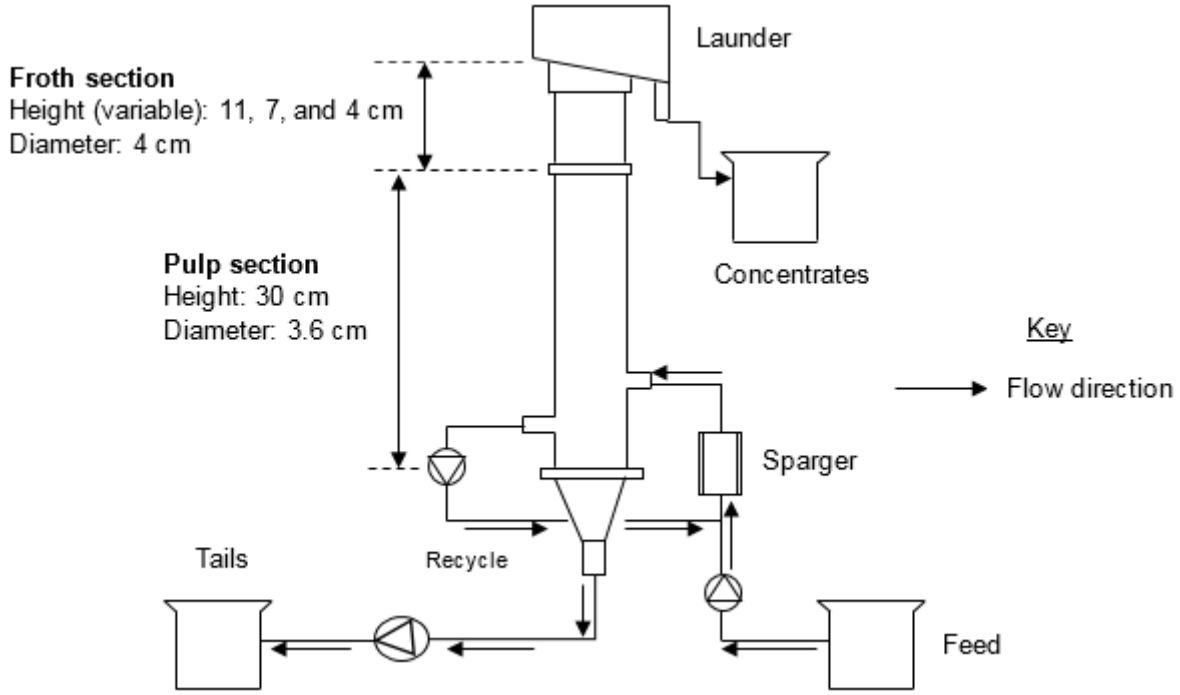

Figure 3.4: Schematic showing setup and operation of the bench-scale continuous flotation column

3.4. Limitations and recommended future improvements to the operation of the continuous flotation column

A decision was made to use glass instead of Perspex for the froth phase section. This was in order to study the bubble coalescence profile above the pulp-froth interface.

Perspex is not well suited for this as bubbles are prone to adhere to it making it difficult to measure their size and subsequently account for increases in size above the pulp-froth interface. However, glass is hydrophilic and this resulted in a high drainage rate at the glass interface, which caused a lower apparent froth stability. This necessitated using a high frother dosage to enable the formation of froth of adequate volume. Numerous attempts were made in choosing the correct combination of frother dosage and air flow rate. 100 ppm frother dosage was found to be sufficient and was thus chosen as the dosage at which all experiments were carried out. It may be useful to explore other options of intermediate hydrophobicity in the construction material of the froth zone.

Flotation conditions needed to be such that maximum froth heights of 11 cm were attainable under all particle size and particle hydrophobicity conditions. Since the range of particle sizes produced such a large difference in froth characteristics, it was extremely difficult to find a set of conditions that suited all particle sizes. Coarse particles needed high air flow rates and frother concentrations to produce sufficient froth, while under these air and frother conditions small particle sizes produced a froth that was too stable. The variables that had most influence on the froth characteristics were the frother concentration, pulp bubble size and air flow rate. Unfortunately, it was impossible to decouple these variables. Air flow rate, as well as feed and recycle flow rates, had an effect on the bubble size. Thus, the aeration rate of 0.7 L/min, giving a superficial gas rate of approximately 1 cm/s, resulted in such a stable froth at small particle sizes (-25 μm) that it was impossible to obtain an interface between the pulp and the froth phases. It is recommended for future designs to have independent control over the bubble size and the air flow rate by installing glass frits of different pore sizes.

CHAPTER FOUR

4. EXPERIMENTAL METHOD

This Chapter details the equipment, materials and methods employed to meet the research objectives of this thesis.

4.1. Equipment

4.1.1. Froth stability column

In order to measure dynamic froth stability, a non-overflowing stability column as shown in Figure 4.1 was constructed from Perspex. Since images of the side of the froth were not analysed in this piece of equipment, the hydrophobicity of the wall was not an issue as discussed in Chapter 3. The column has a height of 1 m and an internal diameter of 9.3 cm. A sintered glass frit placed at the bottom through which air is sparged is used for bubble generation in this thesis. All work was conducted using a P2 frit which has a pore size of 40 – 100 µm. A stainless steel impeller operating at 1100 rpm was inserted inside the column to keep the solids in the slurry in suspension, and to assist in particle-bubble attachment.

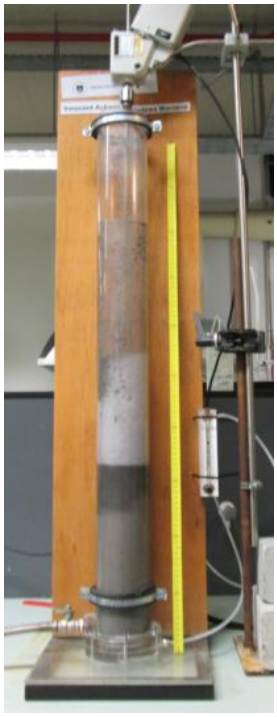

Figure 4.1: Stability column.

Well mixed slurry was pumped through an inlet near the bottom of the column to the 2 L mark. This was sufficient that the particles did not become the limiting factor during the growth of the froth. The impeller was then turned on to keep the solid particles suspended in the fluid. The level attained by the slurry was noted. Air was turned on at the required flow rate and the height attained by the froth was tracked as a function of time. Once the maximum froth height was achieved, the air was turned off. The slurry was then pumped out of the column and was subsequently used for flotation tests in the bench-scale flotation column.

Froth stability was determined in this way for each continuous column flotation experiment conducted.

Dynamic froth stability factor, ∑, is defined as (Bikerman, 1973):

$$\Sigma = \frac{H_{max} \times A}{Q} \qquad \textit{Equation 4.1}$$

Where H_{max} = the maximum height attained by the froth; A = Column surface area and Q = Air flow rate. Using Equation 4.1, a dynamic froth stability factor was calculated for each experimental condition.

H_{max} was determined by measuring the growth rate of the froth and making use of the expression:

$$H(t) = H_{max}(1 - e^{-t/\tau}) \qquad \textit{Equation 4.2}$$

Equation 4.2 was developed by Barbian *et al.*, (2003). Where τ = froth residence time, t = time, and $H(t)$ = height of froth at any time t.

Figure 4.2 shows the variation of froth height with time for three particle size fractions generated using the froth stability column at constant conditions of air flow rate (0.98 cm/s) and frother concentration (100 ppm). All froth stability data generated using the stability column were analysed using Equation 4.2.

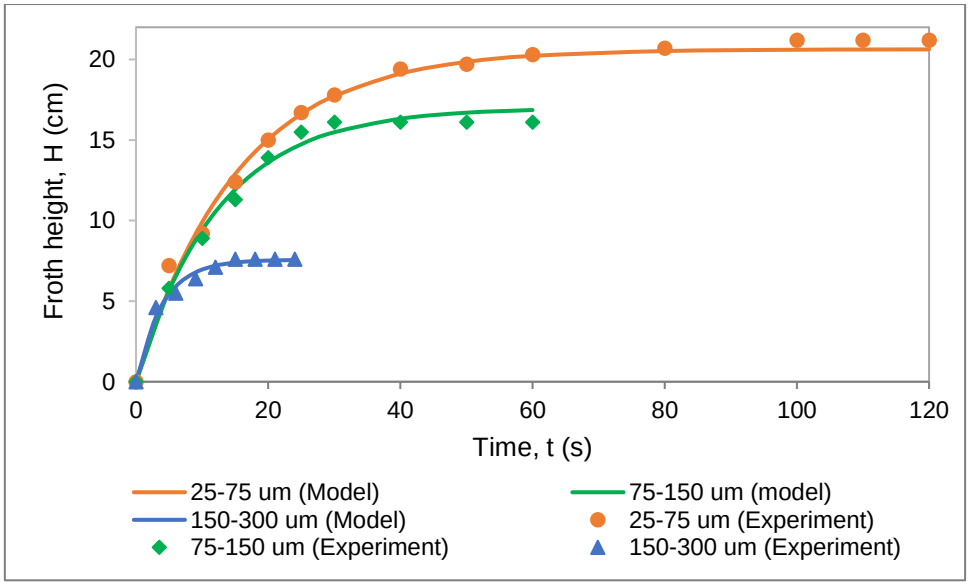

Figure 4.2: Froth growth as a function of time for three particle size fractions (25-75, 75-150, & 150-300 um).

The stability column was initially run at varying air flow rates, but fixed frother dosage, in order to enable selection of a fixed aeration rate at which all experiments could be conducted. Figure 4.3 shows the variation of the maximum froth height as a function of aeration rate for two different ore systems; (1) a mixture of 75-150 and 150-300 um size classes at a ratio of 4:1 dosed with collector corresponding to 300% surface coverage of pyrite made up in a slurry at 25% pulp density, and (2) 150-300 um size class dosed with collector corresponding to 25% surface coverage of pyrite made up in a slurry at 20% pulp density.

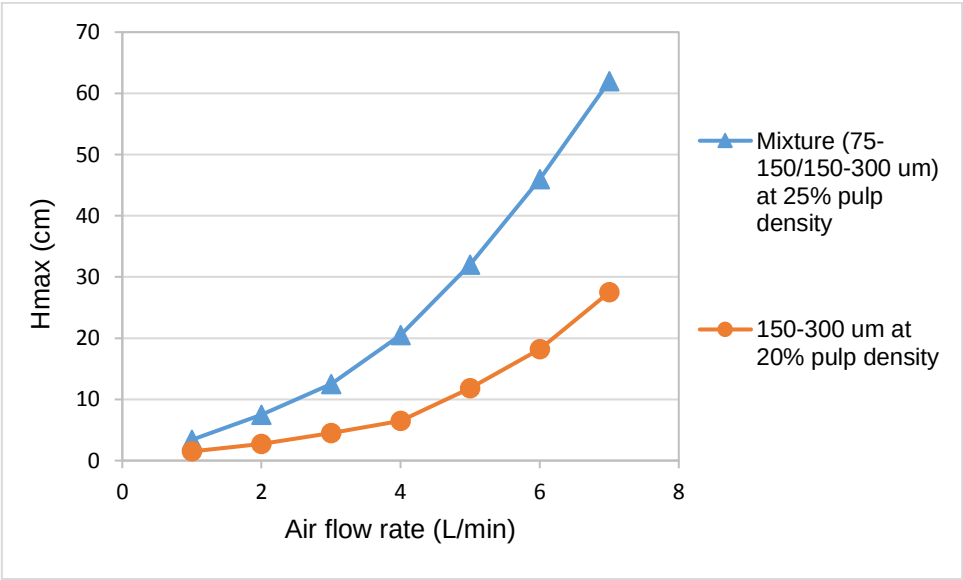

Figure 4.3: Effect of aeration rate on maximum froth height (Hmax) for two different ore systems.

There is an initial non-linear region at low air flow rates, which after about 4 L/min enters a linear region. This is where the froth stability is directly proportional to the air flow rate and is the region at which it was desired to work. Consequently, an aeration rate of 4 L/min was chosen for all column experiments. This corresponds to a superficial air velocity of 1 cm/s similar to that used in operating the bench-scale continuous flotation column.

4.1.2. Bench-scale continuous flotation column

The performance of the flotation process as the system variables changed was also monitored using a bench-scale flotation column operated at steady state. This column including its set-up, and operation, has been extensively described in Chapter 3. The column flotation cell was used to predict froth stability using two proxies i.e. water recovery and top-of-froth bubble burst rate.

4.1.3. Microflotation apparatus

One method of quantifying hydrophobicity was a University of Cape Town (UCT) microflotation cell (shown in Figure 4.4). The unit operates without a froth phase and was used to determine the hydrophobicity of pyrite samples that were reacted with different dosages of potassium amyl xanthate (PAX) collector. This microflotation cell, which is made of glass, has been used in several studies that have earlier been described (Bradshaw, 1997; Bradshaw & O'Connor, 1996; Min, 2010). It uses single bubble streams generated by air flowing through a micro-litre syringe to float particles in the pulp zone. A peristaltic pump is used to achieve an upward circulatory flow in order to keep the mineral particles in suspension. On reaching the upper conical section of the cell, the bubbles burst releasing their load onto the launder. All other parameters being constant, the greater a particle's hydrophobicity, the greater the likelihood of a bubble-particle attachment and the greater the mineral recovery. Thus a higher mineral recovery is associated with a greater degree of hydrophobicity.

Sample preparation: 3 g of pyrite was added to a 250 ml glass beaker, 100 ml of synthetic plant water was added to it and the slurry was conditioned with the required dosage of PAX collector for 5 minutes. An overhead stirrer was used to keep the solids in suspension. After conditioning, the pyrite was filtered out and used for hydrophobicity determination in the microflotation cell.

Microflotation cell experimental procedure: To conduct an experiment, air was turned on and the U-tube manometer given at least 30 minutes for the air distribution to reach steady state. The cell was then half filled with synthetic plant water with the pump turned on. 3 g of dry pyrite sample of size 38 – 106 µm that had earlier been conditioned with collector was added to the cell. The water was topped up to the mark and the flotation test started after the air supply to the cell was connected through a micro-litre syringe at the base of the cell. An aeration rate of 10 cm^3/min was used and the peristaltic pump was set at 100 rpm. Concentrate samples were collected for 2, 4, 6 and 8 minutes in the concentrate launder, filtered, dried and then weighed. Experimental data was fitted to the first order kinetic expression in Equation 4.3:

$$R(t) = R_{max}(1 - e^{-kt}) \qquad \textit{Equation 4.3}$$

Where $R(t)$ = recovery at any time, t, R_{max} = maximum recovery, t = time, and k = rate constant.

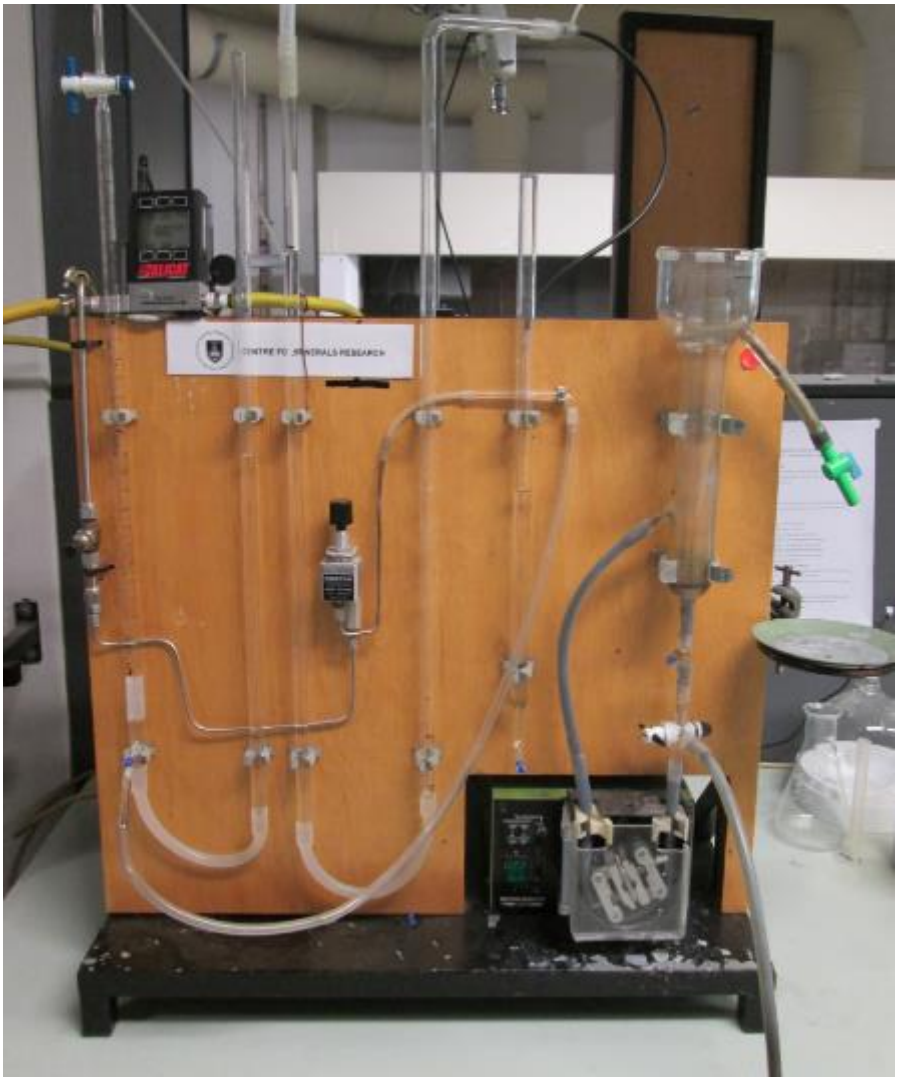

Figure 4.4: UCT Microflotation cell used for hydrophobicity determination.

4.2. Materials

4.2.1. Minerals

Pure pyrite and talc were sourced as bulk samples from Wards Scientific and quartz from Consol Glass (Pty). A synthetic ore made up of these three components was used in all experiments conducted in the stability column and in the bench scale flotation column. Pyrite was the hydrophobic component while quartz was the hydrophilic component. It was necessary to use talc, a naturally floating gangue mineral, in order to aid in stabilising the froth. The synthetic ore contained 1.2% talc, 5% pyrite and 93.8% quartz. The quartz was milled using a 1 kg capacity stainless steel mill and rods supplied by Eriez Magnetics and sieved into the same size fractions as the pyrite and talc samples. The pyrite and talc were pulverised using a Sieb mill supplied by Ferguson Industrial Group. All milling and screening were done on dry

samples as received. The screens used to obtain the different size fractions had aperture sizes of 25, 38, 75, 106, 150, and 300 µm. Prepared pyrite samples were kept under nitrogen at -30 ^{o}C to minimise surface alterations by oxidation. All three minerals were sized into the following size classes: - 25, 25 – 75, 75 – 150, 150 – 300 and 38 – 106 µm. These particle size classes were chosen as being representative of typical ranges of size classes found in most conventional flotation systems. The sub-25 µm range is the very fine range, where much of the material would report to the concentrate by entrainment. The 150 – 300 µm size class is a very coarse and difficult-to-float region.

The particle size distribution of the ore samples was determined using a Malvern Mastersizer 2000 (Hydro 2000 MU) particle analyser. The measurement technique is based on the principle of laser ensemble light scattering.

In order to calculate the amount of collector required to achieve a specific surface coverage the specific surface area (in m^2/g) of pyrite was determined for each size class using the B.E.T. (Brunauer, Emmett and Teller) gas adsorption method. This was based on the BET surface area of the pyrite and assuming the cross-sectional area of the thiol head group of xanthate to be 28.8 Å (Grano *et al.,* 1997).

4.2.2. Reagents

In all tests carried out in the flotation column and the non-over-flowing stability column, potassium amyl xanthate (PAX) was used as the collector. It was supplied by Senmin in powder form and prepared on a daily basis using deionised water. PAX was chosen since it is a strong collector that can be used to alter the hydrophobicity of the mineral surface. At very low dosages, low contact angles could be attained using any xanthate collector. But a strong collector such as PAX was required to induce the very large contact angles required to investigate high hydrophobicity.

A polypropylene glycol ether, Dowfroth 250, supplied in liquid form by Betachem (Pty) Ltd, was used as frother at a constant dosage of 100 ppm. This high frother dosage was necessary in order to run all the experiments in the bench-scale flotation column under the same conditions as the froth volume obtained with coarse particles at a lower frother dosage would be insufficient to obtain an acceptable solids and water mass flow to the concentrate. The glass wall of the flotation column did not have a stabilising effect as it is hydrophilic and drainage would be high at the surface.

4.2.3. Synthetic plant water

Synthetic plant water was used to prepare slurries used in both the stability column and the bench scale flotation column as well as to run all experiments in the UCT microflotation cell. Synthetic plant water mimics the inorganic ions found in recycled plant water, which is essential to a realistic assessment of flotation conditions. Six different salts were dissolved in pure distilled water as reported by Wiese (2005) in order to be able to simulate industrial platinum group minerals (PGM) process water. Each of the salts was weighed as shown in Table 4.1 and dissolved in distilled water to make up 40 L batches of synthetic plant water.

Table 4.1: Composition of salts in each 40 L batch of synthetic plant water

Salt	Formula	Mass composition (g)
Magnesium Sulphate Heptahydrate	$MgSO_4$. $7H_20$	24.6
Magnesium Nitrate Hexahydrate	$Mg(NO_3)_2.6H_20$	4.28
Calcium Nitrate Tetrahydrate	$Ca(NO_3)_2.4H_20$	9.44
Calcium Chloride Dihydrate	$CaCl_2.2H_2$	5.88
Anhydrous Sodium Chloride	NaCl	14.24
Anhydrous Sodium Carbonate	Na_2CO_3	1.20

4.3. Mineral analysis

The quartz used in this study was assayed for iron impurities (that may influence the results obtained for assays of pyrite) using atomic absorption spectroscopy (AAS). The amount of iron in the quartz was found to be negligible. BET specific surface area of both quartz and pyrite were very similar within each size class. Table 4.2 shows the specific surface area of pyrite for each size class. Concentrates and tails from the column flotation tests were assayed for Fe and Mg using AAS after acid digestion. Concentrates were also analysed for particle size and surface area by Malvern particle analyser.

Table 4.2: BET specific surface area of pyrite for each particle size class

Size class (μm)	BET Specific surface area (m^2/g)
- 25	0.8956
25-75	0.2419
75-150	0.0818
150-300	0.0478

4.4. Contact angle measurement and manipulation

Samples for the capillary rise experiments were prepared by a technique first proposed by Burt and Fewtrell (1970) for preparing beds of powders for air permeability measurements. A Kruss K-12 tensiometer (shown in Figure 4.5) was used for the contact angle determination. Capillary tubes were manually filled with samples of the pyrite particles and the sample beds compacted by centrifugal force using a laboratory centrifuge. Hexane, a perfectly wetting liquid was first used to determine the material constant, after which the contact angle of pyrite was determined using water in the capillary rise experiments. The hydrophobicity of pyrite was varied by using different dosages of collector. The dosage of collector required for different coverages on the surface were calculated from the specific surface area of the pyrite. A description of how contact angle is calculated using the Washburn technique has earlier been reported in Chapter 2.

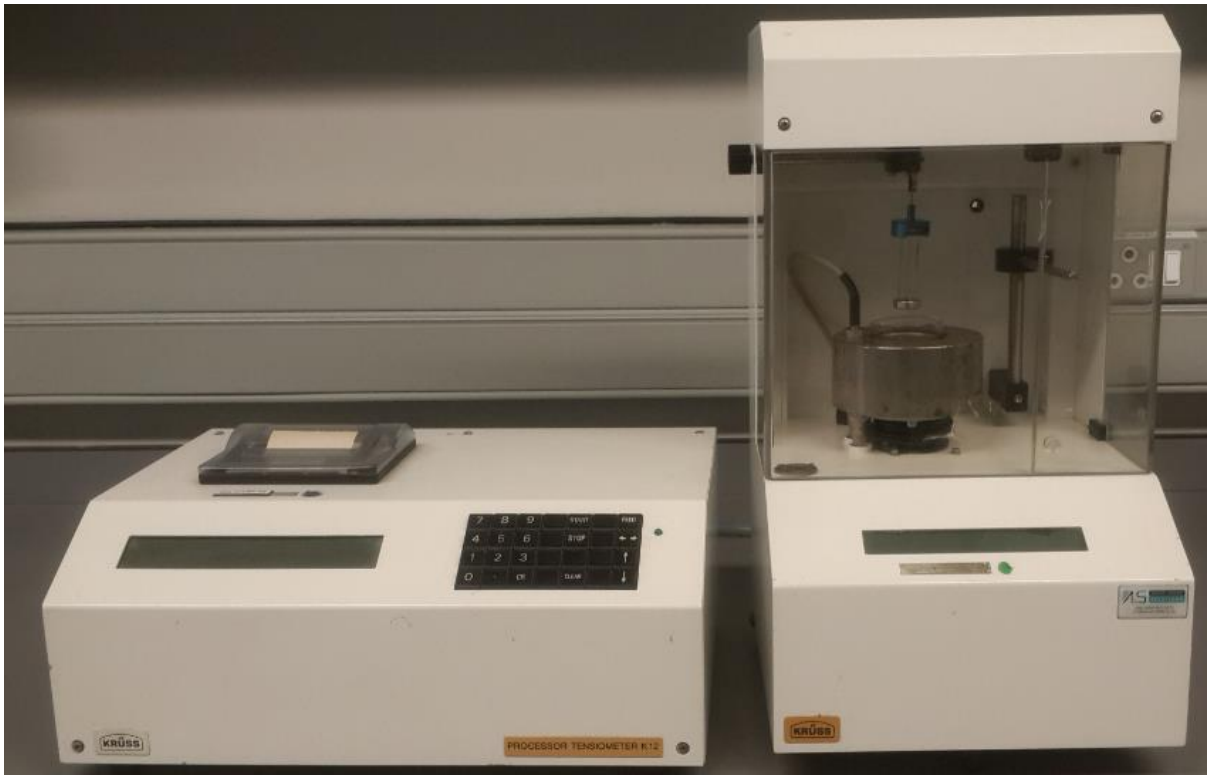

Figure 4.5: Kruss K-12 tensiometer used for contact angle determination

4.5. Froth recovery

Froth recovery is defined as the fraction of particles that are delivered to the pulp-froth interface that make it to the concentrate launder. It is used as a measure of the performance of the flotation system, specifically the froth phase. Froth recovery is related to froth stability (Zanin *et al*., 2009); high froth recovery is achieved with stable froths. Unstable froths in which there is rapid bubble collapse and volume depletion yield lower froth recoveries.

The technique developed by Feteris *et al.* (1987) which involves carrying out flotation tests for at least three different froth depths and calculating the different collection zone rate constants was employed. In this technique, a linear relationship between flotation rate constant and froth depth is obtained. The flotation rate constant at zero froth depth, k_c, is used to calculate froth recovery, R_f by the expression:

$$R_f = \frac{k}{k_c} \qquad \textit{Equation 4.4}$$

Where k is the rate constant at a given froth depth other than zero.

4.6. Representation of particle size data

The geometric mean is defined as the nth root of the product of n numbers, i.e: $(\prod_{i=1}^{n} x_i)^{1/n}$ whereas the harmonic mean is defined as $\frac{n}{\sum_{i=1}^{n}\frac{1}{x_i}}$ where x_1, x_2, ……, x_n are positive real numbers. In this study, a geometric mean size was used to represent size for particle size classes. Where a mixture of two size classes was used, a weighted average geometric mean size was used to represent size. The harmonic mean size was calculated and found to be similar to the geometric mean size as shown in Table 4.3 for all size classes. As such the harmonic mean sizes as well as their weighted averages were not used in the results presented here.

Table 4.3: Geometric and harmonic means of discrete size fractions and mixtures of particle size fractions.

Percentage particles by mass from each size class (%)				***Geometric mean size (µm)***	***Harmonic mean size (µm)***
-25 µm	***25-75 µm***	***75-150 µm***	***150-300 µm***		
80	20			15.59	11.79
80		20		28.14	24.29
20	80			36.37	31.07
	100			43.30	37.50
80			20	49.35	44.29
	80	20		55.85	50.00
	80		20	77.07	70.00
20		80		86.58	81.07
	20	80		93.51	87.50
		100		106.07	100.00
		80	20	127.28	120.00
20			80	171.44	161.07
	20		80	178.37	167.50
		20	80	190.92	180.00
			100	212.13	200.00

Experiments to determine the effect of particle size on froth stability were conducted with discrete particle size classes as well as mixtures of these size fractions at two ratios, 1:4 (20% and 80%) and 4:1 (80% and 20%) as shown in Table 4.3.

4.7. Particle size distributions

A characterisation of the particles in terms of distribution was done. Initially, the particles were screened into different fractions using wire mesh sieves aided by mechanical vibration. This was the most appropriate way to characterise the particles as it enabled preparation of large quantities of feed particles, especially quartz which was required in large amounts. A Malvern mastersizer 2000 was used to determine the size of the particles in the concentrates obtained from the flotation process and the results are shown in Figure 4.6, Figure 4.7 and Figure 4.8. This was found to be very effective for the small amounts of concentrates obtained from the flotation tests.

Figure 4.6 shows the particle size distribution for the concentrates of 1:4 ratios. As expected, a distribution of sizes was obtained. The following observations are made:

- 93% of the particles in the –25/25–75, –25/75–150 and the 25–75/75–150 µm mixtures were below 212 µm in size.
- In the case of the –25/150–300, 25–75/150–300, and the 75–150/150–300 µm mixtures, 93% of the particles were below 425 µm in size.

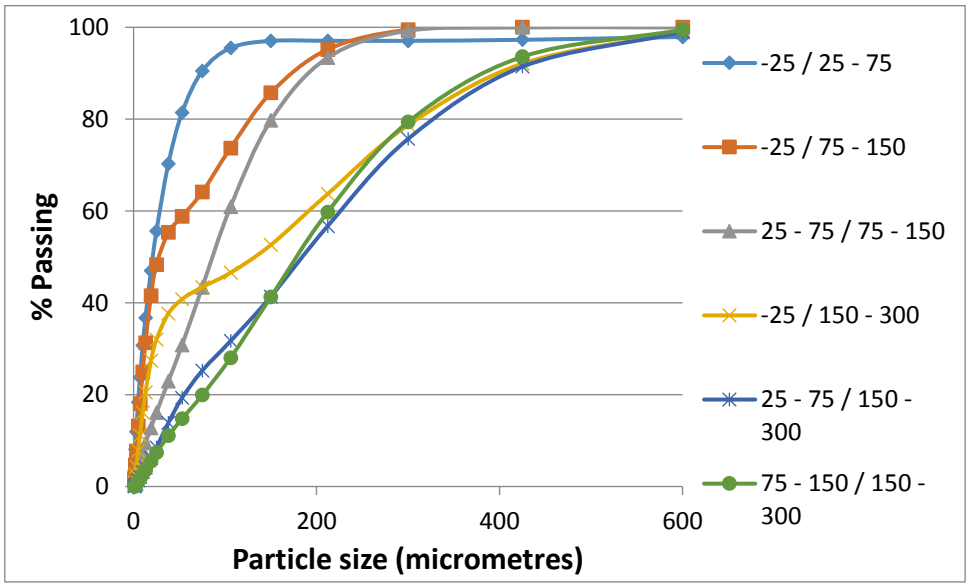

Figure 4.6: Concentrate particle size distribution for the 1:4 ratio. Sauter mean particle sizes from the Malvern mastersizer were used for this plot.

Figure 4.7 shows the particle size distributions for the 4:1 ratio. The following observations are made:

- 94% of the particles in the –25/25–75, –25/75–150, and –25/150–300 mixtures were smaller than 53 µm in size.
- In the case of the 25–75/75–150 and the 25–75/150–300 mixtures, 86% of the particles were smaller than 106 µm in size.
- 93% of the particles in the 75–150/150–300 µm mixtures were smaller than 300 µm in size.

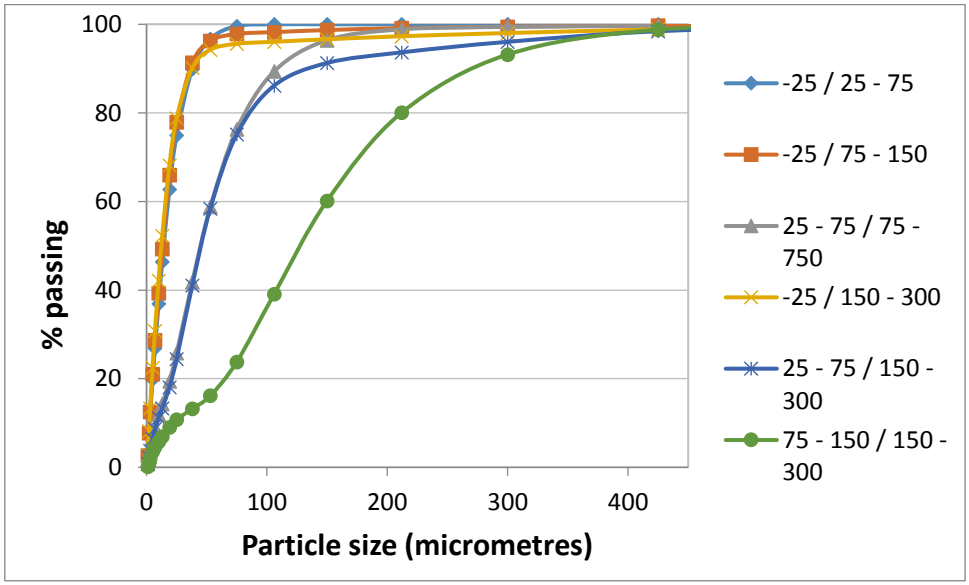

Figure 4.7: Concentrate particle size distribution for the 4:1 ratio. Sauter mean particle sizes from the Malvern mastersizer were used for this plot.

Figure 4.8 shows the particle size distributions for discrete size fractions of concentrates from the flotation process. The following observations are made:

- 85.9% of the particles in the 25 – 75 µm size class were smaller than 75 µm in size.
- 44.3% of the particles in the particles in the 75 – 150 µm size class were smaller than 150 µm in size.
- In the 150 -300 µm size class, 67.45% of the particles were smaller than 300 µm in size.

The results obtained using mechanically agitated stacked screens are expected to be different from those in which the Malvern Mastersizer was used for non-spherical particles. This is expected since each of these two methods measure particle size in different ways. Laser diffraction techniques require well described optical properties and assume that particles are perfect spheres.

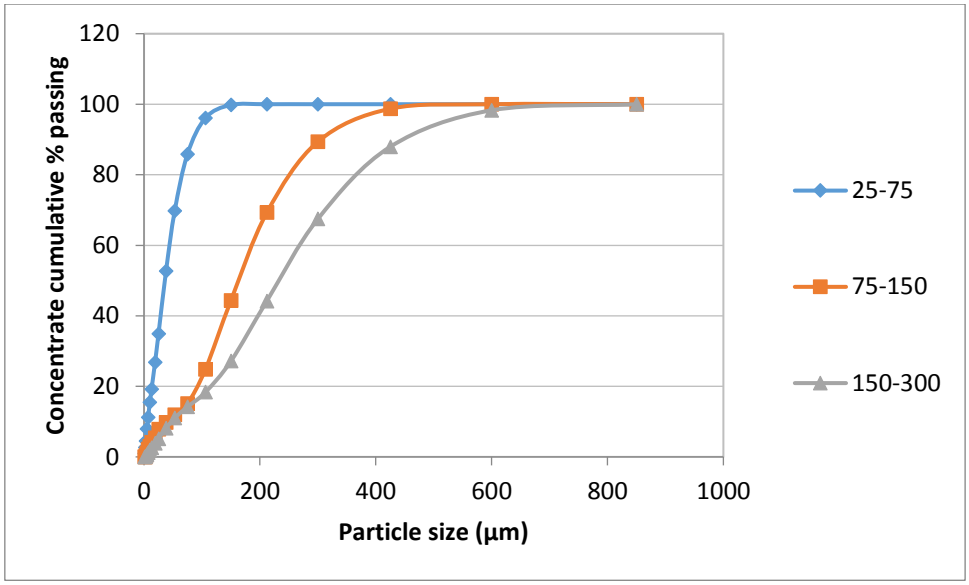

Figure 4.8: Concentrate particle size distribution for the discrete size fractions. Sauter mean particle sizes from the Malvern mastersizer were used for this plot.

4.7. Bubble burst rate

The number of bubbles bursting at the top of the concentrate launder can be used as a measure of froth stability. Videos were captured of the top of the froth using a Sony Handycam video camera. The videos were analysed using VirtualDub, a free online video analysis software. By scrolling through the video frame by frame, it was possible to count and record the number of bursting bubbles per unit time.

CHAPTER FIVE

5. THE EFFECT OF PARTICLE SIZE ON FROTH STABILITY

5.1. Introduction

Mineral particle size has been known to significantly affect the quality of froths and subsequently froth stability in flotation tests. This impacts on the overall grade and recovery tenable.

This chapter presents experimental findings and discussions on the effect that mineral particle size has on froth stability. The hypotheses being tested here are:

"Hypothesis 1: *Froth stability increases with decreasing particle size and this is due to increased viscosity of the thin liquid films between bubbles which leads to a slower liquid drainage rate."*

"Hypothesis 2: *Froth stability will increase as a function of the increasing particle surface area in the froth because thin film liquid drainage will be directly affected by the surface area of particles retarding drainage."*

The aims of this chapter are to establish a relationship between particle size and froth stability for a set of well-characterised particles and to establish this methodology as a small-scale particle characterisation test that could be used for flotation froth modelling. Stabilities of froths resulting from discrete particle sizes as well as mixtures of size fractions were investigated. A novel bench scale continuously operated flotation column with a well-defined froth phase (as described in Chapter 3) was used for the flotation tests and a non-overflowing stability column for stability tests. Froth stability was quantified using water recovery, top-of-froth bubble burst rate, and maximum height attained by the froth at a fixed aeration rate (dynamic froth stability factor).

5.2. Results and discussion

5.2.1. Feed versus concentrate particle size

Naturally, the particles that will affect the froth stability are not the feed particles, but those that report to the froth phase. However, in the first phase of the data analysis, froth stability was analysed as a function of feed particle size, rather than concentrate

particle size. Since, on a full-scale operation or in ore characterisation, feed particle size is generally a more easily measured property than concentrate particle size, and it is a more useful property for froth characterisation. Figure 5.1 illustrates the relationship between feed particle diameter and concentrate particle diameter for all the particle size ranges used in this Chapter. The feed consists of pyrite, quartz and talc in different proportions as earlier reported in Section 4.2.1. It is clear that the particles reporting to the concentrate have a slightly smaller average diameter than the feed particles, as would be expected. However, the concentrate particle diameter is a linear function of feed particle diameter and plots of froth stability as a function of either feed or concentrate particle diameter follow the same trend. It was decided to analyse the data in terms of the feed particle diameter since this is a parameter that is more useful as a predictive tool.

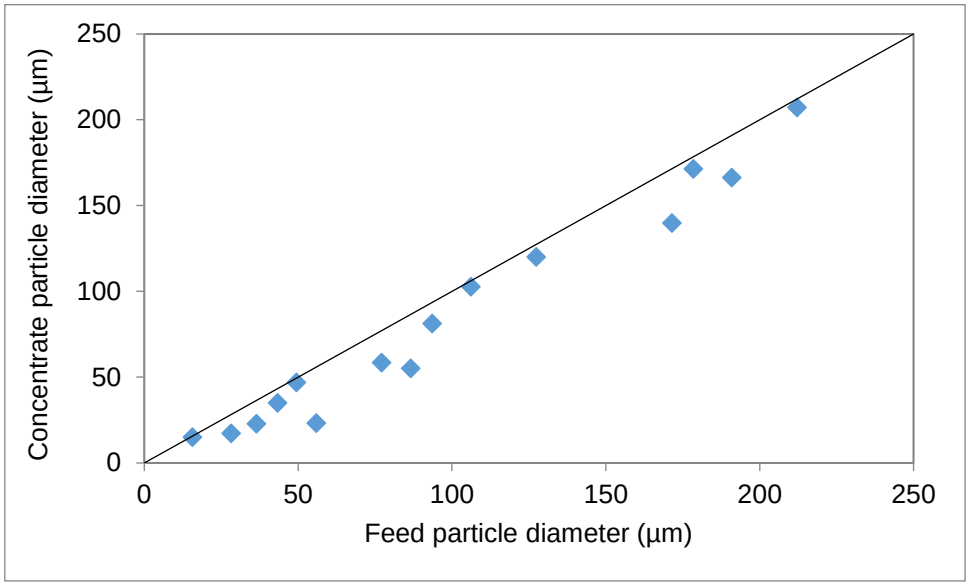

Figure 5.1: Feed particle diameter as a function of concentrate particle diameter. The line represents the xy function.

5.2.2. Relationship between froth stability and feed particle size

Dynamic froth stability data was generated by the non-overflowing froth stability column. This was accomplished by measuring the froth growth rate at a fixed superficial gas rate of 1 cm/s. Figure 5.2 shows the variation of the dynamic froth stability with feed particle size at a constant pulp density of 25% and constant collector surface coverage of 25%, corresponding to pyrite contact angle of 46°. This was chosen as an intermediate contact angle that would generate some pyrite recovery,

but not be high enough to destabilise the froth. The general trend of the graph shows a power law dependence of the froth stability on particle size. The froth is most stable at small particle sizes, with the highest froth stability of 68 s, and least stable at large particle sizes, with the lowest froth stability of 7.7 s. There is a steep initial decrease in the froth stability as the particle size increases up until about 50 µm, whereafter the dependence of froth stability on particle size becomes less pronounced.

It was observed visually in the stability column that fine particles formed fine bubbles that grew steadily up the pulp-froth interface. The froth was very stable and carried a high amount of water and solid particles. In contrast, coarse particles formed froths with larger bubbles that were very unstable. The froth had a low concentration of particles. As such, the froth height obtained for coarse particles was low.

It is interesting to note that the data points fall on the same relationship irrespective of whether they are for mixtures or discrete particle sizes. Thus, the weighted geometric mean (as described earlier in Chapter 4) seems to be a good approximation of the characteristics of the particle size distribution as applied to froth stability. The particles stabilise the froth to the same extent whether they are, for example, a mixture of small and large particles or a narrow size range of medium sized particles. This may be unexpected due to the work of Dippenaar (1982b) who found that the rate determining step in the rupture of bubbles by hydrophobic particles of different sizes was the rate at which the thinning of the films occurred. Large particles ruptured films faster since less film thinning was required before the particle could bridge the film and cause migration of the three-phase boundary lines to the same point. Thus, it may have been expected that a single large particle would be sufficient to bridge the film and cause rupture. However, it is clear from Figure 5.2 that all particle size combinations fall on the same relationship. For example, the geometric mean of 49.4 µm represents 80% particles less than 25 µm and 20% particles in the 150 to 300 µm size class. Thus, it might be expected that the 20% of large particles would have a disproportionate effect and destabilise the froth to a greater extent than a mixture with less large particles. However, this was clearly not the case.

The horizontal line in Figure 5.2 shows the froth stability of the 2-phase system. Thus, it is evident that any mixture with an average diameter greater than about 30 µm acts as a destabilising force on the froth. These would be conditions that have a large ratio

of hydrophobic to hydrophilic particles reporting to the froth, since there will be less particles reporting to the froth by entrainment and more by true flotation. These particles may be classified as film breakers due to their froth destabilising effect.

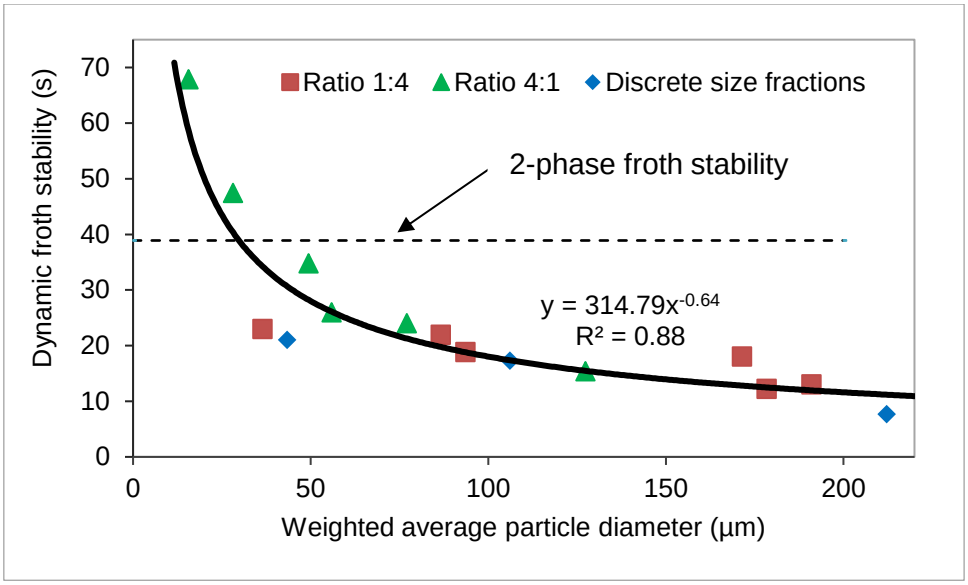

Figure 5.2: Effect of particle size on dynamic froth stability at 25% pulp density and a pyrite contact angle of 46° in a non-overflowing stability column. Ratio 1:4 refers to a mixture with 20% of one size class and 80% of another size class. The reader is referred to Table 4.3 in Chapter 4.

Froth stability was also measured using the continuously operated flotation cell. It is well known that the characteristics of the froth such as its stability, mobility and gas hold-up are influenced by the amount of water entering the froth phase and this will ultimately influence the water and solids recoveries to the concentrate launder (Zheng *et al.*, 2006). Figure 5.3 shows the variation in water recovery as a function of the feed particle size.

Similarly, to the stability column data, it can be seen that the water recovery has a power law dependence on the particle size. Small particles result in a higher water recovery than large particles and this dependence becomes less pronounced as the particle size increases. It was seen during the experimentation stage that the fine particles formed froths that were very mobile and had a high mass pull. On the contrary, froths formed with coarse particles were low in volume, with a low mass pull. Again, the dependence of froth stability on particle size is more pronounced below a particle size of 50 µm.

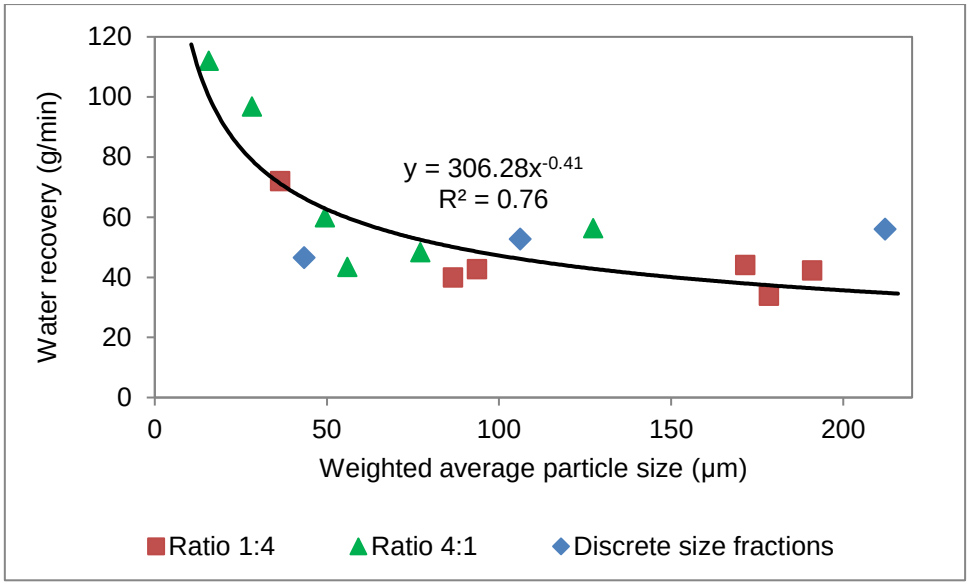

Figure 5.3: Recovery of water as a function of particle size at a constant pulp density of 25% and a pyrite contact angle of 46° in a continuously operated bench-scale flotation column. Ratio 1:4 refers to a mixture with 20% of once size class and 80% of another size class. The reader is referred to Table 4.3 in Chapter 4.

The water recovery versus particle size results are consistent with experimental findings earlier reported by Feng & Aldrich (1999) who investigated particle size effects on flotation performance of complex sulphide ores and showed that water recovery decreased as particle size increased, although this is the first time that such a detailed relationship between water recovery (froth stability) and particle size has been established.

The bubble bursting phenomena at the froth surface also provides an indication of the extent of the stability of the froth. A higher burst rate indicates a lower froth stability. Figure 5.4 shows the top-of-froth bubble burst rate as a function of feed particle size. A power law relationship is seen to exist between particle size and bubble burst rate. As particle size increases, the burst rate increases. This relationship is obeyed by both particle mixtures and the discrete particle size fractions used in the experiments. The shape of the bubble burst rate versus particle size graph is the inverse of the water recovery versus particle size graph (Figure 5.3), as expected. As can be seen, coarse particles generally form froths with a high burst rate compared to small particles. The variation in the bubble bursting phenomena is between 2 to 5 bubbles bursting per second.

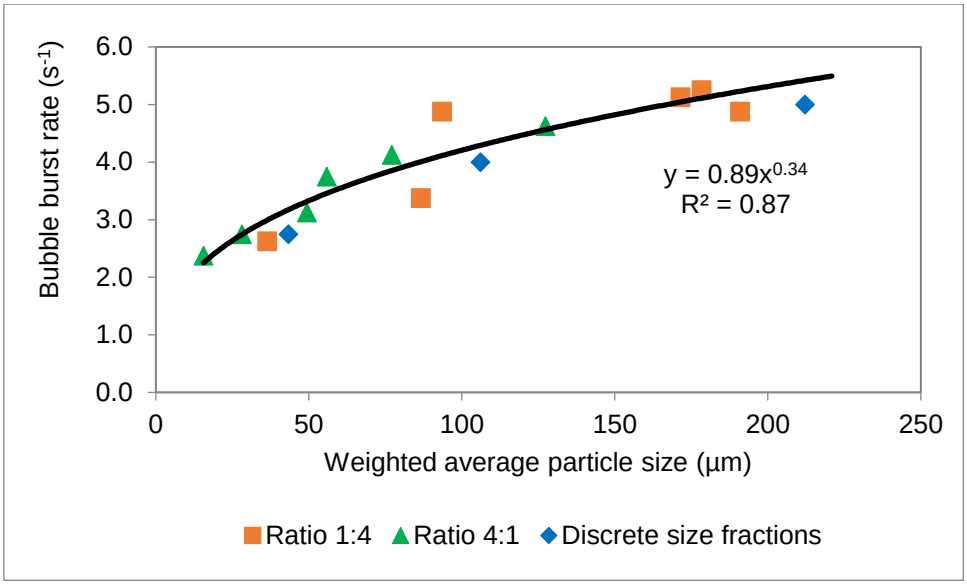

Figure 5.4: Effect of particle size on bubble burst rate at a constant pulp density of 25% and pyrite contact angle of 46°as measured from a continuously operated bench-scale flotation column. Ratio 1:4 refers to a mixture with 20% of once size class and 80% of another size class. The reader is referred to Table 4.3 in Chapter 4.

5.2.3. Relationship between froth stability and feed particle specific surface area

An inverse relation exists between particle size and specific surface area (Jiqiao and Baiyun, 2001; Hosokawa *et al., 2012*), i.e.

$$d = \frac{\alpha}{A_{BET}\,\rho} \qquad \text{Equation 5.1}$$

Where d = particle diameter (cm), α = shape factor (6 ≤ α ≤ 18; α = 6 for spherical particles), A_{BET} = specific surface area as determined by the BET technique (cm^2/g), and ρ = particle density (g/cm^3).

A particle with a large surface area will have a small size. On the contrary, large particles have small surface area relative to smaller particles of similar mass. This implies that in studying froth stabilisation, the effects of size and surface area should be considered concurrently. It is important to note that flotation is a kinetic process which is surface area driven. The relationship between particle surface area, size, and the froth phase stability can be looked at by considering the adsorption of the particle at the air-water interface. Binks (2002) provides an extensive discussion on particles as surfactants. Particles can act as surfactant molecules when they adsorb at the air-water interface and in so doing stabilise froths. A greater adsorption at the air-water

interface results in a more stable interface. When particles adsorb at the air-water interface, they can form a dense film (monolayer or multilayer) around the dispersed bubble surfaces impeding rupture and coalescence. The extent to which they can prevent rupture and coalescence may be dependent on the particles' surface area.

The reciprocal relationship between particle size and specific surface area, as shown in Equation 5.2, is used in Figure 5.5 to illustrate the relationship between the dynamic froth stability, $\sum$, and feed particle specific surface area. This shows that the dynamic froth stability is linearly dependent on the specific surface area of the particles. Small particles with a high surface area will create froths with high dynamic stability. Coarse particles on the other hand, because of their large size and small surface area, will have a low influence in raising the stability of the froth. In the same way that the strength of a frother increases with molecular weight, the increasing specific surface area of the particles can be visualised as the "strength" of their ability to stabilise the froth. The more surface area available per unit mass, the greater the froth stabilising effect. This may be due to a greater adsorbed surface area, leading to changes in capillary pressure and also a greater viscosity because of an increase in fine particles reporting to the froth by entrainment. It may be expected that the slope of the line will be related to the hydrophobicity, or froth stabilising/destabilising effect of the particles. Particles with optimum hydrophobicities for froth stabilisation will have a greater slope than particles of low hydrophobicity, which will have poor froth stabilising ability. Particles of very high hydrophobicities may also have a lesser slope due to their destabilising effect on the froth. The y-intercept may represent the lowest froth stability at very large particle sizes. These aspects will be discussed further in the following chapter. This relationship may prove to be a useful way in which to characterise an ore in terms of its frothing properties, which traditional batch flotation tests do not provide for.

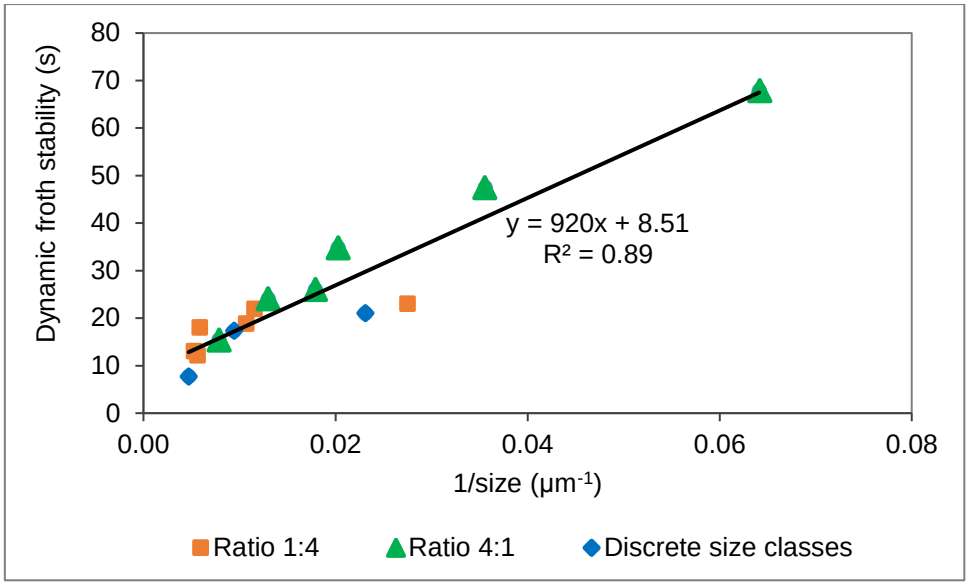

Figure 5.5: Relationship between dynamic froth stability and reciprocal particle size, representing specific surface area

Analysis of water recovery based on surface area is shown Figure 5.6. The linear dependence of water recovery on surface area is seen to be similar to the dynamic froth stability data.

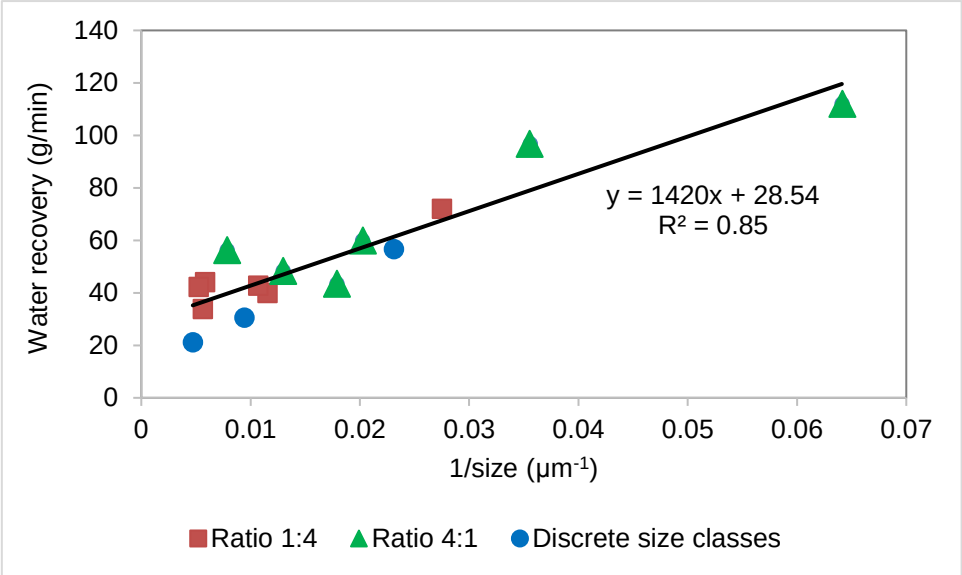

Figure 5.6: Dependence of water recovery on specific surface area

Figure 5.7 shows the dependence of the bubble burst rate on specific surface area. 1/bubble burst rate is defined here as the time taken for a given number of bubbles to burst. It thus depicts the life time of a given number of bubbles. This time is seen to increase with increasing surface area. An increase in particle surface area leads to a more stable froth and less bubble bursting events.

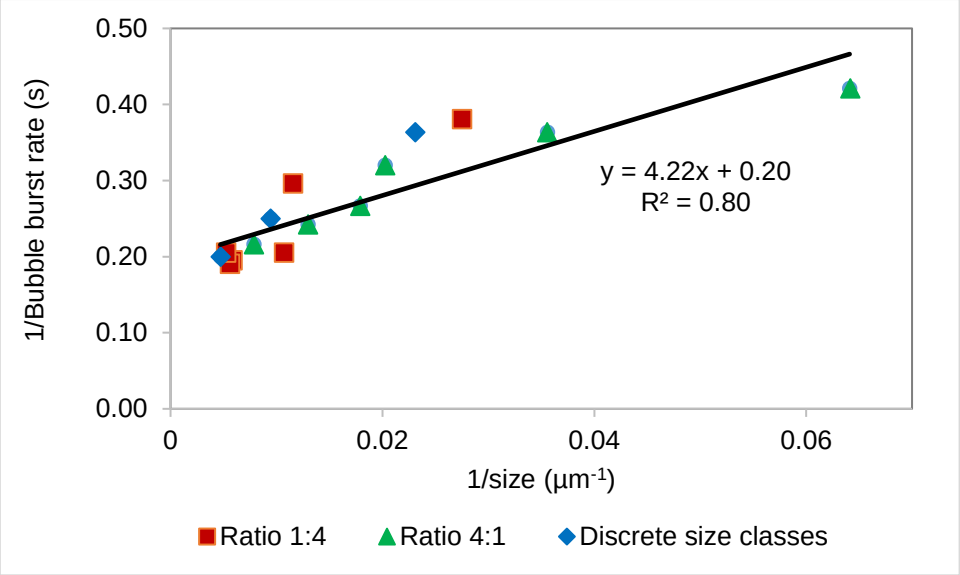

Figure 5.7: Influence of particle surface area on reciprocal bubble burst rate

It is clearly seen in Figure 5.7 that coarse particles cause an increase in bubble bursting events over fine particles. The bubble life time at the froth surface is thus higher with fine particles than with coarse particles.

The reciprocal feed particle size has provided an important relationship with froth stability. For modelling purposes, it is a simple process to use the feed particle size distribution as this can easily be measured from the feed being sent to the flotation process. The relationship between froth stability and the reciprocal of feed particle size is a simple linear relationship. Should this relationship hold for other conditions and ore types, it may prove extremely valuable in predicting frothing characteristics that could be used to predict mass pull and flotation recovery.

5.2.4. A model describing the relationship between froth stability and concentrate particle surface area

It is evident that it is the particles in the froth phase that affect the froth stability and not the feed particles, which have been analysed up until now. In addition, it is not only the size of particles in the froth that affect the stability, but the amount of these particles. Therefore, it was hypothesised that the froth stability is a function of the concentrate particle surface area.

The effect of surface area on froth stability can be visualised in terms of the packing of particles at the interface. The packing of particles in the films can be considered as an adsorption process. The fundamental concept uses the adsorption isotherm to

relate the quantity of the adsorbed material to the pressure or concentration in the bulk phase at constant temperature. The adsorption isotherm enables the efficiency of the separation process to be assessed based upon the adsorption of the adsorbate to the adsorbent. One of several equations that has been proposed to explain the adsorption phenomenon is the Langmuir isotherm equation. It was derived kinetically based on the assumption that there is a definite and energetically equivalent number of adsorption sites at each of which one molecule of adsorbate may be adsorbed (Dabrowski, 2001). Two main types of adsorption processes can be identified; physisorption resulting from Van der Waals forces or chemisorption resulting from a chemical process. Physisorption is a reversible phenomenon, which occurs at a temperature lower or close to the critical temperature of an adsorbed substance. In contrast, chemisorption is a specific process occurring at a temperature usually much higher than the critical temperature. This theory can be loosely applied to the process of particle adsorption at the air-water interface and the resultant froth stability in the same way that a surfactant molecule may adsorb at the air-water interface.

Using the above assumptions, a Langmuir type isotherm relationship shown in Equation 5.2 can be used to model the data obtained:

$$\sigma = \sigma_0 + \sigma_{max}\left(\frac{p.a_s}{1+p.a_s}\right) \qquad \text{Equation 5.2}$$

Where σ is the froth stability, σ_0 is the initial froth stability, σ_{max} is the maximum froth stability, p is a stabilisation constant and a_s is the surface area of the particles in the concentrate.

The fitted model is shown in Figure 5.8 showing the variation of dynamic froth stability with concentrate surface area at constant hydrophobicity (particles contact angle of 46°).

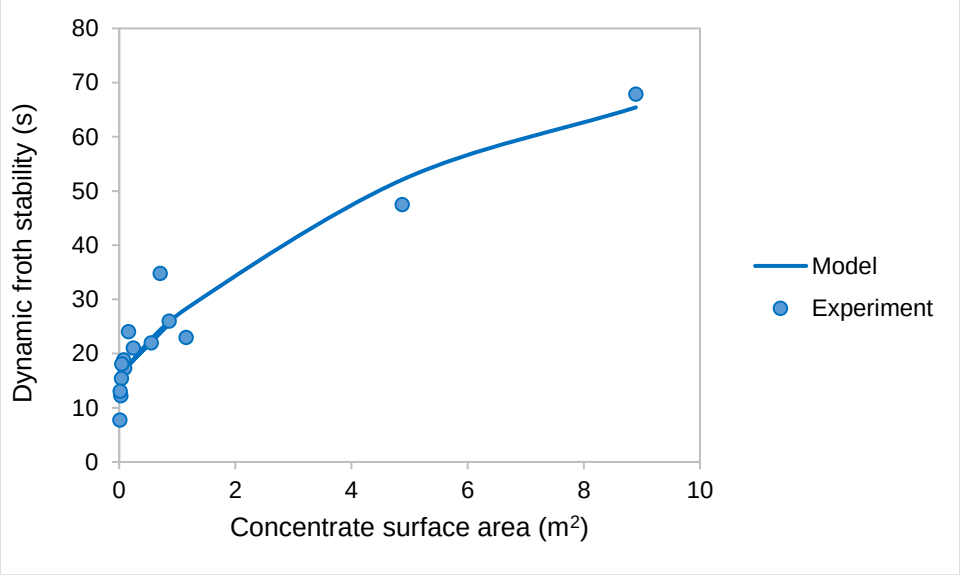

Figure 5.8: Influence of particle surface area on dynamic froth stability at a constant hydrophobicity of contact angle 46°.

It is clear that the Langmuir isotherm model is a relatively good fit to the experimental dynamic froth stability data. This shows that it is possible to model froth stability in terms of the particle packing at the air-water interface in much the same way that surfactant molecular packing at the interface is modelled. The particle packing affects the surface tension in the same way that surfactant molecules do. The fitted constants for the data set in Figure 5.9 were: σ_{max} = 89.52 s, σ_0 = 15.91 s and p = 0.14. The initial froth stability, σ_0, is not the 2-phase froth stability, as might be supposed since this was measured for the case of the non-overflowing stability column and was found to be higher than the modelled value, i.e. considering the stability column, it was 39 s for the experiment versus 15.91 s for the case of the model. This shows that there are a substantial number of particles above a certain size that break down the structure of the foam. The constant, p, can be approximated as the ability of the particles to reduce film drainage and bubble coalescence. In essence, it can be referred to as a stabilisation constant. This model will be discussed in more detail in the following chapter (Chapter 6) when the effects of particle hydrophobicity are also considered.

5.2.5. Comparison of froth stability measurements

The non-overflowing froth stability column provides a practical and simple method for determining froth stability, which is not taken into account by standard laboratory batch flotation tests. In addition, it is a potentially scalable measure, which is the subject of ongoing research at the Centre for Minerals Research. However, it does not provide

any metallurgical data, which is why the bench-scale continuous column flotation cell was designed to simultaneously collect froth stability and metallurgical data. Three froth stability measures were used in the continuous column flotation cell: water recovery, top-of-froth bubble burst rate and side-of-froth bubble coalescence rate. The side-of-froth bubble coalescence rate data was discarded since the growth rate of the bubbles up the column length was not sufficient to distinguish between different conditions. Water recovery has often been used as a proxy for froth stability since a more stable froth will hold more water in the thin films and Plateau borders (Triffet & Cilliers, 2006).

The following discussion compares the three measurement techniques and the two measurement devices with specific reference to the factors affecting the froth stability.

- Bubble generation was by means of a ceramic tubular sparger for the bench scale flotation column, whereas a sintered glass P2 frit with a pore size of 40 – 100 µm placed at the bottom of the column was used in the non-overflowing stability column. Bubble size generated by the frit was approximately 1.5 mm, while those generated by the sparger were smaller than 1 mm. This would certainly have an effect on the froth stability. Smaller pulp bubble sizes result in larger apparent froth stabilities (Geldenhuys, 2017). However, since the bubble sizes in both devices were held constant, the trends would be expected to be the same. Thus, absolute values of froth stability would differ between the different measurement types and devices, but the *p* constant in Equation 5.2, which defines the ability of the particles to stabilise the froth, should be expected to be similar.
- The superficial air velocity used for both pieces of equipment was 1 cm/s. The air flow rate will govern how much water reports to the froth and subsequently to the concentrate launder. Likewise, this should also govern the growth rate of the froth if the frother dosage is held constant in both devices. Since both parameters were held constant, these were not expected to differ between the two devices or different measurement techniques.
- The two devices employed were of different diameters. It is expected that the rate of drainage will be higher in the continuous flotation column due to its higher wall-to-froth surface area ratio (smaller diameter). The wall has been shown to have a higher drainage rate than the froth in previous studies

(Geldenhuys, 2017). However, since this difference holds constant between the two devices, it is expected to have an effect on the absolute value of the froth stability measurement, but not on the ability of the particles to stabilise the froth, the p value.

- The two devices differ in operating mode. The bench-scale flotation column was operated continuously at steady state whereas the non-overflowing stability column was operated in batch mode. Thus, once the maximum froth height is achieved in the stability column, further particles reporting to the froth serve to overload the froth and there is a collapse in froth height. However, the particles then build again and the froth height can be shown to oscillate around a mean, which is the maximum froth height. If it can be shown that the two devices show similar trends, then it can be assumed that the froth stability column is a suitable device for measuring froth stability. This will be shown in Figure 5.9.
- Both devices are dynamic processes, meaning that liquid is reporting to the froth phase continuously while drainage is occurring simultaneously. This is as opposed to a static process, where there is no air input and only drainage is occurring. The froth growth height, bubble burst rate and water recovery will all be driven by these two processes: water and particles reporting into the froth, while simultaneously draining. Liquid content of the froth at the surface affects the liquid films at the top of the froth (Neethling and Cilliers, 2003). Wet froths have smaller bubbles and therefore contain more water, whereas dry froths have larger bubbles and contain less water (Morar *et al.*, 2012a; Neethling and Cilliers, 2003). Since bubble coalescence causes materials (particles and liquid trapped within the lamella) to detach from the bubbles, the rate of coalescence will be higher in a dry froth than in a wet froth. The bubble burst rate at the top of the froth is related to the incoming bubble size as well as pulp conditions. It is expected that the wet froth will experience less surface bubble bursting phenomena than the dry froth. Less surface bubble bursting phenomena implies more water flow over the weir and therefore a higher water recovery.

It was seen in section 5.2.4. that the Langmuir isotherm expression is a good way to model experimental froth stability data. In this section, a comparison of the model predictions for the three froth stability measurement proxies is explored as shown in

Figure 5.9. It can be seen that the model predictions are in good agreement with the experimental data for all three froth stability measurement proxies.

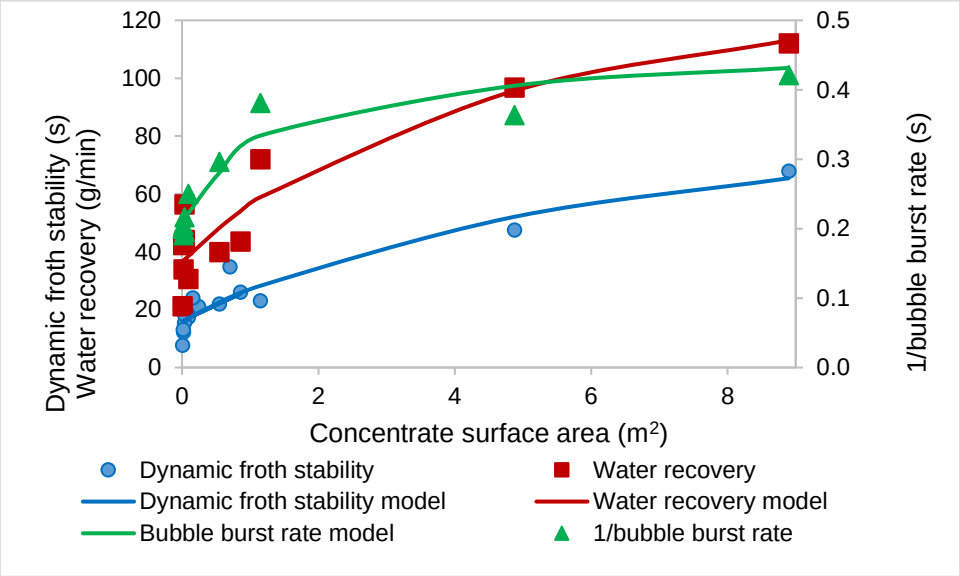

Figure 5.9: The Langmuir isotherm expression predictions for each of the three froth stability measurement proxies data set.

Table 5.1 shows values of the initial froth stabilities, σ_0, maximum froth stabilities, σ_{max}, and the stabilisation constant, p for each of the three froth stability measurement proxies. The values of p are very similar for all the three proxies as expected and as discussed above. This shows that the same mechanisms are driving the froth stability in both devices. Thus, the froth stability column has been shown to be a simple device that produces similar results to a continuous device and has the possibility of being scalable.

Table 5.1: Values of the initial froth stabilities and the stability constant, p for each froth stability measurement proxy

	Dynamic froth stability	1/burst bubble rate	Water recovery
σ_0	15.91 s	0.20 s	36.29 g/min
σ_{max}	89.52 s	0.42 s	119.29 g/min
p	0.14	0.15	0.20

5.2.6. Particle size and flotation performance

5.2.6.1. Overall recovery and froth recovery

Flotation performance was monitored concurrently with the froth stability measurements. Figure 5.10 shows that the pyrite recovery follows the same type of

power law dependence on particle size as the froth stability data, albeit with some scatter in the data. This recovery is a combination of the pulp phase and froth phase recovery. According to the literature, pulp phase recovery follows the classic dependence on particle size first put forward by Gaudin *et al*. (1931), where smaller particles and larger particles are more difficult to recover than intermediate sized particles. These recovery losses occur mainly due to limitations associated with bubble-particle adhesion and collision rates, detachment and buoyancy (Kohmuench *et al.*, 2010). Interestingly, Figure 5.10 shows that there is not a decrease in the pyrite recovery at smaller particle sizes. This indicates that the froth zone is more important to the recovery of pyrite than the pulp zone. The expected decrease in pyrite recovery in the pulp zone at smaller particle sizes is offset by the higher froth stability at those particle sizes, which aids in the recovery of pyrite.

This is supported by the froth recovery data shown in Figure 5.11. This shows that the amount of pyrite entering the froth that is recovered to the final concentrate is greater for the small particle sizes than for the large particle sizes. This supports the fact that the more stable froth at smaller particle sizes allows for greater overall recovery than would normally be expected. This also serves to show the strong role that froth stability plays in valuable mineral recovery. With an increase in froth stability, there is a concomitant increase in valuable mineral recovery as shown in Figure 5.14. This shows the value of being able to predict froth stability for different particle properties. The incorporation of froth stability values into a phenomenological froth flotation model is a subject of ongoing research within the Centre for Minerals Research.

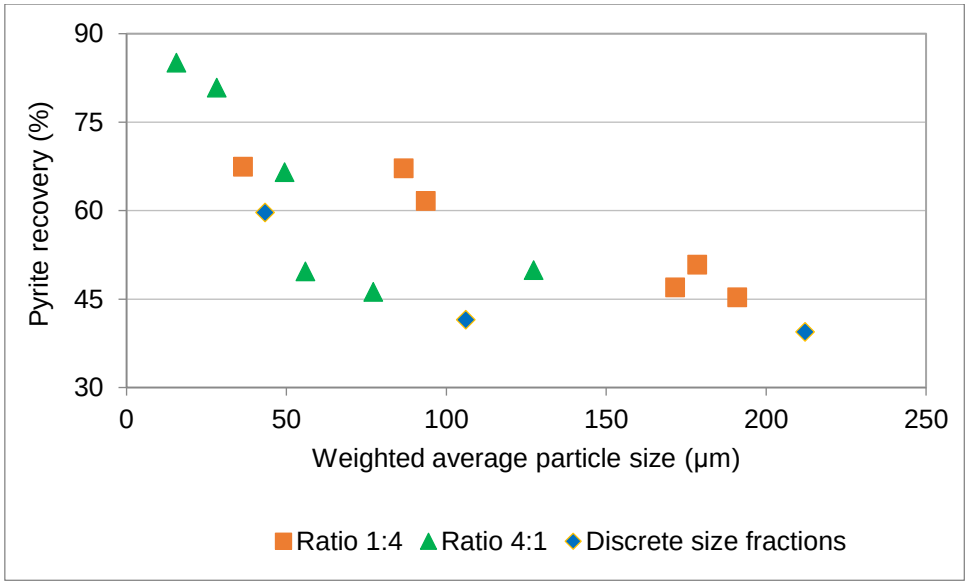

Figure 5.10: Effect of particle size on pyrite recovery at 25% pulp density in the continuously operated bench-scale flotation column cell

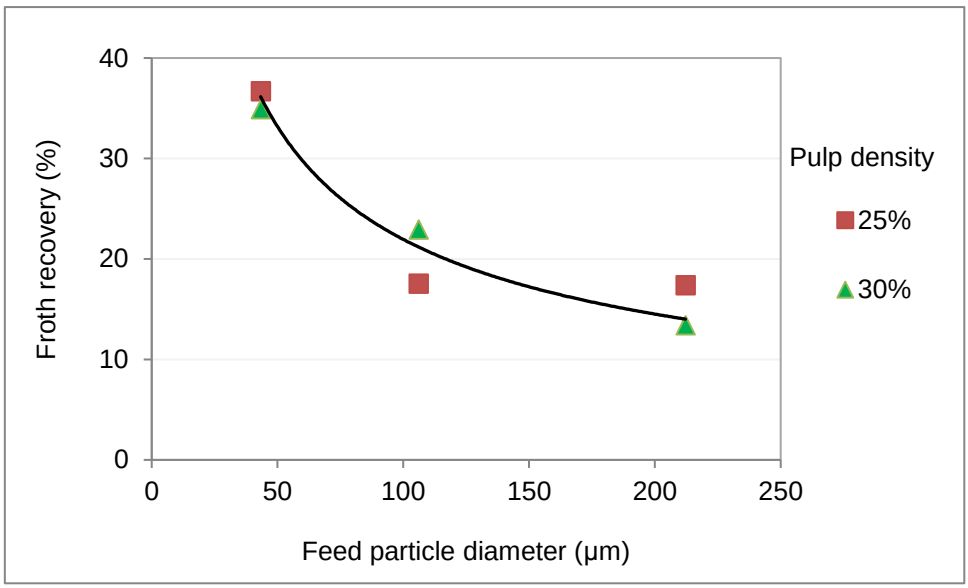

Figure 5.11: Variation of froth recovery with particle size and concentration (25% and 30% pulp density)

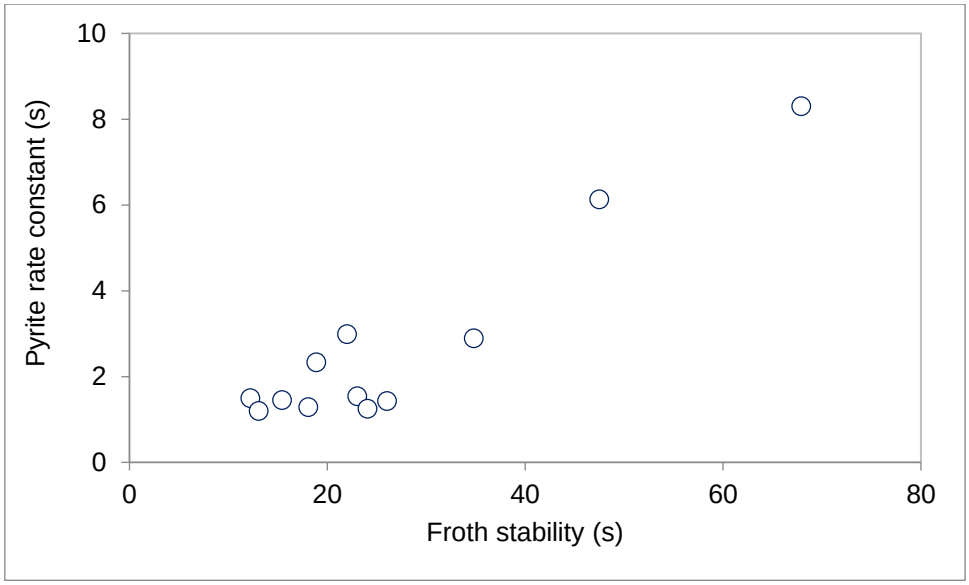

Figure 5.12: Rate constants for pyrite flotation as a function of froth stability

5.2.6.2. Effect of hydrophobic and hydrophilic particles

In order to further understand the effect of particles on froth stability, the concentrate was characterised in terms of the particles' hydrophobicity or hydrophilicity. This is because mechanical carry-over of unattached hydrophilic particles in the water flowing through the froth lamellae occurs alongside true flotation of attached particles to bubble surfaces. Entrainment functions were calculated for each of the size classes by assuming that all the quartz was recovered by entrainment only, since quartz is highly hydrophilic. The slope of the quartz versus water recovery graph gives the classic straight line entrainment function as shown in Figure 5.13. This is similar to the works of Kracht (2016) and Moyo (2005). The slope of the graph gives the entrainability or entrainment factor. It is clearly seen that the quartz particles with a size range of 25 – 75 µm are easily entrained. However, the coarse particles in the size ranges of 75 – 150 and 150 – 300 µm are not affected by entrainment. Coarse quartz particles are not entrained to the concentrate launder.

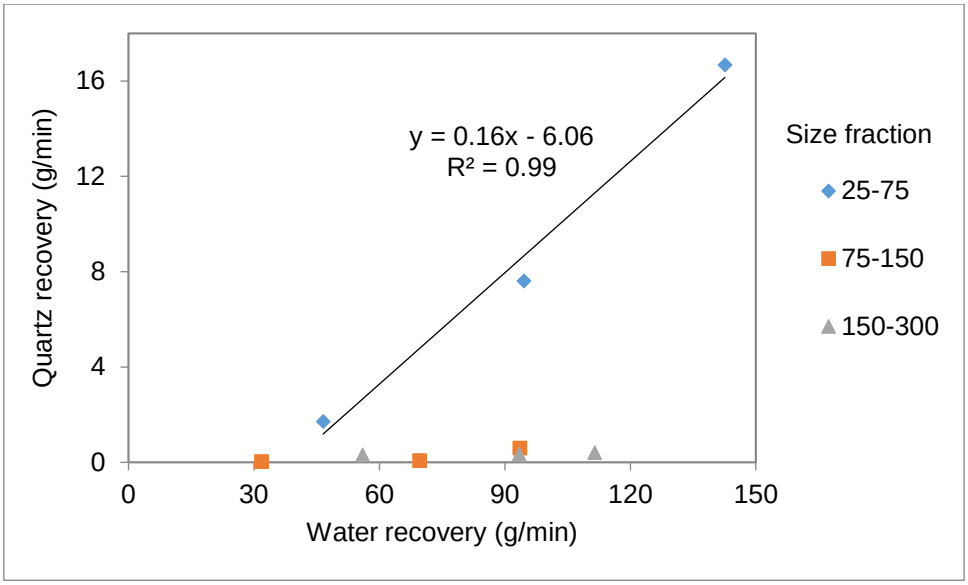

Figure 5.13: Entrainment of quartz particles of different size fractions

It is significant that froth stability rises sharply for a feed size less than 50 µm (as shown in Figure 5.2, and Figure 5.3). This raises the question of whether the froth is stabilised by entrained particles, since the amount of these would be expected to rise sharply at a particle size of less than 50 µm, or by naturally floatable particles that are attached at the interface, or by a combination of the two. The proposed mechanisms of film stabilisation incorporate particles attached at the air-water interface as well as particles with complete wettability that reside within the films, as discussed in Chapter three.

Figure 5.14 shows the amount of total solids reporting to the concentrate as a function of the feed particle size. In addition, the total solids have been separated into hydrophilic material (the quartz), which is presumed to be recovered mostly by entrainment and the hydrophobic material (the pyrite and talc), which is recovered mostly by true flotation and is attached at the air-water interface. It is evident from Figure 5.14 that the amount of hydrophilic quartz reporting to the concentrate increases sharply below a feed size of 50 µm. Although there is some scatter in the data, little quartz is recovered to the concentrate above a feed size of 50 µm. This is in line with many previous studies that have shown entrainment to be significant below a particle size of 50 µm (Smith & Warren, 1989). The recovery of hydrophobic material follows a gradual, linear increase as particle size decreases. Thus, it is evident that the dramatic increase in froth stability below a particle size of 50 µm can be attributed to the large increase in the amount of hydrophilic particles reporting to the froth. This

suggests that the drainage of the thin films is affected by the presence of hydrophilic particles within the films and that this has a large effect on the froth stability. The drainage is affected by an increase in viscosity of the liquid making up the films, which will increase with decreasing particle size and increasing particle mass or area. In addition, froth stability may be described by the pressure gradient between bubbles and interfilm fluid, or the capillary pressure. The maximum capillary pressure is inversely proportional to the particle size (as discussed in Chapter 4), which shows that smaller particles are more effective at preventing drainage and stabilising froths. Thus, it is expected that the main mechanism stabilising froths with feed particle sizes of less than 50 µm is the increased capillary pressure gradients and viscosities of the thin films. Above 50 µm, the majority of particles reporting to the froth phase are hydrophobic in nature. The line in Figure 5.14 shows the froth stability of the 2-phase system. Thus, it is evident that any mixture with an average diameter greater than 30 µm acts as a destabilising force on the froth. These would be conditions that have a large ratio of hydrophobic to hydrophilic particles reporting to the froth. These particles may be classified as film breakers due to their froth destabilising effect.

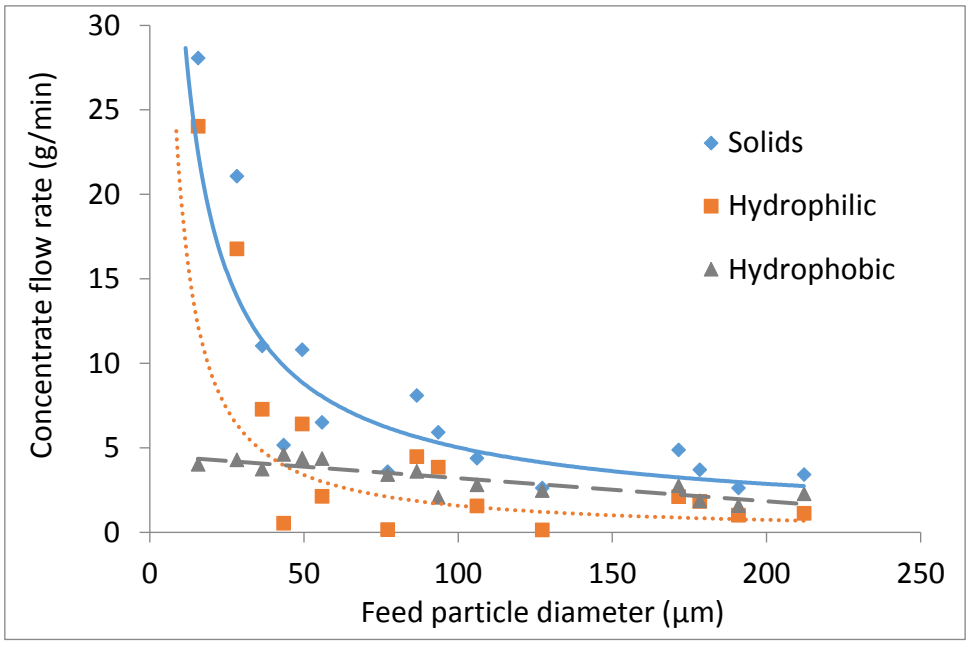

Figure 5.14: Flowrate of total solids (blue diamonds), hydrophilic material in the form of quartz (orange squares) and hydrophobic material in the form of pyrite and talc (grey triangles) as a function of feed particle diameter.

5.3. Conclusions

The effect of particle size on froth stability has been studied experimentally using a synthetic ore made of three components, i.e. pyrite, talc, and quartz. Experiments were performed using particles of discrete size classes as well as mixtures of discrete size classes. These were floated in a non-overflowing froth stability column and in a continuously operated bench-scale column flotation cell and the froth stability was measured.

There was a power law relationship between froth stability and feed particle size, with all particle size combinations falling onto the same relationship. Froth stability was shown to decrease with increasing particle size. There was a large increase in froth stabilities for average feed particle sizes below 50 μm and this was shown to be largely due to the large increase in particles reporting to the froth by entrainment. It was suggested that these particles modified the viscosity of the thin films, reducing drainage and thus stabilising the froths. The same trend was found to be consistent for both water recovery and bubble burst rate techniques.

Froth stability was shown to have a linear relationship with the reciprocal of feed particle size. The reciprocal of feed particle size is used to represent the specific surface area of the feed particles as shown in Equation 5.2. The larger the specific surface area of the particles, the greater their froth stabilising effect. This is the first time that such a linear relationship has been shown and may prove a useful tool in predicting the froth characteristics of ore samples.

A Langmuir-type equation was used to model the relationship between froth stability and concentrate surface area. It was found that the model was a good fit to the experimental data. This shows that it is possible to model froth stability in terms of the particle packing at the air-water interface in much the same way that surfactant molecular packing at the interface is modelled. The increasing particle surface area affects the surface tension of the films and reduces film drainage. The model has three constants: the initial froth stability, σ_o, the maximum froth stability, σ_{max}, and a constant, p, that defines the curvature of the plot and describes the ability of the particles to stabilise the froth. When comparing the two different flotation devices and the three different measurement techniques, it was found that, as expected, the

absolute values of froth stability differed between the measurements. However, the stability constant, *p*, was similar between the three different measurements. This showed that the three measurements and two devices were consistent in their determination of the froth stabilising abilities of the different particle size conditions. This was found to be encouraging for the future use of the froth stability column as a simple and effective method of characterising froth stability for scale-up and design.

The continuous flotation column was used to measure, not only froth stability, but the flotation performance at the different particle size conditions. This confirmed that froth stability was an overriding factor in the recovery of valuable particles. There was an approximately linear relationship between froth stability and the valuable mineral rate constant, with an increase in froth stability resulting in an increase in the pyrite rate constant. This affirms the need for froth characteristics to be taken into account during scale-up and design, which are neglected in the current batch flotation methodology.

CHAPTER SIX

6. THE EFFECT OF PARTICLE HYDROPHOBICITY AND THE INTERACTIVE EFFECTS OF PARTICLE SIZE AND HYDROPHOBICITY ON FROTH STABILITY

6.1. Introduction

The degree of hydrophobicity of a mineral surface affects the recovery of valuable mineral particles in the flotation process. Certain mineral surfaces possess an inherent hydrophobicity, although this may be improved with the use of surface active reagents known as collectors. For the flotation process to be successful, a mineral particle must attach to an air bubble. In so doing, the air bubble will displace water from the mineral particle surface making an effective contact. However, for this to occur, the mineral particle surface has to be hydrophobic to an appreciable degree. The extent to which the bubble will displace water from the mineral surface forms the basis for the measure of the degree of hydrophobicity (Rao, 2013).

In Chapter 5, the effects of particle size on froth stability have been explored in great detail. This chapter presents experimental findings and discussions on the effect that mineral particle hydrophobicity and the interactive effects of particle size and hydrophobicity have on froth stability. The hypotheses being tested here are:

"Hypothesis 3: *Froth stability is greatest at a critical contact angle, below or above which froth stability decreases. This is due to bridging effects causing film rupture in highly hydrophobic particles."*

"Hypothesis 4: *Optimum froth stability is obtained with small particles of intermediate hydrophobicity. This is because large particles and particles of very high hydrophobicity rupture liquid films and so suppress the froth stability."*

The aim of this work was to develop a relationship between mineral particle hydrophobicity and froth stability. To achieve this aim, two devices were used, i.e. a bench-scale continuously operated flotation column and a non-overflowing stability column in which froth stability was quantified by means of water recovery and froth growth rate, respectively. A synthetic ore made up of hydrophilic (quartz) and

hydrophobic (pyrite and talc) components was used. The pyrite was rendered hydrophobic by conditioning the prepared slurry with potassium amyl xanthate collector. A pulp density of 25% was used for all tests. Firstly, the effect of different hydrophobicities was investigated at a constant size class of +38 -106 µm. Thereafter, mixtures of particles of different sizes were used at varying hydrophobicities.

6.2. Results and discussion

6.2.1. Quantifying mineral particle hydrophobicity – microflotation and contact angle measurements

The control of particle hydrophobicity is key to attaining the separation of minerals in flotation. In order to characterise the hydrophobicity of pyrite particles, two measurement techniques were employed. The first technique involved measuring the pyrite recovery in a microflotation cell and the second technique employed the Washburn method to measure the particle contact angle. Particle hydrophobicity was varied by increasing collector surface coverage. This is explained in detail in the Experimental section.

Figure 6.1 shows the reproducibility measurements for the microflotation tests. Three identical tests were carried out with no collector addition to ascertain the degree of reproducibility. The results obtained were within a maximum relative standard deviation of less than 10% for the recovery of pyrite over a 20-minute period.

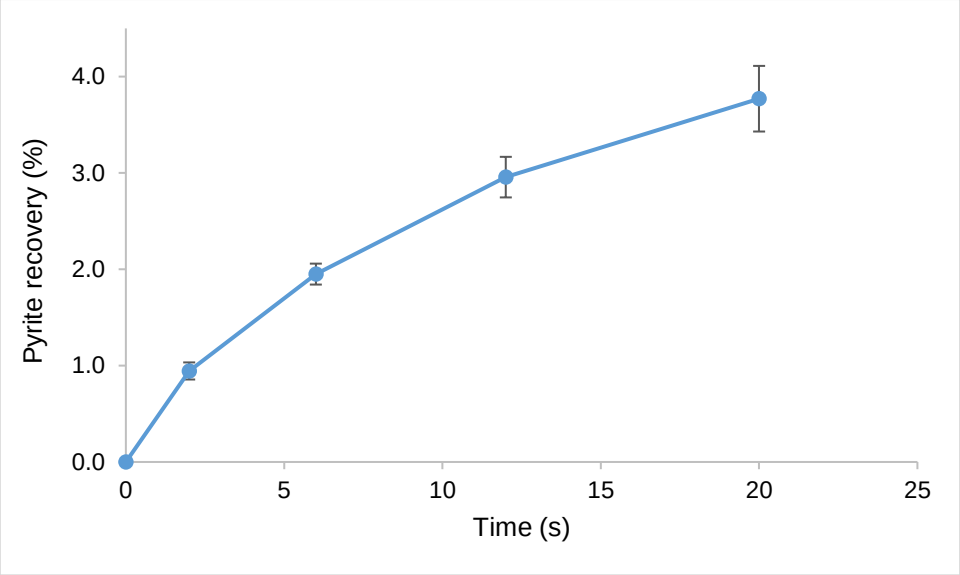

Figure 6.1: Variation of pyrite recovery with time in the microflotation cell at no collector coverage of the particle surface.

The Washburn method for studying the wettability of a solid by a liquid was employed to measure the contact angle of a bed of pyrite particles as described in the Experimental section. n-Hexane, a perfectly wetting liquid was used to determine the capillary constant. The average value of the capillary constant in both the presence and absence of collector is $(1.22 \pm 0.08)\times10^{-5}$ for three identical tests carried out. This was then used to obtain the contact angle of pyrite in water at varying collector surface coverages. Contact angle tests were done in triplicate at each collector surface coverage and an average value calculated. Maximum relative standard deviation for each test was less than 10%.

It is seen in Figure 6.2 that the pyrite particles had an initial contact angle of 37° in the absence of collector. The pyrite contact angle increases linearly with surface coverage up to approximately 80% surface coverage, where the contact angle is 64°, and thereafter, levels off. It can be clearly seen that there is not a significant increase in contact angle above one monolayer coverage. The maximum contact angle is 73.4° at 300% surface coverage.

The UCT microflotation device was used to measure the recovery of pyrite over time as explained in the experimental section. Figure 6.2 shows that there is a non-linear relationship between collector surface coverage (or contact angle) and the cumulative pyrite recovery.

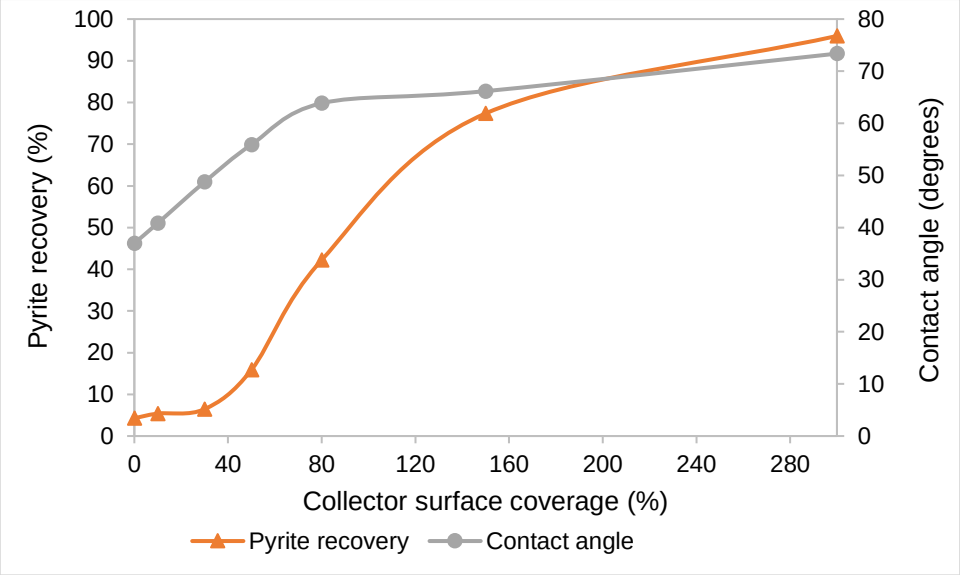

Figure 6.2: Relating the collector surface coverage to pyrite recovery in the microflotation cell and contact angles measured using the Kruss tensiometer.

Below 50% collector surface coverage, the pyrite recovery was below 20%. However, above 50% collector surface coverage, a sharp increase in pyrite recovery occurred. This is similar to results published by Blake and Ralston (1985), Crawford and Ralston (1988) and Prestidge and Ralston (1996) where they found that there existed a critical contact angle above which flotation recovery significantly increases. They observed this in the flotation of galena and hydrophobised quartz particles. The range of surface coverages from zero to 300% resulted in the presence of particles with a large range of different hydrophobicities, from particles that barely float with no collector present on the surface, to particles that are almost 100% floatable at collector surface coverage of 300%.

A measure of the particle hydrophobicity can either be made using contact angle measurements or using the recovery of the pure mineral from the microflotation cell. Johansson and Pugh (1992) plotted froth stability as a function of the recovery from the microflotation cell, but acknowledged that particle recovery is not an absolute hydrophobicity measure since it is dependent on the kinetics of the process, much as it is an easy way to conveniently represent hydrophobicity. Although contact angle measurements have been used widely as a measure of hydrophobicity, challenges do exist in obtaining reproducible results in its determination. This work has focussed on linking froth stability to contact angles measured using the Washburn technique since this is a more routinely acceptable measure of surface hydrophobicity.

6.2.2. Froth stability as a function of hydrophobicity

The froth stability was measured using the dynamic froth stability factor obtained from the non-overflowing stability column and water recovery from the continuously operated column cell. Froth stability experimental results are plotted versus the particle hydrophobicity measured in terms of contact angle. The bubble burst rate technique was abandoned in this Chapter since it is more prone to scatter. However, water recovery was maintained as a control to determine that the non-overflowing stability column continued to give equivalent results to the continuously operated bench-scale flotation column.

The results in Figure 6.3 show that increasing particle hydrophobicity results in an increase in froth stability up until a maximum, which in this case corresponds to a contact angle of between 56° and 64°. Above 64°, there is a decrease in froth stability with increasing hydrophobicity. Maximum froth stability of 78.6 g/min for water recovery and 34.6 s for dynamic stability factor are obtained. The response of the non-overflowing stability column to changes in froth stability as collector dosage was varied is within a narrow range of 22 – 35 s. This is as opposed to large variations observed with particle size differences (between 8 s and 68 s). This shows that froth stability is more sensitive to changes in particle size than particle hydrophobicity over the ranges tested. The continuously operated flotation column also showed less variability in water recovery over the hydrophobicity range than the particle size range that was tested.

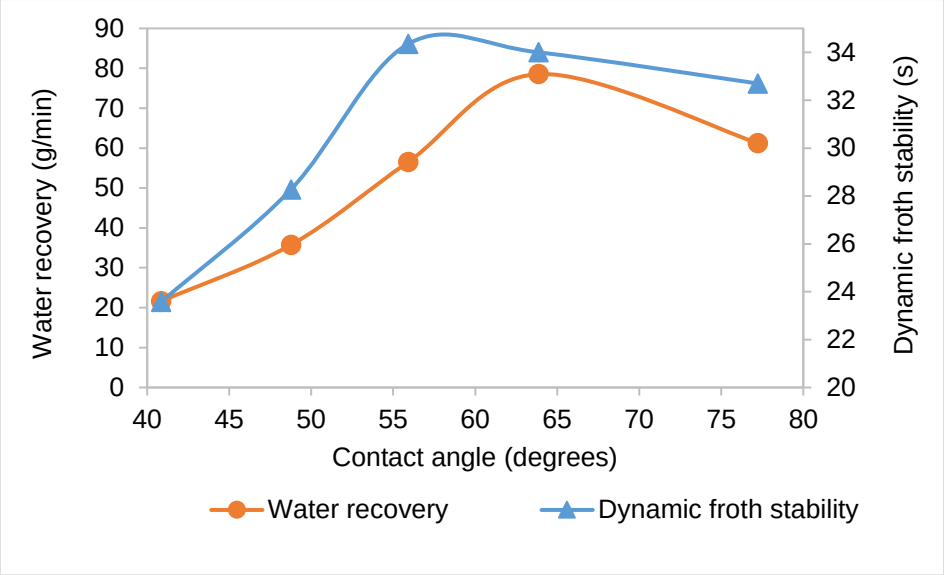

Figure 6.3: Effect of particle hydrophobicity on froth stability as measured using a non-overflowing stability column and a bench-scale continuously operated flotation column for a particle size of 38 – 106 µm.

Taking into account both froth stability factor and water recovery, the approximate contact angle that gives the optimum froth stability for the pyrite particles of +38-106 µm size range used in these experiments is 64°. This optimal contact angle is very close to the optimum experimental value of 65˚ obtained in a study by Johansson and Pugh (1992) in which they used a sparsely mineralised froth consisting of methylated quartz particles. Also, utilizing the concepts of froth stabilisation by the particle detachment theory and the maximum capillary pressure of coalescence, Kaptay (2006) was able to show that an optimum contact angle of 70˚ on particles within a foam system provided the highest stability. The system used in the current study was very different to the sparsely mineralised froth of Johansson and Pugh or the model results of Kaptay. However, it still produced results that were very similar to those obtained by these authors.

Particles with an intermediate degree of hydrophobicity interact with the air-water interface and produce stable films during the process of film formation. As a result of particles packing at the interface of the Plateau borders, the strength, rigidity and surface viscosity of the froth structure will increase. However, if the particles are weakly hydrophobic, they will stream out into the lamella, remaining dispersed and thus have little influence on froth stability. On the other hand, if the particles are highly hydrophobic, they will penetrate the interface, causing bridging and rupture (Johansson and Pugh, 1992).

Figure 6.4 shows the recovery of solids from the continuously operated flotation column as a function of the particle hydrophobicity. The total solids recovered have been decoupled into the hydrophobic components, consisting of pyrite and talc, and the hydrophilic components, consisting of quartz particles. It is clear that at low hydrophobicity (below a contact angle of 47°) and at very high hydrophobicity (above a contact angle of 70°), the amounts of both hydrophilic and hydrophobic particles reporting to the concentrate decrease and the decrease in solids recovery represents the effects of very low and very high hydrophobicities respectively on the amount of particles reporting to the concentrate launder. This is indicative that conditions of low and high hydrophobicity are not favourable for flotation recovery. However, it has already been shown in Chapter 5 that the amount of particles (and, hence, the surface area of these particles) reporting to the froth phase has a large influence on froth stability. Particles of low hydrophobicity are less floatable than particles of high hydrophobicity as shown in Figure 6.2. Therefore, less of these particles will report to the froth phase and the froth will be less stable as a result. However, at higher hydrophobicities (above 64°), Figure 6.2 shows that particle recovery in the pulp phase continues to increase. This is not reflected by an increase in froth stability, but rather a decrease in froth stability. This has been attributed to the bridging and rupture of the films by these very hydrophobic particles (Dippenaar, 1982a; Johansson and Pugh, 1992). The influence of particle surface area on froth stability will be discussed in more detail in Section 6.2.5

The theory of particle detachment energy suggests that increasing contact angle, up to 90°, results in an increase in froth stability. This suggests that, as the hydrophobic particles attach onto the air-liquid interface, the liquid films thicken and froth stability increases. This packing of hydrophobic particles at the air-liquid interface of the Plateau border will increase the rigidity and surface viscosity and strength of the froth structure. This favours the accumulation of hydrophilic quartz particles into the plateau borders by entrainment hence enhancing their recovery. The highest recovery of hydrophilic quartz is obtained at the highest froth stability when the contact angle of pyrite is 64°. A decrease in hydrophilic quartz recovery occurs as the particles attain a hydrophobicity beyond the optimum value.

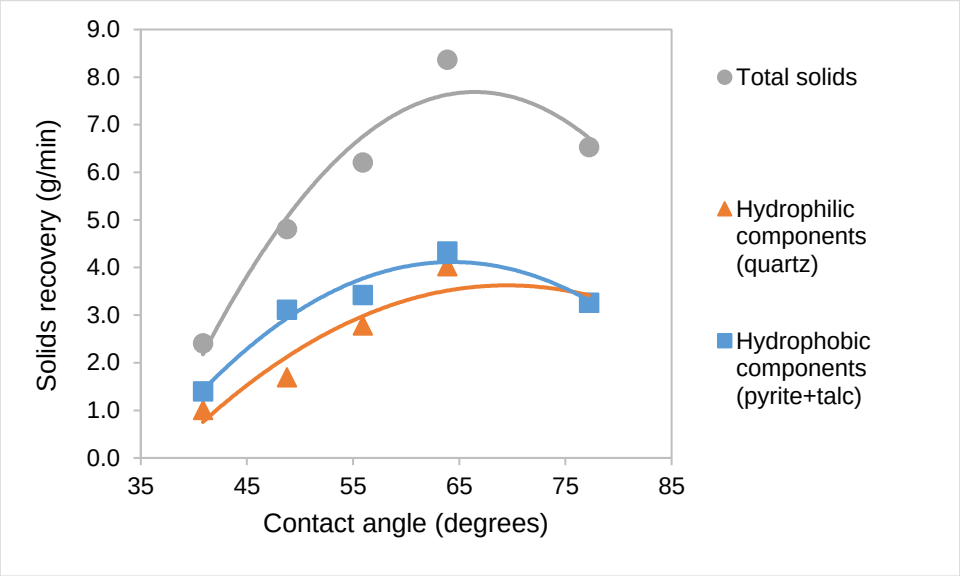

Figure 6.4: Recovery of solids (total solids, hydrophilic and hydrophobic components) as a function of hydrophobicity for a constant particle size of 38 – 106 µm.

Figure 6.5 shows the flotation performance in terms of the froth recovery and overall recovery of pyrite as a function of the particle hydrophobicity. It is clear that both froth recovery and overall pyrite recovery are initially low at low hydrophobicity. Then they increase with an increase in hydrophobicity until a maximum value is obtained, thereafter, a decrease in both is observed. The trends of the plots for recovery as a function of hydrophobicity are very similar to those for froth stability (as measured by water recovery and dynamic froth stability) as a function of hydrophobicity.

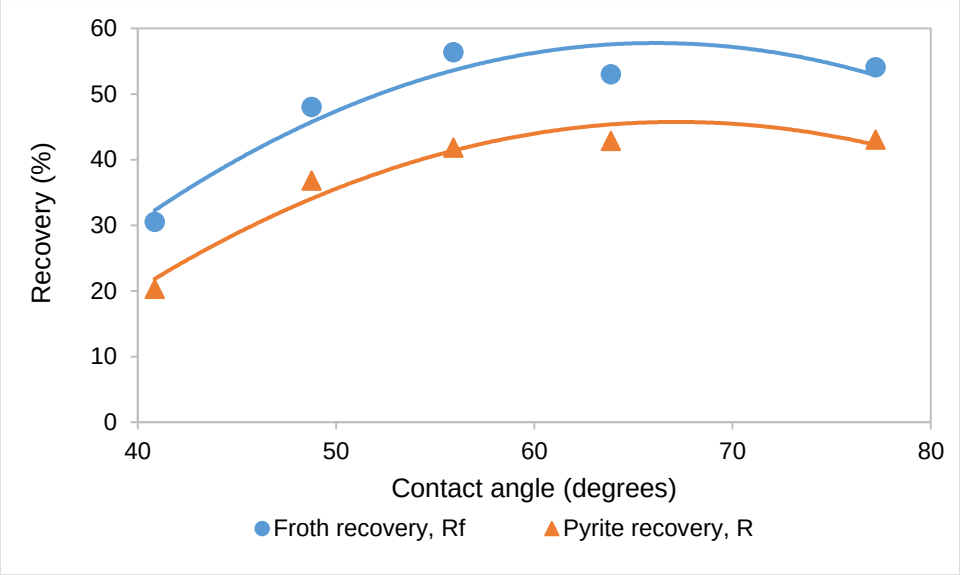

Figure 6.5: Effect of particle hydrophobicity on pyrite recovery and froth recovery for size class of 38 – 106 µm

It is clear that froth stability will affect the froth recovery, which in turn affects the overall recovery. The froth phase has the overriding influence on pyrite recovery since pulp phase recovery continues to increase with increasing hydrophobicity as shown in Figure 6.2, whereas overall recovery (and froth stability) decreases above a contact angle of 64°. This illustrates the importance of taking froth characteristics into account in flotation modelling.

6.2.3. Froth stability as a function of hydrophobicity at varying particle sizes

The influence of particle hydrophobicity on froth stability has also been studied on mixtures of particles having varying geometric mean sizes. Figure 6.6 shows the effect of particle hydrophobicity on dynamic froth stability for mixtures of particles of varying geometric mean sizes. The fine particles (28 µm mean size) gave the largest variation in froth stability while the coarse particles (127 µm mean size) generated froths with the lowest volume and the least variation with increasing hydrophobicity. Dynamic froth stability generally increased with increasing hydrophobicity up to a maximum value at a contact angle of between 68 and 69° for all particles. The life time of froths obtained with coarse particles varied between 15 and 20 s. For particles of intermediate size (mean sizes 36 and 56 µm), it varied between 30 and 50 s whereas that of fine particles (28 µm) varied between 50 and 94 s. At the optimum contact

angle, the maximum life times of these particles were: 94 s for the fine particles, 50 s for the intermediate particles (36 µm) and 20 s for the coarse particles.

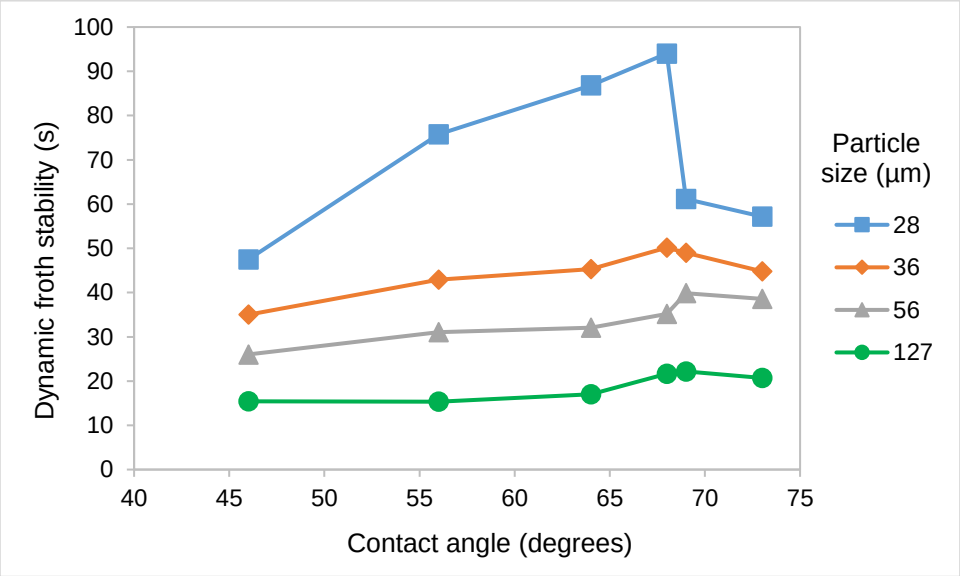

Figure 6.6: The variation of dynamic froth stability with particle hydrophobicity for particle mixtures of different geometric mean sizes.

Figure 6.7 shows the variation in water recovery from the continuously operated flotation column as a function of particle hydrophobicity for the particle mixtures of varying geometric mean sizes. Again as can be seen in comparison with the stability column data, a similar variation in froth stability (as measured by the water recovery proxy) with particle hydrophobicity for different geometric mean sizes of the particles is seen. The water recovery is initially low at low hydrophobicity and it increases as hydrophobicity increases reaching a maximum value before it decreases or levels off.

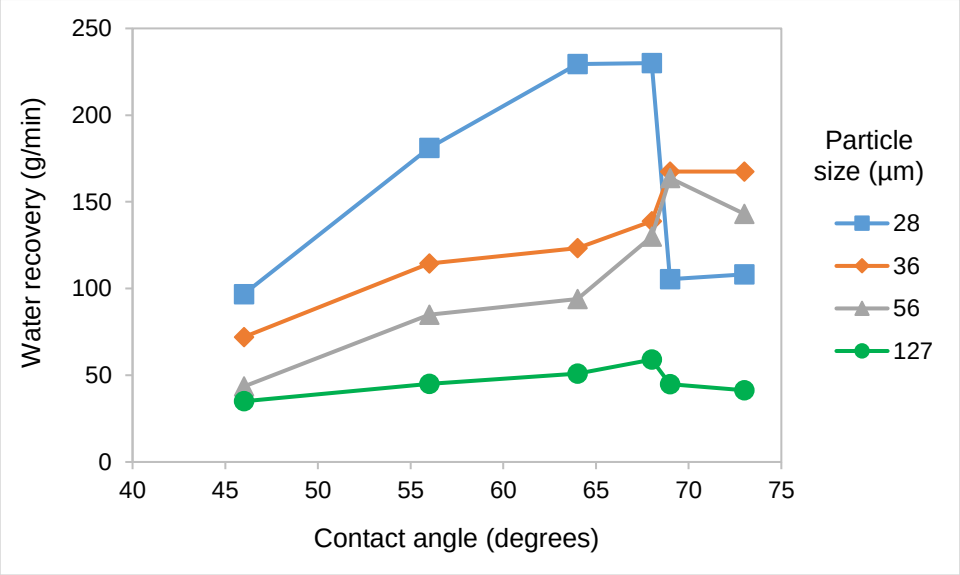

Figure 6.7: The variation of water recovery with particle hydrophobicity for particle mixtures of different geometric mean sizes.

Fine particles show significantly larger variability in froth stability with changing hydrophobicity than do larger particles. This accounts for the relatively small changes in variability that were seen in Section 6.2.2 since this particle size distribution contained no fine particles (38-106 µm). The reason for the larger variability in froth stability at fine particle sizes is proposed to be due to the large difference in the amounts (and, therefore, surface area) of these particles that report to the froth. This will be discussed in more detail in the following sections.

As discussed in Section 6.2.2, particle size still has a larger effect on froth stability than hydrophobicity with the largest difference between different particle size distributions being 72 s, while the largest difference between different contact angles was 44 s.

Results from flotation tests showing the amount of solids recovered to the concentrate as a function of particle hydrophobicity for varying particle sizes are shown in Figure 6.8. These follow similar trends to the froth stability data and contribute to the argument that high froth stabilities are related to a high surface area of particles in the froth. There was a significant decrease in the amount of solids recovered for the fine particles after the maximum froth stability was reached at a contact angle of 69°. These particles also produced the highest froth stabilities as well as the highest solids recovery below a contact angle of 68°. The coarse particles produced froths with the lowest stabilities as well as the lowest solids recoveries at all hydrophobicities. As

discussed in Section 6.2.2, the amount of particles recovered to the concentrate will be as a result of the combined recovery in the pulp phase and the froth phase. Predictions of pulp phase recovery can be inferred from the microflotation recoveries (Figure 6.2), which showed increasing recovery with increasing hydrophobicity. However, it is evident that the froth phase has the overriding effect on solids recovery since the solids recovery follows the general trend of froth stability and not of the pulp phase recovery.

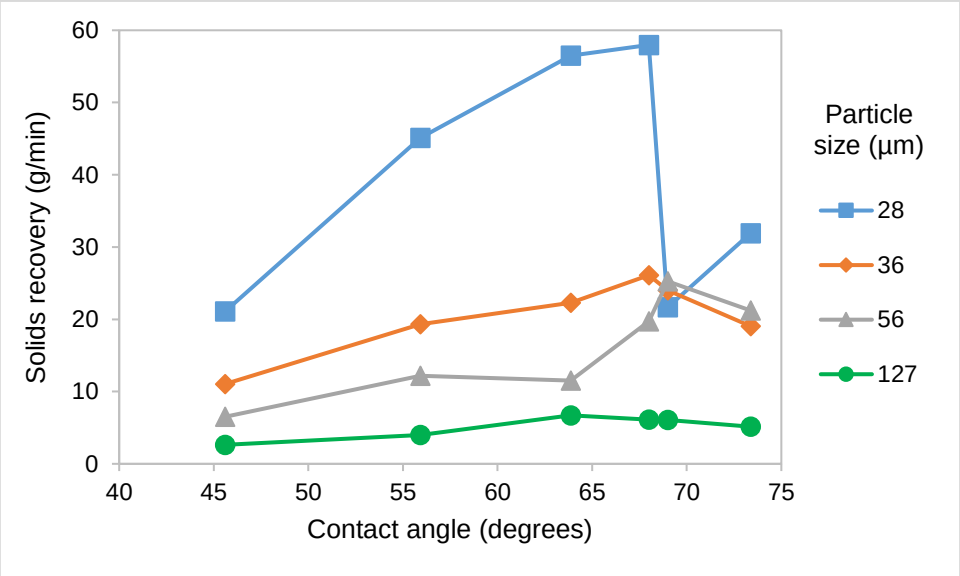

Figure 6.8: The variation of solids recovery with particle hydrophobicity for particle mixtures of different geometric mean sizes.

It is well known that the overall froth stability is determined by the liquid film stability (Aktas *et al.*, 1982; Dippenaar, 1982b) which is related to the lamellae thickness. The extent of drainage affects the lamellae thickness and the drainage is affected by the particle size and the nature of the particles. It has been reported by Johannsson and Pugh (1992) that particles with high hydrophobicity may break the liquid films and destabilise the froth. This was seen especially with the fine particles of mean size 28 µm during flotation tests using collector dosages above 100% surface coverage in this study. These particles may destabilise the froth and reduce the solids holding capacity of the froth. The particles with low hydrophobicity will remain dispersed within the lamellae and therefore, will have less effect on froth stability, particularly at larger particle sizes. Aveyard *et al.* (1994) and Kumagai *et al.* (1991) have also correlated the feasibility of the liquid films rupture to the wettability of particles. Kumagai *et al.* (1991) proposed that hydrophobic particles may modify the Laplace pressure between

the Plateau border and the three liquid films when they pack at the air-water interface and in so doing influence froth stability. This will reduce the pressure difference, and thus stabilise the froth since the liquid drainage will be restricted. Aveyard *et al.* (1994) quantified the hydrophobicity in terms of contact angles (θ) and proposed two possibilities in which hydrophobicity could affect liquid film drainage. The first instance is when θ<90°, in which the particles are expected to decrease the rate of liquid film thinning. In the second instance when θ>90°, film rupture is promoted. The 2 three-phase lines of contact are forced to meet since both surfaces of the film are on the same side of the centre of the particle. In essence, a particle that has entered a film and bridged two interfaces will have to position itself in such a way as to meet the contact angle requirement. The contact angle will determine if the froth will remain in a stable orientation or it will become destabilised.

6.2.4. Froth stability as a function of specific surface area at varying hydrophobicities

Chapter 5 showed how the froth stability as a function of the reciprocal of feed particle size (specific surface area) had a linear relationship. The specific surface area of the particles was described as the ability of the particles to stabilise the froth. This ability increased in a linear fashion with increasing specific surface area.

Figure 6.9 shows the relationship between dynamic froth stability and the reciprocal of feed particle size at varying hydrophobicities. Linear relationships are maintained for contact angles of 46°, 69° and 73°. However, for the intermediate hydrophobicities (contact angles of 56°, 64°, and 68°), the linear relationship is maintained only up to a particle size of 56 µm. Deviation from linearity occurs as the particles become finer at the smallest particle size of 28 µm. This shows that at optimum hydrophobicities and very small particle sizes, there is a substantial increase in froth stability, above the predicted linear trend. This is probably because the froth is stabilised, not only by the specific surface area of the particles, but by the amount of those particles reporting to the froth phase. It seems that the feed particle specific surface area, as shown in Chapter 5, was a good predictor of the froth stability because the feed particle size is also a good predictor of the amount of a given size of particles that will report to the froth phase. It is well known that fewer large particles report to the froth by true flotation and almost none by entrainment. There is an optimum size of particle, which will report

to the froth by true flotation and an increasing amount of particles will report to the froth by entrainment as the particle size decreases. From an examination of the data shown in Figure 6.9 it appears that, at low or high hydrophobicities, the particle size is a good predictor of the amount of particles of any size class that will report to the froth. However, at optimum hydrophobicities, more fine particles report to the froth than is predicted by their particle size. This may be due to the increased amount of fine particles reporting to the froth by true flotation at these hydrophobicities.

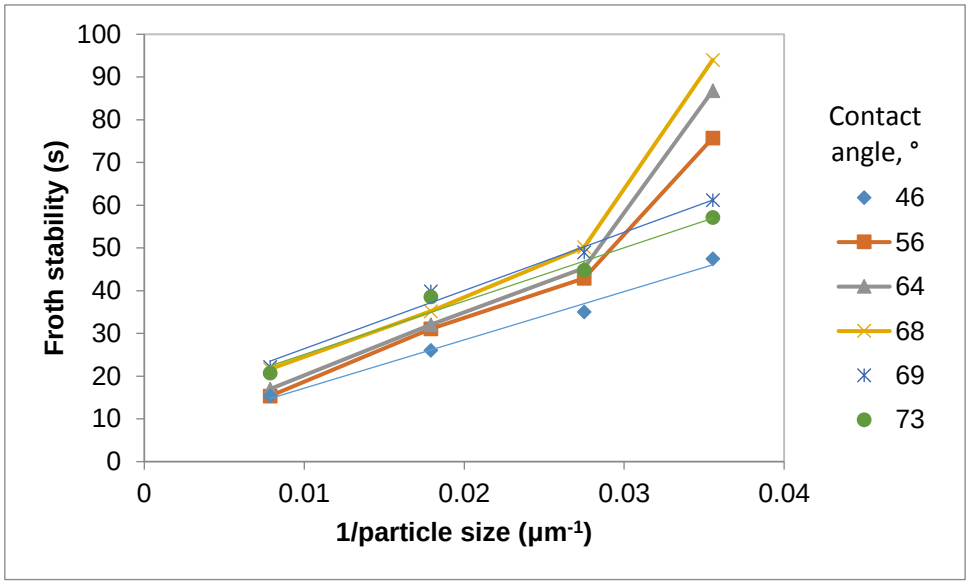

Figure 6.9: Froth stability as a function of the inverse of feed particle size at varying hydrophobicities.

Since most concentrator plant streams will have d_{50}s of greater than 28 µm, the final data point in Figure 6.9 was discarded and a linear trend plotted for each of the contact angles. The slopes of these lines and the R^2 value are given in Table 6.1.

Table 6.1: Slopes of the froth stability - inverse feed particle size graphs at each contact angle

Contact angle (°)	Slope	R^2
46	999	0.998
56	1404	0.995
64	1444	0.999
68	1451	0.998
69	1367	0.972
73	1231	0.935

If these slopes are plotted as a function of the contact angle, the plot in Figure 6.10 is obtained. As discussed in Chapter 5, this is the expected trend in the slopes of the froth stability versus reciprocal particle size graphs. The slope increases up until an optimal hydrophobicity, whereafter the slope decreases as froth stability decreases at

higher hydrophobicities. The slope of the line is the predictor for all particle sizes of that particular hydrophobicity or for that particular type of ore. This could be useful when characterising the froth for a particular ore type or drill core sample.

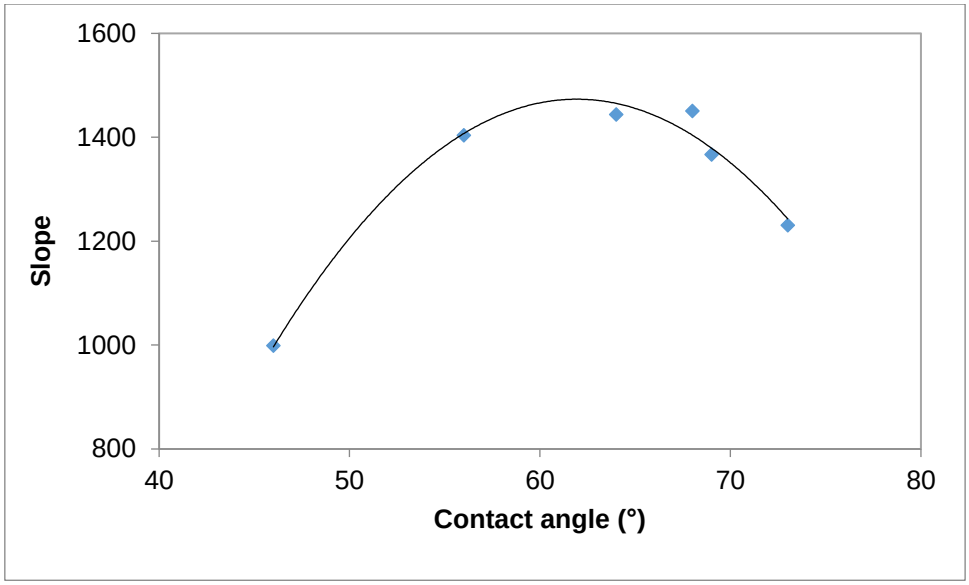

Figure 6.10: Slope of the froth stability - inverse feed particle size graph as a function of hydrophobicity.

Figure 6.11 shows an example of a graph showing froth stability as a function of reciprocal particle size for some real ores. The raw data comes from the study by Chidzanira (2016). Froth stability was measured using a froth stability column under the same conditions that were used in this study. The ores that were investigated were an Itabirite ore and a UG2 ore at various particle sizes and solids concentrations. The Itabirite iron ore consists of a large percentage of floatable quartz, while the UG2 is a platinum-bearing ore whose froth consists mainly of floatable gangue species. Both ores at all solids concentrations conform to the straight line relationship. The iron ore, with more floatable particles than the UG2 ore has a higher froth stability. In addition, the iron ore shows increasing slopes when going from 15% to 20% to 25% solids (Table 6.2). This is to be expected since there will be more floatable material present at a higher solids concentration. All solids concentrations of the UG2 ore fall on the same line. This may be due to the fact that the UG2 froth is sparsely mineralised and changes in solids concentration have less effect than in a heavily mineralised froth. A comparison between the slopes of the lines in Figure 6.11 show that the UG2 has less hydrophobic material present than the iron ore since the slope is smaller for the UG2

ore (Table 6.2). The information given in Figure 6.11 may be of use to a plant to predict how the froth would react to changes in grind and solids concentration.

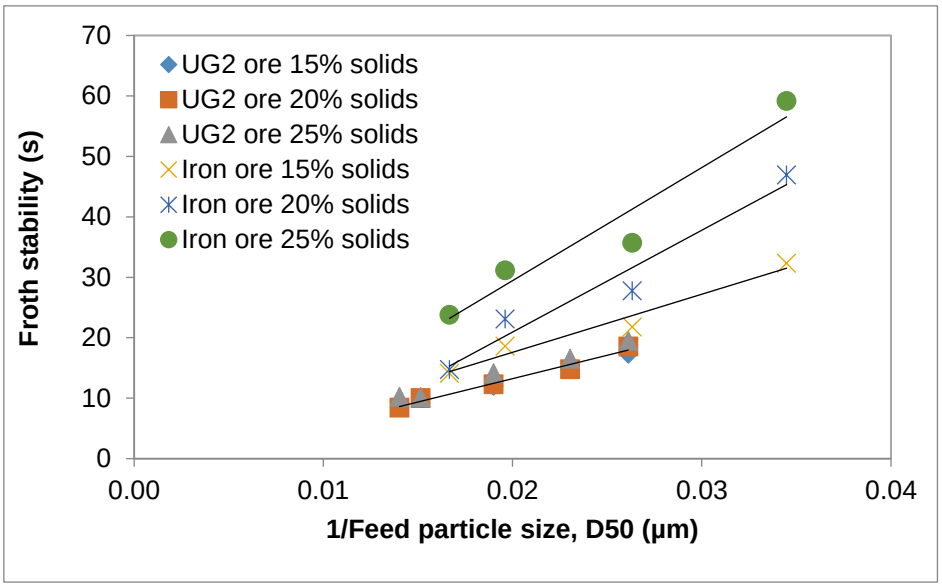

Figure 6.11: Dynamic froth stability as a function of the inverse feed particle size for UG2 and Iron ores at 15 and 20% solids concentrations (Chidzanira, 2016).

Table 6.2: Slope of the lines in Figure 6.11. (Chidzanira, 2016)

Ore type, solids concentration	Slope of the line in Figure 6.11
Iron ore, 25%	1870
Iron ore, 20%	1685
Iron ore, 15%	961
UG2 ore, 15, 20 & 25%	773

6.2.5. Modelling froth stability as a function of concentrate particle surface area

Chapter 5 discussed how it was it is not simply the size (or hydrophobicity) of the particles in the froth that affect froth stability, but also the amount of these particles in the froth. This developed into a theory on the relationship between particle surface area and froth stability. Figure 6.12 shows that as the specific surface area of the particles increased, so did their recovery to the concentrate. This was more pronounced at contact angles that afforded the maximum froth stability. This simply shows that, not only does surface area increase as the particle size decreases, but that there is an additional contribution to the surface area from the increased mass recovered at smaller particle sizes.

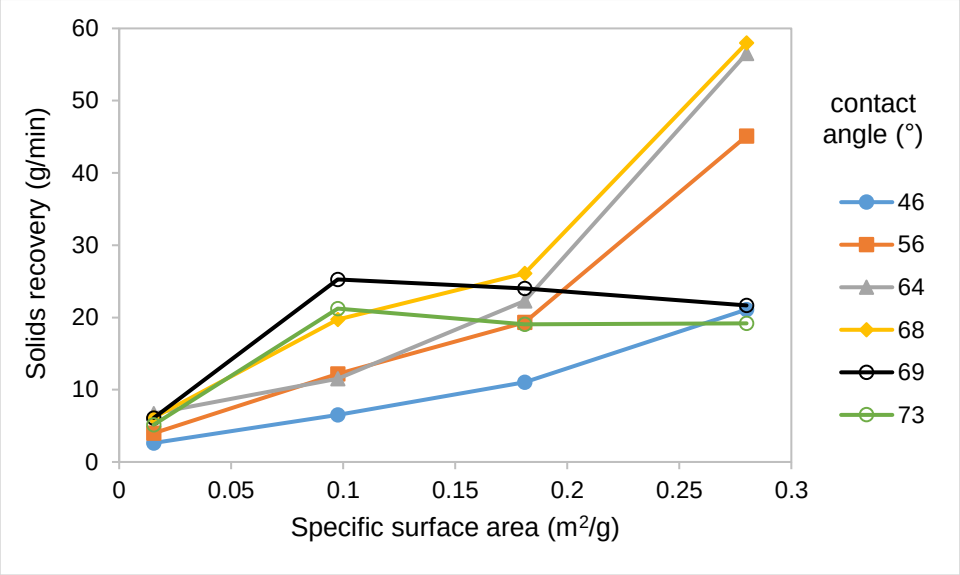

Figure 6.12: Relationship between solids recovery in the continuously operated flotation column and specific surface area at varying hydrophobicities (contact angles).

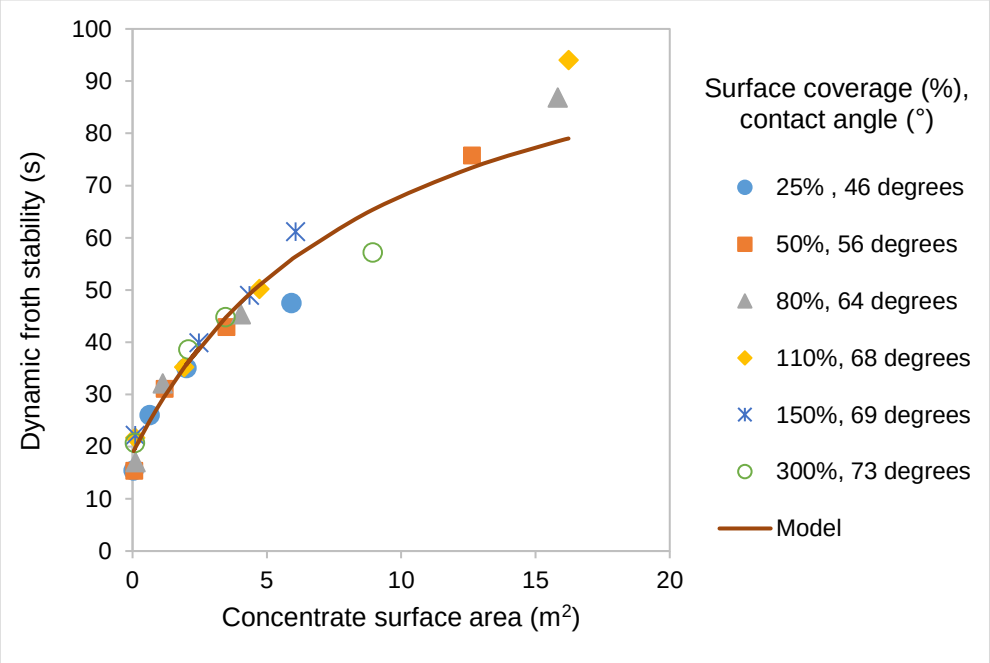

Figure 6.13: Dynamic froth stability as a function of concentrate surface area for all hydrophobicity values explored. A Langmuir isotherm model that describes this relationship is also included. Each of the shape markers represents the particle hydrophobicity measured in terms of the particle surface coverage with a corresponding contact angle.

Equation 5.2 developed in Chapter 5 was used to model this relationship between froth stability and the concentrate surface area. It is reproduced here below to aid in the discussion in this section:

$$\sigma = \sigma_0 + \sigma_{max}\left(\frac{p.a_s}{1+p.a_s}\right) \qquad \text{Equation 6.1}$$

Where σ is the froth stability, σ_0 is the initial froth stability, σ_{max} is the maximum froth stability, p is a stabilisation constant and a_s is the surface area of the particles in the concentrate.

Figure 6.13 shows the froth stability as a function of concentrate particle surface area. It is clear that the data points for all of the different hydrophobicities fall on the same relationship. The fitted constants σ_0, σ_{max} and p are: 18.73 s, 94.01 s, and 0.11, respectively.

It was expected that particles of the same hydrophobicities, but decreasing size, would fall onto the same relationship. As discussed in Chapter 5, particle packing affects froth stability in much the same way that surfactant molecules affect surface tension. Both can be fitted by a Langmuir-type isotherm. However, surfactant molecules of different hydrophobicities have different equilibrium constants. The equilibrium constant (p in Equation 6.1) defines the curvature of the adsorption isotherm. A higher p value corresponds to a greater affinity of the surfactant for the air-water interface. Surfactants may have greater affinities for the interface for such reasons as their molecular weight or their chemical structure. Therefore, it was expected that particles of different hydrophobicities would have different affinities for the air-water interface and would, therefore, have different p values. This was found not to be the case as shown in Figure 6.13. There is no clearly defined difference between the different hydrophobicities and all hydrophobicities appear to fall on the same relationship with the same p value.

Figure 6.6 showed that particles of high hydrophobicity had a lower froth stability than particles of optimum hydrophobicity. The result of this was that the surface area of these particles in the froth was lower and, thus, the froth stability was lower. However, they still fell on the same froth stability versus surface area relationship. It appears that for a given volume, geometry and initial bubble size, there is an associated surface area of particles with a given stability. The surface area of the particles reporting to the froth may change according to the hydrophobicity of the particles, but will fall somewhere along the relationship. That is, the surface area of particles in the froth defines the stability attainable under those conditions. Therefore, the contact angle/mineralogy defines the amount of particular particles that report to the froth. But it is their surface area once they are there that will define the froth stability.

6.3. Conclusion

This chapter has demonstrated the relationship between froth stability and particle hydrophobicity at different particle size distributions using a synthetic ore made up of three components, i.e. pyrite, quartz, and talc. Froth stability was measured using two laboratory devices, i.e. a non-overflowing stability column and a continuously operated column flotation cell. Firstly, the effect of varying pyrite hydrophobicity was tested on a distinct particle size class of +38-106 µm. Thereafter, particle size distributions of varying mean sizes were used to study this effect.

It was found, in common with other studies, that froth stability increased with increasing particle hydrophobicity until a maximum value was obtained at a contact angle of between 66° and 69°. At higher contact angles there was a decrease in froth stability. Both the non-overflowing stability column and the continuous column produced similar results, showing that the results were not device-specific. It was found that the greatest differences in froth stability with increasing hydrophobicity were for the smallest size particles (geometric mean of 28 µm). Although larger particles followed a similar trend to the smaller particles, the response was less pronounced. Froth stability was found to be more sensitive to changes in particle size than changes in hydrophobicity over the relatively large range of size and hydrophobicity values tested.

The relationship between the froth stability and the feed specific surface area was found to be linear at most practical particle sizes. However, it deviated from linearity at very small mean particle sizes (28 µm) for particles of optimum hydrophobicities. This was attributed to the increase in particles reporting to the froth by both entrainment and true flotation at smaller particle sizes with optimum hydrophobicities. The slopes of the relationships for froth stability as a function of feed specific surface area in the linear region were found to increase with increasing hydrophobicity, up until an optimum contact angle of between 64° and 68°, whereafter they decreased. Thus, this family of curves would allow the prediction of froth stability of varying hydrophobicities on a size-by-size basis.

It was demonstrated how this relationship can be used to characterise the froth stability of real ores at different grinds and how the slopes of these curves change with changes in solids concentration and different ore mineralogy.

The Langmuir-type model that related the froth stability to the concentrate particle surface area was fitted to all of the data points at all particle sizes of varying contact angles. It was found that all data points fell on the same relationship. It was shown that particle hydrophobicity and size determine the amount of particles that will report to the froth phase, but that once the particles are in the froth, it is their surface area which defines the froth stability.

CHAPTER SEVEN

7. CONCLUSIONS AND RECOMMENDATIONS

7.1. Conclusions

The main aim of this thesis was to study the effect that mineral particle properties have on froth stability. The two main particle properties which were varied in order to quantify their effects are size and hydrophobicity. At first, each of these particle properties were studied independently and their effects on froth stability quantified. Thereafter, the interactive effects of the two variables on froth stability were quantified.

A summary of the results are presented here as answers to the key questions put forward in Chapter 1.

(i) What forms the basis of a good experimental measure for froth stability?

Techniques employed to predict froth stability ought to focus on the factors that affect it. In this regard, the prediction of indicators like water recovery, top-of-the-froth bubble burst rate, froth growth rate, and froth lifetime, among other factors, should provide a good understanding of the stability of the froth. In order to answer the above key question, two devices were built in the laboratory.

The non-overflowing stability column which predicts the froth growth rate was built in the laboratory. It provides a practical and simple method for determining froth stability, which is not taken into account by standard laboratory batch flotation tests. It is important that flotation tests should be accompanied by metallurgical data. Since this is a shortcoming of the non-overflowing stability column, a continuously operated bench-scale flotation column was constructed, and in addition it is able to predict froth stability using water recovery and the bubble burst rate.

The differences and similarities between the two devices as well as among the three froth stability measurement proxies have been substantially discussed in Chapter 5.

- The two devices were operated with the same superficial air velocity of 1 cm/s. At a constant frother dosage, the froth growth rate and the amount of water

reporting to the froth will be the same. In addition, both devices are dynamic processes, meaning liquid reports to the froth while drainage occurs continuously. The froth growth height, bubble burst rate and water recovery will all be driven by these two processes.

- Differences do exist between the two devices and this is brought about by differences in operating mode, column diameters, and the bubble generation techniques employed. Whereas the bench-scale flotation column was operated continuously at steady state, the non-overflowing stability column was operated in batch mode. The bench-scale flotation column had a smaller diameter than the froth stability column (higher wall-to-froth surface area ratio) meaning it experienced a higher rate of drainage. Bubble generation was by means of a ceramic tubular sparger for the bench scale flotation column, whereas a sintered glass P2 frit with a pore size of 40 – 100 µm placed at the bottom of the column was used in the non-overflowing stability column.

Differences between the two devices should bring about differences in the absolute values of froth stability, but this is not expected to bring about a difference in the ability of the mineral particles to stabilise the froth. This was confirmed by the fact that the two devices, along with 3 different measurement types (dynamic froth stability, water recovery and bubble burst rate) all had similar stability constants, *p*, in the froth stability versus particle surface area model.

(ii) What is the relationship between froth stability and particles of varying size distributions?

The influence of particle size on froth stability was studied experimentally and results obtained discussed in Chapter 5. It was found that froth stability decreased with increasing particle size. It was seen that small particles had the biggest influence on froth stability. However, coarse particles had a destructive effect on froths and the froth volume was low. There was a large increase in froth stabilities for average feed particle sizes below 50 µm and this was shown to be largely due to the large increase in particles reporting to the froth by entrainment. It was suggested that these particles modified the viscosity of the thin films, reducing drainage and thus stabilising the froths. In addition, the maximum capillary pressure is inversely proportional to particle size, which predicts that smaller particles increase the capillary pressure gradients.

On the other hand, coarse particles tend to break the liquid films in between bubbles rendering the froth unstable.

Froth stability was shown to increase linearly with feed particle specific surface area. This useful relationship was shown to hold for two different ore types at different percent solids.

Froth stability was related to the packing of particles at the air-water interface. A Langmuir-type equation was thus used to model the froth stability data in much the same way that one would model surfactant packing at the interface. It was found that this model is a good fit to the experimental data.

Thus, the first two hypotheses were answered in this section of work:

Hypothesis 1: Froth stability increases with decreasing particle size and this is due to increased viscosity of the thin liquid films between bubbles which leads to a slower liquid drainage rate.

> Froth stability was found to increase with decreasing particle size and the relationship was shown. Determining the mechanism for this was beyond the scope of this work, but it was shown that very fine, entrained particles increased the froth stability substantially and it is known that these would have a significant effect on viscosity.

Hypothesis 2: Froth stability will increase as a function of the increasing particle surface area in the froth because thin film liquid drainage will be directly affected by the surface area of particles retarding drainage.

> A relationship and model have been put forward and the froth stability has been shown to increase in a systematic manner with increasing surface area.

(iii) What is the relationship between froth stability and particles of varying hydrophobicities?

Particle hydrophobicity was quantified using three main proxies, i.e. collector surface coverage, recovery of pyrite in the microflotation cell and contact angle. It was found

that pyrite recovery in the microflotation cell followed a sigmoid shape as a function of the collector coverage on the mineral surface, as opposed to overall recovery, which decreased after a particular surface coverage. Contact angle increased linearly until a value of about 64°, which corresponded to a collector surface coverage of 80%, whereafter it levelled off.

The effect of particle hydrophobicity was initially tested on particles of a size range 38-106 μm. It was found that froth stability was initially low at low particle hydrophobicity. It then increased with increasing hydrophobicity, reaching a maximum value at a contact angle of 64°, before finally decreasing as particle hydrophobicity continued to increase. The optimal condition at 80% collector surface coverage (contact angle of 64°) which offered the highest froth stability also gave the best flotation performance in terms of recovery. The lowest froth stabilities as well as flotation recoveries were obtained at conditions of very high and very low hydrophobicities. This indicates the importance of froth stability in overall valuable mineral recovery. It was shown that the recovery of pyrite in the microflotation cell continued to increase with increasing collector dosage, indicating that the particle hydrophobicity kept increasing and thus favoured their recovery in the pulp zone. However, this was not reflected by a continuous increase in froth stability, but rather, a maximum stability was reached and this was followed by a decrease. The decrease in froth stability beyond the optimal hydrophobicity has been attributed to bridging and rupture of the thin liquid films by these very hydrophobic particles.

Hypothesis 3: Froth stability is greatest at a critical contact angle, below or above which froth stability decreases. This is due to bridging effects causing film rupture in highly hydrophobic particles.

> Froth stability was shown to increase until a critical contact angle, after which the froth stability decreased.

(iv) What are the interactive effects of particle size and hydrophobicity on froth stability?

The interactive effects of particle size and hydrophobicity on froth stability was studied extensively in Chapter 6 using mixtures of particles of different sizes and varying hydrophobicities.

In common with the single size range studied initially, the different size classes followed the same trend of increasing froth stability with increasing hydrophobicity up until a contact angle of about 68° to 69°, whereafter froth stability decreased. The effect on small particles of 28 μm mean size were far more dramatic than on coarser particles, but all followed a similar trend. This trend was found to be in common with previous flotation studies that have found greatest froth stabilities between 63° and 69°. This provides confirmation of the robustness and accuracy of the techniques employed in this study. However, this study extended our understanding of particle-stabilised froths by characterising the froth stability in terms of surface areas of particles.

The effect of particle surface area on froth stability

The reciprocal relationship between particle size and specific surface area was used to investigate the relationship between froth stability and feed particle specific surface area. It was shown that froth stability was linearly dependent on the feed specific surface area for most practical flotation particle sizes. The slopes of the froth stability versus feed specific surface area relationships in the linear region were found to increase with increasing hydrophobicity, up until an optimum contact angle of between 64° and 68°, whereafter they decreased. Thus, this family of curves would allow the prediction of froth stability of varying hydrophobicities on a size-by-size basis. It was demonstrated how this relationship can be used to characterise the froth stability of real ores at different grinds and how the slopes of these curves change with changing solids concentrations and different ore mineralogy.

A Langmuir-type model that related the froth stability to the concentrate particle surface area was fitted to all of the data points at all particle sizes of varying contact angles. It was found that all data points fell on the same relationship. This showed that particle hydrophobicity and size determine the amount of particles that will report to the froth phase, but that once the particles are in the froth, it is their surface area which defines the froth stability.

Hypothesis 4: Optimum froth stability is obtained with small particles of intermediate hydrophobicity. This is because large particles and particles of very high hydrophobicity rupture liquid films and so suppress the froth stability.

This hypothesis was shown to be true. This was shown most clearly in Figure 6.6 where small particles of optimum hydrophobicity had a significantly higher froth stability than other particles.

7.2. Recommendations

Much as the continuously operated flotation column provided a good framework for froth stability prediction using water recovery and the bubble burst rate technique, let alone froth recovery determination by the variable froth depths method, it was however, unable to provide for the prediction of the bubble coalescence rate due to the small diameter of the column. A redesign of this column that provides for a large surface area in which bubble size variation is seen up the pulp-froth interface would be a worthy venture in enabling the bubble coalescence rate to be predicted by measuring the bubble sizes in the froth phase. A column with flat surfaces would be a preferred choice for this instead of the cylindrical column employed in this work.

Another important step in furthering this work would be to build an image analysis technique to measure the bubble bursting phenomena at the top of the flotation cell. It would be impossible to quantify the bubble bursting phenomena visually for a flotation cell with a large surface area at the top.

In this study, a pyrite-quartz-talc system was used to study the effect of particle properties on froth stability. It would be interesting to carry out similar studies with a mineral system which has a different density, e.g. a galena-quartz-talc system.

REFERENCES

Aktas, Z., Cilliers, J. J., and Banford, A. W. (2008). Dynamic froth stability: Particle size, airflow rate and conditioning time effects. *International Journal of Mineral Processing, 87*, 65-71.

Alexander, D. J., Franzidis, J. P., and Manlapig, E. V. (2003). Froth recovery measurement in plant scale flotation cells. *Minerals Engineering, 16*, 1197-1203.

Ata, S. (2012). Phenomena in the froth phase of flotation - A review. *International Journal of Mineral Processing, 102-103*, 1-12.

Ata, S., Ahmed, N., and Jameson, G., J. (2003). A study of bubble coalescence in flotation froths. *International Journal of Mineral Processing, 72*, 255-266.

Aveyard, R., Binks, B. P., Fletcher, P. D. I., Peck, T. G., and Rutherford, C. E. (1994). Aspects of aqueous foam stability in the presence of hydrocarbon oils and solid particles. *Advances in colloid and interface science, 48*, 93-120.

Barbian, N., Cilliers, J. J., Morar, S. H., and Bradshaw, D. J. (2007). Froth imaging, air recovery and bubble loading to describe flotation bank performance. *International Journal of Mineral Processing, 84*, 81-88.

Barbian, N., Hadler, K., Ventura-Medina, E., and Cilliers, J. J. (2005). THe froth stability column: linking froth stability and flotation performance. *Minerals Engineering, 18*, 317-324.

Barbian, N., Ventura-Medina, E., and Cilliers, J. J. (2003). Dynamic froth stability in froth flotation. *Minerals Engineering, 16*, 1111-1116.

Bikerman, J. J. (1973). *Foams*: Springer-Verlag.

Binks, B. P. (2002). Particles as surfactants - similarities and differences. *Current Opinion in Colloid and Interface Science, 7*, 21-41.

Blake, P., & Ralston, J. (1985). Particle size, surface coverage and flotation response. *Colloids and surfaces, 16*, 41-53.

Bradshaw, D. J. (1997). *Synergistic effects between thiol collectors used in the flotation of pyrite.* University of Cape Town, Cape Town.

Bradshaw, D. J., and O'Connor, C. T. (1996). Measurement of the sub-process of bubble loading in flotation. *Minerals Engineering, 9*, 443-448.

Brożek, M., and Mlynarczykowska, A. (2006). Application of the Stochastic model for analysis of flotation kinetics with coal as an example. *Physicochemical Problems of Mineral Processing, 40*, 31-44.

Bulatovic, S. M. (2007). *Handbook of flotation reagents: Chemistry, Theory and Practice: Flotation of Sulphide Ores*. Boston.

Burt, M. W. G., and Fewtrell, C. A. (1970). The preparation of powder beds by a centrifugal compaction technique. In M. J. Groves & J. L. Wyatt-Sargent (Eds.), *Particle size analysis* (pp. 321-338). London: Society for Analytical Chemistry.

Castro, S., Miranda, C., Toledo, P., and Laskowski, J. S. (2013). Effect of frothers on bubble coalescence and foaming in electrolyte solutions and seawater. *International Journal of Mineral Processing, 124*, 8-14.

Chidzanira, T. (2016). *Investigation of the effect of particle size on froth stability.* University of Cape Town, Cape Town.

Chipfunhu, D., Zanin, M., and Grano, S. (2012). Flotation behaviour of fine particles with respect to contact angle. *Chemical Engineering Reseach and Design, 90*, 26-32.

Chipfunhu, D., Zanin, M., and Grano, S. R. (2011). The dependency of the critical contact angle for flotation on particle size - Modelling the limits of fine particle flotation. *Minerals Engineering, 24*, 50-57.

Cho, Y. S., and Laskowski, J. S. (2002). Effect of flotation frothers on bubble size and foam stability. *International Journal of Mineral Processing, 64*, 69-80.

Connolly, J., and Dobby, G. (2009). Benchmarking of flotation plants: A key element of flotation modelling. In *Recent Advances in Mineral Processing Plant Design* (pp. 211-219). Colorado: Society for Mining, Metallurgy and Exploration (SME).

Crawford, R., and Ralston, J. (1988). The influence of particle size and contact angle in mineral flotation. *International Journal of Mineral Processing, 23*, 1-24.

Dabrowski, A. (2001). Adsorption - from theory to practice. *Advances in Colloid and Interface Science, 93*, 135-224.

de Jager, G., Hartfield, D. P., Bradshaw, D. J., Francis, J. J., & Morar, S. H. (2004). A method and a control system for extracting valuable minerals from mined ore. “Smartfroth”, Adams & Adams Patent Attorneys, Pretoria, A&A REF: v16148 (1-9), Provisional Patent lodged 24 Feb 2004.

de Vries, A. J. (1957). *Foam Stability*. Delft, The Netherlands: Rubber-Stichting.

Denkov, N., and Marinova, K. (2006). Antifoam effects of solid particles, oil drops and oil-solid compounds in aqueous foams. In B. P. a. H. T. S. Binks (Ed.), *Colloidal Particles at Liquid Interfaces* (pp. 383-444). Cambridge: Cambridge University Press.

Denkov, N. D., Ivanov, I. B., and Kralchevsky, P. A. (1992). A possible mechanism of stabilization of emulsions by solid particles. *Journal of Colloid and Interface Science, 150*, 589-593.

Diggins, D., Fokkink, L. G. S., and Ralston, J. (1990). The wetting of angular quartz particles: capillary pressure and contact angles. *Colloids and Surfaces, 44*, 299-313.

Dippenaar, A. (1982a). The destabilisation of froth by solids I: The mechanism of film rupture *International Journal of Mineral Processing, 9*, 1-14.

Dippenaar, A. (1982b). The Destabilisation of froth by solids II: The rate determining step. *International Journal of Mineral Processing, 9*, 15-27.

Dunstan, D., and White, L. J. (1986). A capillary pressure method for measurement of contact angles in powders and porous media. *Journal of Colloid and Interface Science, 111*(1), 60-64.

Engelbrecht, J. A., and Woodburn, E. T. (1975). The effect of froth height, aeration rate and gas precipitation on flotation. *Journal of the South African Institute of Mining and Metallurgy, 76*, 125-132.

Estrada-Ruiz, R. H., and Perez-Garibay, R. (2009). Evaluation of models of air recovery in a laboratory flotation column. *Minerals Engineering, 22*, 1193-1199.

Falutsu, M., and Dobby, G. S. (1992). Froth performance in commercial sized flotation columns. *Minerals Engineering, 20*, 121-135.

Farrokhpay, S. (2011). The significance of froth stability in mineral flotation - A review. *Advances in Colloid and Interface Science, 166*, 1-7.

Feng, D., and Aldrich, C. (1999). Effect of particle size on flotation performance of complex sulphide ores. *Minerals Engineering, 12*(7), 721-731.

Feteris, S. M., Frew, J. A., and Jowett, A. (1987). Modelling the effect of froth depth in flotation. *International Journal of Mineral Processing, 20*, 121-135.

Finch, J., A., Nesset, J. E., and Acuna, C. (2008). Role of frother on bubble production and behaviour in flotation. *Minerals Engineering, 21*, 949-957.

Finch, J. A. (1995). Column flotation: A selected review - Part IV: Novel flotation devices. *Minerals Engineering, 8*(6), 587-602.

Finch, J. A., and Dobby, G. S. (1990). *Column flotation* (1st ed. Vol. 89): Pergamon Press.

Frye, G. C., and Berg, J. C. (1989). Antifoam action by solid particles. *Journal of Colloid and Interface Science, 127*(1), 222-239.

Garrett, P. R. (1980). Preliminary considerations concerning the stability of a liquid heterogeneity in a plane-parallel liquid film. *Journal of Colloid and Interface Science, 76*(2), 587-590.

Gaudin, A., Grob, J., and Henderson, H. (1931). *Effect of particle size in flotation*. New York, USA: Technical Publication No. 414.

Geldenhuys, S. (2017). *Froth stability in two-phase system.* University of Cape Town, Cape Town.

Grano, S. R., Prestidge, C. A., and Ralston, J. (1997). Solution interaction of ethy xanthate and sulphite and its effect on galena flotation and xanthate adsorption. *International Journal of Mineral Processing, 52*, 161-186.

Hadler, K., and Cilliers, J. J. (2009). The relationship between the peak in air recovery and flotation bank performance. *Minerals Engineering, 22*, 451-455.

Hadler, K., Smith, C. D., and Cilliers, J. J. (2010). Recovery vs. mass pull: The link to air recovery. *Minerals Engineering, 23*, 994-1002.

Hanumanth, G. S., and Williams, D. J. A. (1990). An experimental study of the effects of froth height on flotation of China clay. *Powder Technology, 60*, 131-144.

Harris, M. (2011). *Development of a phenomenological model of the froth.* Paper presented at the The optimisation of mineral processes by modelling and simulation.

Hernáinz, F., and Calero, M. (2001). Froth flotation: kinetic models based on chemical analogy. *Chemical Engineering and Processing, 40*, 269-275.

Horozov, T., S. (2008). Foams and foam films stabilised by solid particles. *Current Opinion in Colloid and Interface Science, 13*, 134-140.

Hosokawa, M., Nogi, K., Naito, M., and Yokoyama, T. (2012). *Nanoparticle Technology Handbook* (2 ed.): Elsevier.

Hu, S., Ofori, P., and Firth, B. (2009). Monitoring of froth stability using electrical impedance spectroscopy. *International Journal of Mineral Processing, 92*, 15-21.

Hunter, T., N., Pugh, R. J., Franks, G., V., and Jameson, G., J. (2008). The role of particles in stabilising foams and emulsions. *Advances in Colloid and Interface Science, 137*, 57-81.

Iglesias, E., Anderez, J., Forgiarini, A., and Salager, J.-L. (1995). A new method to estimate the stability of short-life foams. *Colloids and Surfaces A: Physicochemical and Engineering Aspects, 98*, 167-174.

Ip, S. W., Wang, Y., and Toguri, J. M. (1999). Aluminium foam stabilisation by solid particles. *Canadian Metallurgical Quartery, 38*(1), 81-92.

Ityokumbul, M., T. (1992). A mass transfer approach to flotation column design. *Chemical Engineering Science, 47*(13/14), 3605-3612.

Jiqiao, L., and Baiyun, H. (2001). Particle size characterization of ultrafine tungsten powder. *International Journal of Refractory Metals & Hard Materials, 19*, 89-99.

Johansson, G., and Pugh, R. J. (1992). The influence of particle size and hydrophobicity on the stability of mineralized froths. *International Journal of Mineral Processing, 34*(1-2), 1-21.

Johnson, N. W., McKee, D. J., and Lynch, A. J. (1974). Flotation rates of nonsulfide minerals in chalcopyrite flotation processes. *Trans. AIME, 256*, 204-209.

Kaptay, G. (2006). On the equation of the maximum capillary pressure induced by solid particles to stabilize emulsions and foams and on the emulsion stability diagrams. *Colloids and Surfaces A: Physicochemical and Engineering Aspects, 282-283*, 387-401.

Kaptay, G. (2012). On the optimum contact angle of stability of foams by particles. *Advances in Colloid and Interface Science, 170*, 87-88.

Kawatra, S., Komar, and Carlson, J. T. (2013). *Beneficiation of Phosphate Ore*. Englewood, Colorado: Society for Mining, Metallurgy, and Exploration (SME).

King, R. P. (July 1978). A pilot-plant investigation of a kinetic model for flotation. *Journal of the South African Institute of Mining and Metallurgy*, 325-338.

Kirjavainen, V. M. (1989). Application of a probability model for the entrainment of hydrophilic particles in froth flotation. *International Journal of Mineral Processing, 27*, 63-74.

Kirjavainen, V. M. (1992). *Study on entrainment mechanism in dispersed flotation suspensions* (Vol. 206).

Kirjavainen, V. M. (1996). Review ana analysis of factors controlling the mechanical flotation of gangue minerals. *International Journal of Mineral Processing, 46*, 21-34.

Kohmuench, J., Mankosa, M., Yan, E., and Luttrel, G. H. (2010). *Advances in coarse particle recovery - fluidised bed flotation.* Paper presented at the XXV International Mineral Processing Congress (IMPC), Brisbane, Australia.

Kracht, W., Orozco, Y., and Acuna, C. (2016). Effect of surfactant type on the entrainment factor and selectivity of flotation at laboratory scale. *Minerals Engineering, 92*, 216-220.

Kumagai, H., Torikata, Y., Yoshimura, H., Kato, M., and Yano, T. (1991). Estimation of the stability of faom containing hydrophobic particles by parameters in the capillary model. *Agric. Biol. Chem., 55*(7), 1823-1829.

Laplante, A. R. (1980). *The effect of air flow rate on the kinetics of flotation.* University of Toronto, Toronto.

Laplante, A. R., Kaya, M., and Smith, H. W. (1989). The effect of froth on flotation kinetics - a mass transfer approach. In J. S. Laskowski (Ed.), *Frothing in flotation*. New York: Gordon and Breach.

Laplante, A. R., Toguri, J. M., and Smith, H. W. (1983). The effect of air flow on the kinetics of flotation: Part 1. The transfer of material from the slurry to the froth. *International Journal of Mineral Processing, 11*, 203-219.

Laskowski, J. S. (2003). Fundamental properties of flotation frothers. In L. Lorenzen & D. J. Bradshaw (Eds.), *Proceedings of the 22nd International Mineral Processing Congress* (Vol. 2, pp. 788-797). Cape Town, South Africa: SAIMM.

Leja, J. (1982). *Surface chemistry of froth flotation*. New York and London: Plenum Press.

Mathe, Z. T., Harris, M. C., and O'Connor, C. T. (1999). A review of methods to model the froth phase in non-steady state flotation systems. *Minerals Engineering, 13*(2), 127-140.

Min, M. A. (2010). *Measuring the floatability of Sulphide minerals and ores.* University of Queensland, Brisbane.

Moolman, D. W., Aldrich, C., and Van Deventer, J. S. J. (1995). The interpretation of flotation froth surfaces by using digital image analysis and neural networks. *Chemical Engineering Science, 50*(22), 3501-1513.

Morar, S., H., Harris, M., C., and Bradshaw, D. J. (2012b). The use of machine vision to predict flotation performance. *Minerals Engineering, 36-38*, 31-36.

Morar, S. H., Bradshaw, D. J., and Harris, M. C. (2012a). The use of the froth surface lamellae burst rate as a flotation froth stability measurement. *Minerals Engineering, 36-38*, 152-159.

Morris, G., Pursell, M. R., Neethling, S. J., and Cilliers, J. J. (2008). The effect of particle hydrophobicity, separation distance and packing patterns on the stability of a thin film. *Journal of Colloid and Interface Science, 327*, 138-144.

Muganda, S., Zanin, M., and Grano, S. R. (2011). Influence of particle size and contact angle on the flotation of chalcopyrite in a laboratory batch flotation cell. *International Journal of Mineral Processing, 98*, 150-162.

Neethling, S. J., and Cilliers, J. J. (2002). The entrainment of gangue into flotation froth. *International Journal of Mineral Processing, 64*, 123-134.

Neethling, S. J., and Cilliers, J. J. (2003). Modelling flotation froths. *International Journal of Mineral Processing, 72*, 267-287.

Nesset, J. E., Hernandez-Aguilar, J. R., Acuna, C., Gomez, C. O., and Finch, J., A. (2006). Some gas dispersion characteristics of mechanical flotation machines. *Minerals Engineering*, 807-815.

Prestidge, C. A., and Ralston, J. (1995). Contact angle studies of galena particles. *Journal of Colloid and Interface Science, 172*(2), 302-310.

Prestidge, C. A., and Ralston, J. (1996). Contact angle studies of particulate sulphide minerals. *Minerals Engineering, 9*(1), 85-102.

Przemyslaw, B. K. (2013). Determination of critical coalescence concentration and bubble size for surfactants used as flotation frothers. *Industrial and Engineering Chemistry Research, 27*(370), 11752-11757.

Pugh, R. J. (1996). Foaming, foam films, antifoaming and defoaming. *Advances in Colloid and Interface Science, 64*, 67-142.

Pugh, R. J. (2005). Experimental techniques for studying the structure of foams and froths. *Advances in colloid and interface science, 114-115*, 239-251.

Rahman, R., M., Ata, S., and Jameson, G. J. (2012). The effect of flotation variables on the recovery of different particle size fractions in the froth and the pulp. *International Journal of Mineral Processing, 106*, 70-77.

Rao, S. R. (2013). *Surface Chemistry of Froth flotation* (2 ed. Vol. 1: Fundamentals): Springer Science & Business Media.

Rosenholm, J., B. (2007). Wetting of surfaces and interfaces: a conceptual equilibrium thermodynamic approach. In T. F. Tadros (Ed.), *Colloid Stability: The role of surface forces, Part II* (Vol. 2).

Runge, K., Crosbie, R., Rivett, T., and McMaster, J. (6-10 September 2010). *An evaluation of froth recovery measurement techniques.* Paper presented at the XXV International Mineral Processing Congress (IMPC), Brisbane, Queensland, Australia.

Savassi, O. N., Alexander, D. J., Franzidis, J. P., and Manlapig, E. V. (1998). An empirical model for entrainment in industrial flotation plants. *Minerals Engineering, 11*(3), 243-256.

Savassi, O. N., Alexander, D. J., Johnson, N. W., Franzidis, J. P., and Manlapig, E. V. (1997). *Measurement of froth recovery of attached particles in industrial flotation cells.* Paper presented at the 6th Annual Mill Operators Conference, Melbourne.

Schwarz, S., and Grano, S. R. (2005). Effect of particle hydrophobicity on particle and water transport across a flotation froth. *Colloids and surfaces A: Physicochemical Engineering aspects, 256*, 157-164.

Seaman, D. R., Manlapig, E. V., and Franzidis, J. P. (2006). Selective transport of attached particles across the pulp-froth interface. *Minerals Engineering, 19*, 841-851.

Shean, B., Hadler, K., and Cilliers, J. J. (2017). A flotation control system to optimise performance using peak air recovery. *Chemical Engineering Research and Design, 117*, 57-65.

Siebold, A., Nardin, M., Schultz, J., Walliser, A., and Oppliger, M. (2000). Effect of dynamic contact angle on capillary rise phenomena. *Colloids and Surfaces A: Physicochemical and Engineering Aspects, 161*, 81-87.

Smith, C. D., Hadler, K., and Cilliers, J. J. (2010). Flotation bank air addition and distribution for optimal performance. *Minerals Engineering, 23*, 1023-1029.

Smith, P. G., and Warren, L. J. (1989). Entrainment of particles into flotation froths. *Mineral Processing and Extractive Metallurgy, 5*, 123-145.

Soto, H. S. (1992). *Development of novel flotation-elutriation method for coarse phosphate beneficiation*: Final report to Florida Institute of Phosphate Research; Publication number 02-070-098.

Subrahmanyam, T. V., and Forssberg, E. (1988). Froth stability, particle entrainment and drainage in flotation - a review. *International Journal of Mineral Processing, 23*, 33-53.

Sutherland, K. L., and Wark, I., William. (1955). *Principles of flotation*: Australian Institute of Mining and Metallurgy.

Szatkowski, M., and Freyberger, W. L. (1985). Kinetics of flotation with fine bubbles. *Transactions of the Institute of Mining and Metallurgy, 94*(C61-C70).

Tao, D., Luttrel, G. H., and Yoon, R.-H. (2000). A parametric study of froth stability and its effect on column flotation of fine particles. *International Journal of Mineral Processing, 59*, 25-43.

Thorne, G. C., Manlapig, E. V., Hall, J. S., and Lynch, A. J. (1976). *Modelling of industrial flotation circuits* (Vol. 2).

Trahar, W. J., and Warren, L. J. (1976). The floatability of very fine particles - a review. *International Journal of Mineral Processing, 3*, 103-131.

Triffett, B., and Cilliers, J. J. L. R. (2006). London, England Patent No.: E. P. Specification.

Tsatouhas, G., Grano, S., and Vera, M. (2006). Case studies on the performance and characterisation of the froth phase in industrial flotation circuits. *Minerals Engineering, 19*, 774-783.

Ulusoy, U., Hicyilman, C., and Yekeler, M. (2004). Role of shape properties of calcite and barite particles on apparent hydrophobicity. *Chemical Engineering and Processing, 43*, 1047-1053.

Ventura-Medina, E., Barbian, N., and Cilliers, J. J. (2004). Solids loading and grade on mineral froth bubble lamellae. *International Journal of Mineral Processing, 74*(1-4), 189-200.

Ventura-Medina, E., and Cilliers, J. J. (2002). A model to describe flotation performance based on physics of foams and froth image analysis. *International Journal of Mineral Processing, 67*, 79-99.

Vera, M. A., Franzidis, J. P., and Manlapig, E. V. (1999). Simultaneous determination of collection zone rate constant and froth zone recovery in a mechanical flotation environment. *Minerals Engineering, 12*(10), 1163-1176.

Vera, M. A., Mathe, Z. T., Franzidis, J. P., Harris, M. C., Manlapig, E. V., and O'Connor, C. T. (2002). The modelling of froth zone recovery in batch and continuously operated laboratory flotation cells. *International Journal of Mineral Processing, 64*, 135-151.

Vieira, A. M., and Peres, A. E. C. (2007). The effect of amine type, pH, and size range in the flotation of quartz. *Minerals Engineering, 20*, 1008-1013.

Vizcarra, T. G., Harmer, S. L., Wightman, E. M., Johnson, N. W., and Manlapig, E. V. (2011). The influence of particle shape properties and associated surface chemistry on the flotation kinetics of chalcophrite. *Minerals Engineering, 24*, 807-816.

Warren, L. J. (1985). Determination of the contributions of true flotation and entrainment. *International Journal of Mineral Processing, 14*, 33-44.

Washburn, E., W. (1921). The dynamics of capillary flow. *Physical review, 17*, 273-283.

Weaire, D., and Hutzler, S. (1999). *The Physics of foams*. Oxford: Clarendon Press.

Wiese, J., Harris, P., and Bradshaw, D. (2005). The influence of the reagent suite on the flotation of ores from the Merensky reef. *Minerals Engineering, 18*, 189-198.

Wills, B., A., and Napier-Munn, T. J. (2006). *Wills' Mineral Processing Technology: An introduction to the practical aspects of ore treatment and mineral recovery* (7th ed.): Elsevier Ltd.

Woodburn, E. T., Austin, L. G., and Stockton, J. B. (1994). A froth-based flotation kinetic model. *Chemical Engineering Research & Design, 74*(2A), 211-226.

Woodburn, E. T., Kropholler, H. W., Green, J. A. A., and Cramer, L. A. (1976). The utility and limitations of mathematical modelling in the prediction of the properties of flotation networks. *Flotation, 2*.

Xu, M., Quinn, P., and Stratton-Crawley. (1996). A feed-line aerated flotation column - Part 1: Batch and continuous testwork. *Minerals Engineering, 9*(5), 499-507.

Yianatos, J. B., Bergh, L. G., and Cortès, G. A. (1998). Froth zone modelling of an industrial flotation column. *Minerals Engineering, 11*(5), 423-435.

Yianatos, J. B., Moys, M. H., Contreras, F., and Villanueva, A. (2008). Froth recovery of industrial flotation cells. *Minerals Engineering, 21*, 817-825.

Zanin, M., Wightman, E., Grano, S. R., and Franzidis, J.-P. (2009). Quantifying contributions to froth stability in porphyry copper plants. *International Journal of Mineral Processing, 91*, 19-27.

Zheng, X., Franzidis, J. P., and Johnson, N. W. (2006). An evaluation of different models of water recovery in flotation. *Minerals Engineering, 19*, 871-882.

Zuniga, H. G. (1935). Flotation recovery is an exponential function of its rate. *Bol. Soc. Nac. Min., 47*, 83-86.

APPENDICES

APPENDIX A

Appendix A presents the data sets on the effect of particle size on froth stability as discussed in Chapter 5.

The froth growth rates were obtained by following the change in height of the froth over time using the froth stability column. The dynamic froth stability was then calculated using the Model:

$$\Sigma = \frac{H_{max} \times A}{Q} \qquad \text{Equation A1}$$

Where H_{max} = the maximum height attained by the froth; A = Column surface area and Q = Air flow rate.

The model fits for the experimental data for each mean particle size are represented in Figure A1.

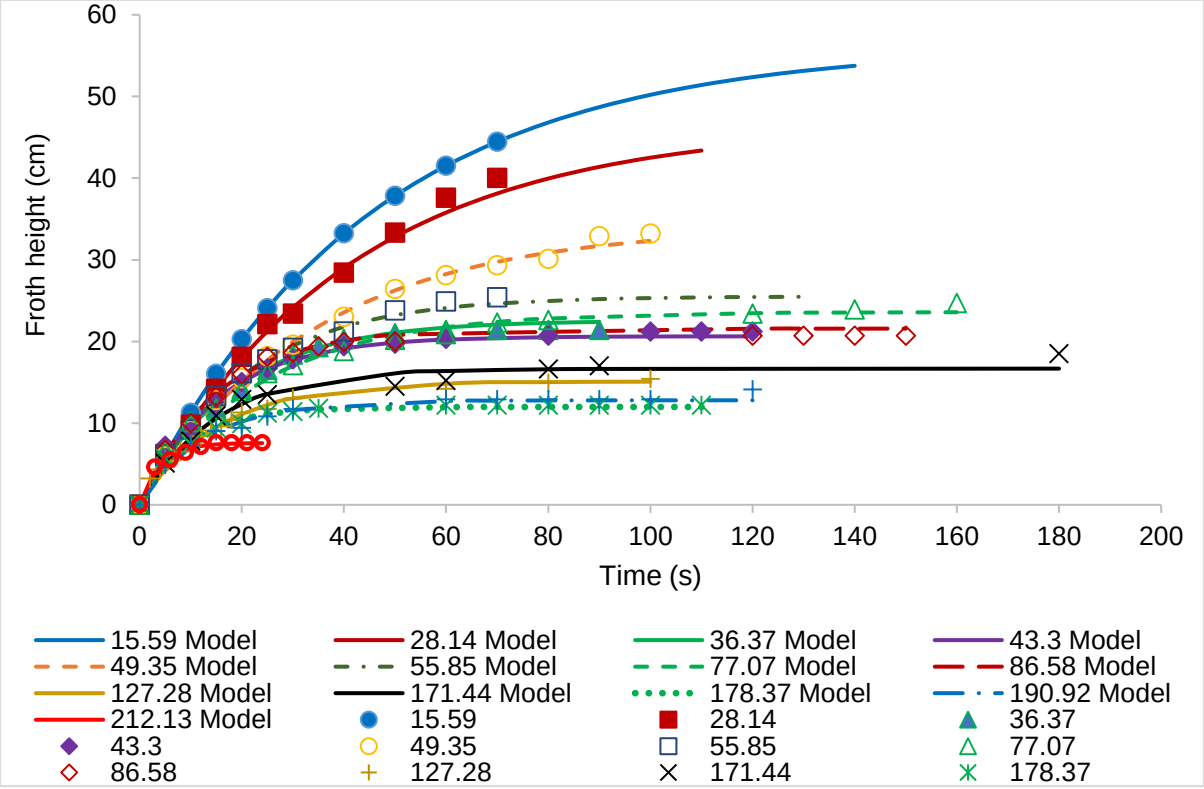

Figure A1: Growth rates of the froth for each mean particle size.

A Langmuir-type model was fitted to the froth stability data. This model is shown below:

$$\sigma = \sigma_0 + \sigma_{max}\left(\frac{p.a_s}{1+p.a_s}\right) \qquad \text{Equation A1}$$

Where σ is the froth stability, σ_0 is the initial froth stability, σ_{max} is the maximum froth stability, p is a stabilisation constant and a_s is the surface area of the particles in the concentrate.

Table A1: Fitting the Langmuir-type model to the dynamic froth stability data.

Feed particle size (µm)	Concentrate Surface Area (m2/min)	Concentrate Surface Area (m^2)	Froth stability (s)	Model
15.59	7.86	8.90	67.89	65.43
28.14	6.16	4.87	47.47	52.08
36.37	2.99	1.15	23.01	28.24
43.30	0.69	0.24	21.03	18.81
49.35	1.21	0.70	34.80	23.88
55.85	1.98	0.86	26.01	25.46
77.07	0.39	0.16	24.06	17.81
86.58	1.49	0.55	21.99	22.24
93.51	0.24	0.07	18.86	16.83
106.07	0.32	0.09	17.33	17.05
127.28	0.13	0.03	15.39	16.33
171.44	0.13	0.04	18.07	16.40
178.37	0.11	0.02	12.21	16.19
190.92	0.07	0.02	13.05	16.10
212.13	0.07	0.01	7.72	16.02

Table A2: Top-of-froth bubble burst rate data

Feed particle size (µm)	Concentrate surface area (m^2/min)	Concentrate surface area (m^2)	Bubble burst rate (s^{-1})	1/Bubble burst rate (s)	Model
15.59	7.862	8.896	2.375	0.421	0.43
28.14	6.158	4.872	2.750	0.364	0.41
36.37	2.995	1.148	2.625	0.381	0.33
86.58	1.492	0.547	3.375	0.296	0.28
106.07	0.323	0.093	4.000	0.250	0.22
127.28	0.134	0.034	4.625	0.216	0.21
171.44	0.133	0.040	5.125	0.195	0.21
178.37	0.113	0.023	5.250	0.190	0.21
190.92	0.071	0.015	4.875	0.205	0.21
212.13	0.069	0.009	5.000	0.200	0.21

Table A3: Water recovery data

Feed particle size (µm)	Concentrate surface area (m^2/min)	Concentrate surface area (m^2)	Water recovery (g/min)	Model
15.59	7.8624	8.896	112.05	113.11
28.14	6.1583	4.872	96.80	95.65
36.37	2.9946	1.148	72.01	58.87
55.85	1.2118	0.858	43.48	54.01
86.58	0.3899	0.547	39.91	48.23
106.07	0.2376	0.093	30.60	38.51
127.28	0.1336	0.034	56.35	37.12
171.44	0.1325	0.040	44.14	37.25
178.37	0.1132	0.023	33.89	36.85
190.92	0.0713	0.015	42.34	36.67
212.13	0.0693	0.009	21.20	36.51

Table A4: Metallurgical analysis of the concentrates from the bench-scale flotation column

Feed particle size (µm)	Concentrate particle size (µm)	Solids recovery (g/min)	Concentrate talc mass (g/min)	Concentrate pyrite mass (g/min)	Concentrate quartz mass (g/min)	Pyrite recovery (%)	Pyrite rate constant, k (s)
15.60	14.99	28.08	0.91	3.13	24.04	85.1	8.30
28.10	17.25	21.09	1.03	3.26	16.80	80.84	6.13
36.40	22.78	11.05	0.72	3.04	7.29	67.46	
43.30	34.88	5.17	0.81	3.81	0.55	59.7	1.54
49.40	46.83	10.82	0.91	3.49	6.42	66.53	
55.90	23.29	3.28	0.86	3.51	2.13	49.68	2.89
77.10	58.55	3.61	0.94	2.49	0.18	46.2	1.43
86.60	55.03	8.11	0.69	2.93	4.48	67.17	1.25
93.50	81.18	5.94	0.54	1.54	3.86	61.62	2.99
106.07	102.74	4.39	0.00	2.15	2.24	30.6	2.33
127.30	120.13	1.76	0.59	1.89	0.15	49.9	
171.40	139.78	4.89	0.60	2.18	2.12	46.99	1.45
178.40	171.42	3.71	0.50	1.37	1.84	50.85	1.29
190.90	166.25	2.63	0.36	1.24	1.03	45.28	1.50
212.13	207.14	3.46	0.13	2.15	1.14	21.20	1.20

APPENDIX B

Appendix B presents the data sets on the effect of particle hydrophobicity and the interactive effects of particle size and hydrophobicity on froth stability as discussed in Chapter 6.

Calculating the amount of collector required for flotation

The amount of collector used for each of the flotation tests was calculated from the BET surface area of pyrite and assuming the cross-sectional area of the thiol head group of xanthate to be 28.8 Å (Grano *et al.,* 1997).

1 g of collector was weighed and dissolved to make 100 mL of solution in a volumetric flask from which calculated volumes required for each flotation test were measured.

Table B1: Calculated volumes of collector solution used in the microflotation tests.

Collector surface coverage (%)	Calculated volume required (µL)
10	100.3
20	200.6
30	300.9
40	401.2
50	501.5
60	601.8
70	702.1
80	802.4
100	1003.0
150	1504.5
200	2006.0
300	3009.0
400	4012.0
500	5015.0

The recovery of pyrite was calculated by the first order kinetic expression:

$$R(t) = R_{max}(1 - e^{-kt}) \qquad \text{Equation B1}$$

Where $R(t)$ = recovery at any time, t, R_{max} = maximum recovery, t = time, and k = rate constant.

Froth recovery, $\mathrm{R_f}$, was calculated from the ratio of the overall flotation rate constant, k and the collection zone rate constant, $\mathrm{k_c}$, i.e.

$$R_f = \frac{k}{k_c}$$ Equation B2

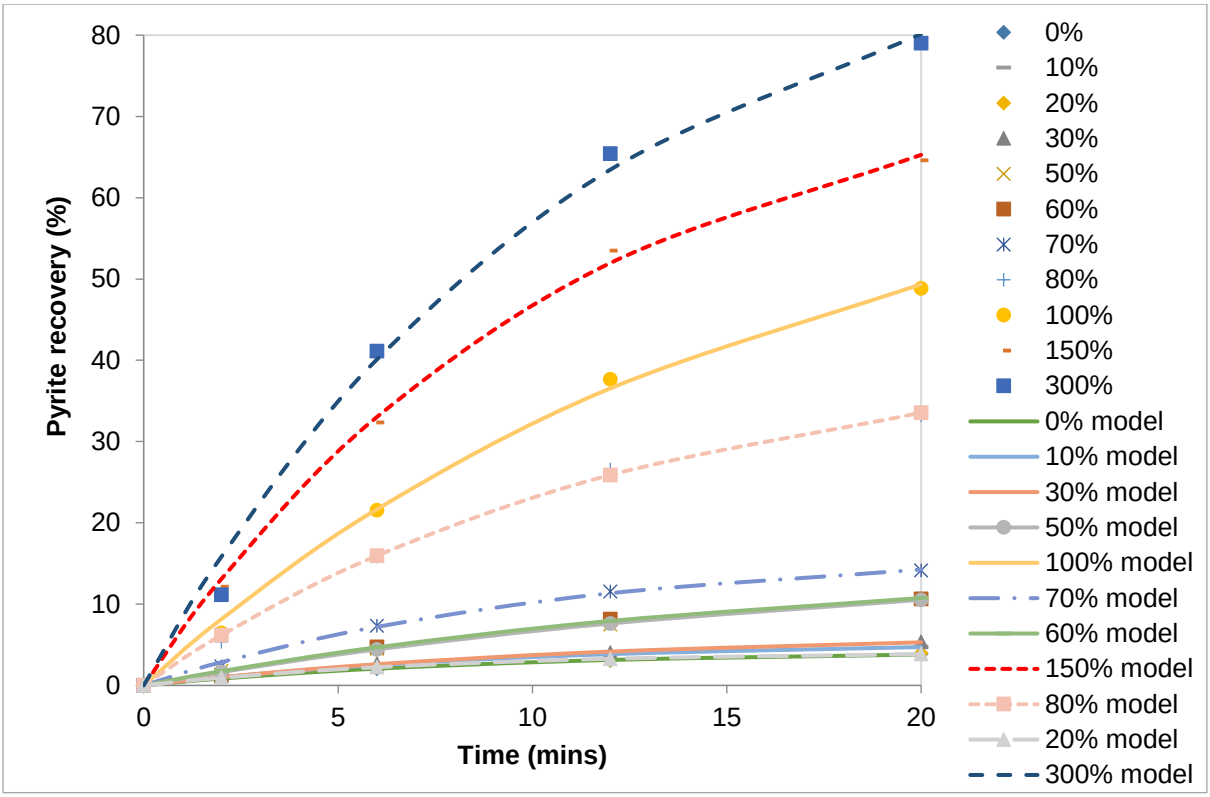

Figure B1: Recovery of pure pyrite as a function of time in the microflotation cell for varying hydrophobicities.

Table B2: Relationship between contact angle, collector surface coverage, and pyrite recovery in the microflotation cell for a particle size class of +38 – 106 µm.

Contact angle (°)	Collector surface coverage (%)	Pyrite recovery (%)
36.99	0	4.28
40.85	10	5.39
48.76	30	6.46
55.91	50	15.88
63.86	80	42.22
66.18	150	77.38
73.37	300	95.95

Table B3: Froth stability of the +38 – 106 µm size class at varying hydrophobicities

Collector surface coverage (%)	Contact angle (°)	Dynamic Froth stability (s)	Water recovery (g/min)
10	40.85	23.57	21.59
30	48.76	28.27	35.72
50	55.91	34.35	56.51
80	63.86	34	78.55
100	77.22	32.7	61.26
150		25.54	43.13

Table B4: Flotation response of the +38 – 106 µm size class at varying hydrophobicities

Collector surface coverage (%)	Total solids mass (g/min)	Hydrophobic mass (g/min)	Quartz mass (g/min)	Grade (%)	Pyrite recovery (%)	Froth recovery, R_f (%)
10	2.41	1.3973	1.0127	29.47	20.32	30.54
30	4.81	3.1131	1.6969	25.21	36.8	48.01
50	6.21	3.4251	2.7849	21.2	41.86	56.37
80	8.37	4.3404	4.0296	14.01	42.84	53.01
100	6.53	3.2663	3.2637	22.58	43.05	54.1
150	5.57	2.2713	3.2987	22.3	37.53	39.62

Table B5: Interactive effectives of particle size and hydrophobicity on dynamic froth stability (s).

	Contact angle (°)					
Mean feed size (µm)	**46**	**56**	**64**	**68**	**69**	**73**
28	47.47	75.74	86.82	94.01	61.16	57.15
36	35.00	42.88	45.32	50.15	48.97	44.79
56	26.01	31.07	32.07	35.2	39.85	38.56
127	15.39	15.34	16.98	21.63	22.18	20.70

Table B6: Interactive effectives of particle size and hydrophobicity on water recovery (g/min) in the bench-scale flotation column.

	Contact angle (°)					
Mean feed size (µm)	**46**	**56**	**64**	**68**	**69**	**73**
28	96.80	181.00	229.54	230.01	105.47	108.22
36	72.01	114.43	123.26	138.83	167.46	167.46
56	43.48	85.00	93.89	130.00	163.71	143.10
127	35.00	45.10	50.93	59.00	44.80	41.44

Table B7: Interactive effectives of particle size and hydrophobicity on solids recovery (g/min) in the bench-scale flotation column.

		Contact angle (°)					
Mean feed size (µm)	**Concentrate specific surface area (m^2/g)**	**46**	**56**	**64**	**68**	**69**	**73**
28	0.2800	21.09	45.10	56.51	57.97	21.68	19.20
36	0.1810	11.05	19.31	22.28	26.10	24.00	19.06
56	0.0976	6.51	12.20	11.53	19.70	25.26	21.23
127	0.0154	2.63	3.98	6.71	6.13	6.09	5.15

Table B8: Surface areas of concentrates (m^2) obtained from studying the interactive effectives of particle size and hydrophobicity on froth stability.

	Contact angle (°)					
Mean feed size (µm)	**46**	**56**	**64**	**68**	**69**	**73**
28	5.905	12.628	15.823	16.232	6.070	8.935
36	2.000	3.495	4.033	4.724	4.344	3.450
56	0.635	1.191	1.125	1.923	2.465	2.072
127	0.041	0.061	0.103	0.094	0.094	0.079